AD-A020 710

PASSIVE NOSETIP TECHNOLOGY (PANT) PROGRAM.
VOLUME XII. NOSETIP TRANSITION AND SHAPE
CHANGE TESTS IN THE AFFDL 50 MW RENT ARC - DATA
REPORT

A. B. Shimizu, et al

Acurex Corporation

Prepared for:

Space and Missile Systems Organization

April 1974

055042

SAMSO-TR-74-36
Volume XII

FDA020710

INTERIM REPORT
PASSIVE NOSETIP TECHNOLOGY
(PANT) PROGRAM

Volume XII.   Nosetip Transition and Shape Change Tests
in the AFFDL 50 MW RENT Arc — Data Report

A. B. Shimizu
J. E. Ferrell
C. A. Powars

Aerotherm Division/Acurex Corporation

SAMSO-TR-74-86

April 1974

AEROTHERM REPORT 74-100

Air Force Space and Missile
Systems Organization
Los Angeles, California

Contract F04701-71-C-0027

INTERIM REPORT
PASSIVE NOSETIP TECHNOLOGY
(PANT) PROGRAM

Volume XII. Nosetip Transition and Shape Change Tests
in the AFFDL 50 MW RENT Arc — Data Report

A. B. Shimizu
J. E. Ferrell
C. A. Powars

This document may be distributed further by any holder
only with specific prior approval of Space and Missile
Systems Organization (SAMSO) Los Angeles, California

Letter on file

1

A

ACKNOWLEDGEMENTS

Preceding page blank

FOREWORD

This document is Volume XII of the Interim Report series for the Passive Nosetip Technology (PANT) program. A summary of the documents in this series prepared to date is as follows:

Volume I   - Program Overview (U)

Volume II   - Environment and Material Response Procedures for Nosetip Design (U)

Volume III   - Surface Roughness Effects

       Part I   - Experimental Data

       Part II   - Roughness Augmented Heating Data Correlation and Analysis (U)

       Part III - Boundary Layer Transition Data Correlation and Analysis (U)

Volume IV   - Heat Transfer and Pressure Distributions on Ablated Shapes

       Part I   - Experimental Data

       Part II   - Data Correlation

Volume V   - Definition of Shape Change Phenomenology from Low Temperature Ablator Experiments

       Part I   - Experimental Data, Series C (Preliminary Test Series)

       Part II   - Experimental Data, Series D (Final Test Series)

       Part III - Shape Change Data Correlation and Analysis

Volume VI   - Graphite Ablation Data Correlation and Analysis (U)

Volume VII   - Computer User's Manual, Steady-State Analysis of Ablating Nosetips (SAANT) Program

Volume VIII - Computer User's Manual, Passive Graphite Ablating Nosetip (PAGAN) Program

Volume IX   - Unsteady Flow on Ablated Nosetip Shapes - PANT Series G Test and Analysis Report

Volume X   - Summary of Experimental and Analytical Results

Volume XI   - Analysis and Review of the ABRES Combustion Test Facility
                for High Pressure Hyperthermal Reentry Nosetip Systems
                Tests

Volume XII   - Nosetip Transition and Shape Change Tests in the AFFDL 50
                MW RENT Arc - Data Report

Volume XIII   - An Experimental Study to Evaluate Heat Transfer Rates to
                Scalloped Surfaces - Data Report

Volume XIV   - An Experimental Study to Evaluate the Irregular Nosetip
                Shape Regime - Data Report

Volume XV   - Roughness Induced Transition Experiments - Data Report

This report was prepared by Aerotherm Division/Acurex Corporation under
Contract F04701-71-C-0027. Volumes I through IX covered PANT activities from
April 1971 through April 1973. Volumes X through XV represent contract efforts
from May 1973 to December 1974. Volume X summarizes the respective test pro-
grams and describes improvements in nosetip analysis capabilities. Volume XI
presents an evaluation of the ABRES test facility in terms of performing ther-
mostructural and reentry flight simulation testing. Volumes XII through XV are
data reports which summarize the experiments performed for the purpose of de-
fining the irregular flight regime. The analysis of these data are presented
in Volume X.

This work was administered under the direction of the Space and Missile
Systems Organization with Lieutenant A. T. Hopkins and Lieutenant E. G. Taylor
as Project Officers with Mr. W. Portenier and Dr. R. L. Baker of the Aerospace
Corporation serving as principal technical monitors. Mr. C. A. Powars, Mr. J.
E. Ferrell, and Mr. A. B. Shimizu were the Aerotherm investigators.

This technical report has been reviewed and is approved.

E G Taylor

E. G. Taylor, Lt., USAF
Project Officer
Aero and Materials Division
Directorate of Systems Engineering
Deputy for Reentry Systems

ABSTRACT

Test results are presented for the Fall 1973 testing performed under the Passive Nosetip Technology Program at the AFFDL 50 MW RENT facility. The purposes of these experiments were:

- Nosetip shape change testing at conditions predicted to produce "irregular" shapes, and

- Testing to obtain data on nose radius and material effects on transition.

Shape change behavior similar to that previously seen on low-temperature ablator testing was observed. Transitional flow was observed on all models. Shape change profiles, recession data, surface temperature measurements and post-test photographs are presented herein. Data correlation activities are in progress and no results, other than very preliminary observations, are presented.

TABLE OF CONTENTS

Preceding page blank

LIST OF FIGURES

LIST OF FIGURES (Concluded)

SECTION 1

INTRODUCTION

This report documents the results of a test series conducted in the AFFDL 50 MM REWT arc during November of 1973 as part of the SAMSO sponsored Passive Nosetip Technology (PANT) Program. The objectives of this test series were to investigate nosetip boundary layer transition and shape change phenomena.

Seventeen models of various sizes and shapes fabricated from ATJ-S graphite, Mod-IIIa carbon/carbon, and reverse dixie cup carbon phenolic were ablation tested at various test conditions with impact pressures ranging from 12 to 40 atmospheres. The overall objectives and specific approach for this test series was documented in detail in the Pre-Test Plan Report, Reference 1. In general, the experiment performed as required and the testing objectives were satisfied.

The rationale for this test series, the test equipment used, and the test conditions achieved are summarized in Section 2. The reduced test data are presented in Section 3 without analysis or comparison to theory. Some preliminary observations relative to the results of this test series are made in Section 4.

SECTION 2

IMPLEMENTATION

The basic test plan as detailed in Reference 1 was maintained. Its principal features are repeated here for completeness, with specific attention paid to those areas where actual practice varied from the plan.

2.1   RATIONALE

As documented in the pretest plan (particularly, Appendices A and B*) considerable effort was devoted to selection of the test conditions. The motivation for this selection is discussed below for both test objectives.

2.1.1   Nosetip Transition

A major uncertainty in calculating the shape change history of an R/V nosetip is associated with predicting the altitude and location of boundary layer transition. This problem was reviewed early in the PANT program (Reference 3), and extensive wind tunnel tests were carried out to measure transition locations on rough wall blunt calorimeter models tested in NOL tunnel 8 (References 4 and 5). These wind tunnel tests provided high quality data on artificially roughened surfaces tested at Reynolds numbers and Mach numbers of interest. However, some uncertainty is associated with the fact that these sorts of tests cannot be conducted on the "real" surfaces (i.e., that of ablating graphite, carbon/carbon, etc.) in a "hyperthermal" environment (i.e., with total enthalpy approaching that experienced in reentry).

Boundary layer transition data can be (and has been) obtained on real ablative materials in hyperthermal environments. However, this data is of somewhat lower quality because:

1.   Boundary layer transition is detected by noting the model shape change pattern (cf., Figure 2-1). This is relatively imprecise. Transition "onset" (i.e., whether transition occurred at all on the nose) can be detected with confidence, but it is difficult to accurately measure transition location.

2.   The test environment produced by facilities capable of these hyperthermal tests (e.g., high pressure arcs) is usually both uncertain

---

*Appendix B is also bound separately as Reference 2.

7018 6.40 5623 4386 3509 2632 1754 877 0 ms
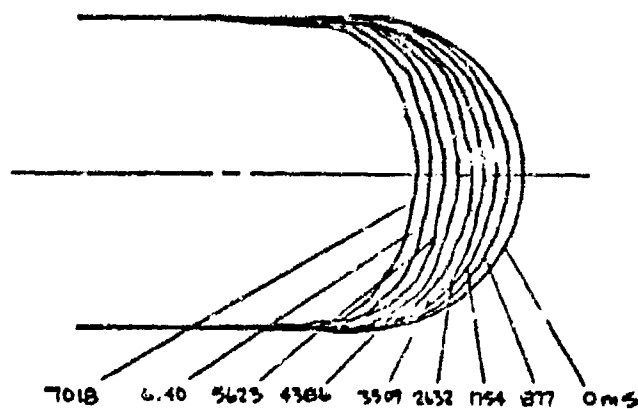
a) Laminar shape; no transition
(Mod-III C/C at P_{t_2} ~ 20 atm)

3000 2750 2500 2250 2000 1750 1500 1250 1000 750 500 250 0 ms
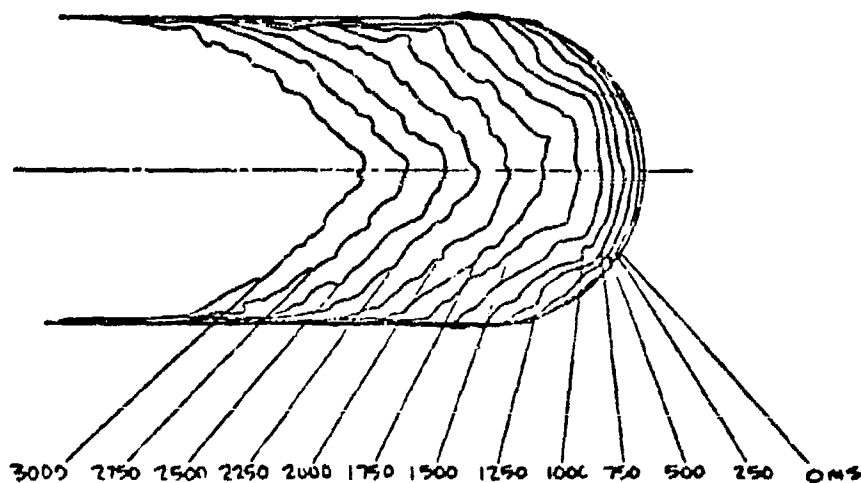
b) Turbulent shape; initial transition in vicinity of sonic point
(Mod-III C/C at P_{t_2} ~ 50 atm)

Figure 2-1. Detection of Boundary Layer Transition from Ablating
Nosetip Model Shape Change Patterns (Example Data
from Fall, 1971 AFML/PANT 50 MW Test Series).

and nonuniform relative to wi ' tunnels ordinarily used for transition testing.

In spite of these factors, much can be learned by analyzing nosetip model ablation data to "back out" transition information. For example, positive conclusions may be drawn regarding the transition potential of one material relative to another.

A preliminary transition analysis of recent nosetip model ablation data obtained in the AFFDL 50 MW RENT arc is included as Appendix A to the pretest plan (Reference 1). This analysis considers only transition onset, not transition location. The analyses of Appendix A of Reference 1 and Reference 5 demonstrate the validity of deducing transition data from ablation data. These analyses indicated a need for certain additional ablation data to answer questions regarding model size effects, material effects, and environmental effects. These requirements formed the basis for the transition tests conducted during this test series.

2.1.2 Nosetip Shape Change

The second objective of this test series was to study the shape change pattern of nosetip materials ablating in a hyperthermal environment. Particular emphasis was placed on the possible development of "irregular" shapes.

"Irregular" shape development, as used here, denotes a peculiar shape change pattern which may occur for certain combinations of flow conditions. Figure 2-2 shows typical irregular shapes assumed by low temperature ablator models (camphor and paradichlorobenzene) tested in the NOL hypersonic tunnel number 8 as part of the PANT program (References 6 and 7). Examples of irregular shapes are:

a. Models which ablate asymmetrically—even though the flow field and material are essentially uniform, and the model is at zero angle of attack (e.g., Figure 2-2a).

b. Models which develop a very long slender pointed shape—where the slender protrusion in the nose region often breaks off due to its fragility (e.g., Figure 2-2b).

c. Models which ablate to an essentially blunt shape except for a sharp protrusion in the stagnation region—this shape can give rise to a high frequency oscillation of the bow shock structure sometimes called "buzz" (e.g., Figure 2-2c).

These irregular shapes are of very practical interest in that their development on a flight nosetip can lead to obvious undesirable effects.

2-3
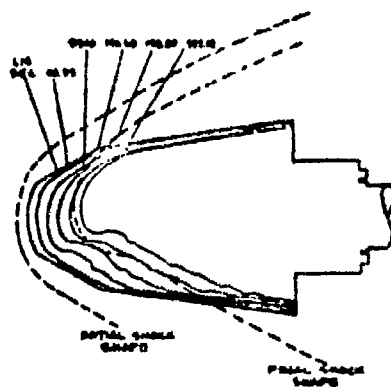
a. Asymmetric Ablation (Run 202: Camphor at $Re_\infty = 2.7 \times 10^6$/ft)
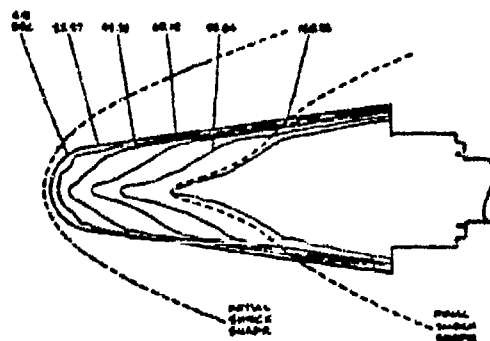
b. Long Slender Fragile Shape Development (Run 209: Camphor at $Re_\infty = 5.2 \times 10^6$/ft)
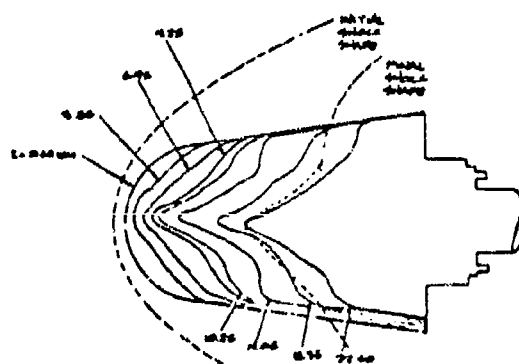
c. Development of Blunt Shape with Sharp Protrusion (Run 20: Paradichlorobenzene at $Re_\infty = 9.2 \times 10^6$)

Figure 2-2. Examples of "Irregular" Nozetip Ablated Shape Development (Data from PANT Low Temperature Ablator Model Tests in NOL Tunnel 8)

The physical event associated with the development of these irregular shapes are not totally understood at present. However, two necessary (though probably not sufficient) flow field conditions are required:

1. The flow field Reynolds number must be high enough (and/or the model must be large and rough enough) to cause boundary layer transition at least as far forward as the sonic point on the nosetip.

2. The flow field Mach number must be high enough (and the model must ablate to a sharp enough shape) to give rise to significant entropy layer effects. That is, the entropy gradient along the boundary layer edge must be substantial enough and must occur far enough forward to cause a significant variation in heat and mass transfer rates to the nose.

The development of irregular shapes as previously defined has never been observed on graphitic materials tested in an arc jet, combustion driven, or other hyperthermal ablation test facility (a possible exception is that asymmetric shapes sometimes develop when transition is incipient). The reason for this is probably due to requirement number 2 above. That is, in order to maximize the impact pressure on the model, nosetip material test facilities usually utilize a low expansion ratio nozzle. Since the stream Mach number is low, the model bow shock is weak and entropy gradient effects on ablation are quite small (cf., Reference 8).

With respect to simulating flight type nosetip shape change in a hyperthermal ground test facility, the following question arises, "How high must the jet Mach number be in order to produce entropy layer affected shape change patterns?" Also, "With the Mach number this high, will the impact pressure be adequate to assure boundary layer transition and turbulent shape development?" A parametric analysis was carried out to answer these questions considering the APFDL 50 MW arc operating capabilities; these calculations are documented in Appendix B to the pretest plan (Reference 2).

The analyses documented in Appendix B indicate the feasibility of testing nosetip models in the 50 MW arc at a Mach number high enough to produce significant entropy layer effects, yet low enough to produce impact pressures adequate to assure transition. The optimum test condition for this objective was shown to be obtained using the 0.9 inch throat diameter, 2.39 inch exit diameter contoured nozzle (which results in a stream Mach number of slightly over 3), an arc chamber pressure of about 100 atm, the "flat enthalpy profile" air injection configuration (to minimize nonuniformities and maximize Reynolds number),

test models based on a 5/8 inch nose (or shoulder) radius, and test times of 20 to 30 seconds. These tradeoffs between impact pressure and Mach number are illustrated in Figure 2-3 from Reference 2.

It was uncertain whether or not these test conditions will give rise to the development of any "irregular" ablated shapes as previously defined. However, it was felt that the test conditions selected were optimum in this respect relative to the basic capabilities of the 50 MW arc. Even if "irregular" shapes did not develop, ablation data at these conditions would be valuable in that they would indicate useful information regarding boundary layer transition and Mach number effects on shape change.

2.2 TEST MATRIX

The testing as actually performed is summarized in Table 2-1. Runs 001, 002, and 003 were devoted to resolving a model positioner malfunction and only calibration data was obtained. Due to the breakage of the first model exposed (Run 004, Strut 1), the schedule was rearranged to allow evaluation of the problem and development of a cure. All test parameters shown in Table 2-1 are the actual values based on measurement of arc heater conditions and interpretation of calibration data.

The test matrix included six arc heater runs:

- Three runs addressed the "nosetip transition" objective (Section 2.1.1)

- Three runs addressed the "nosetip shape change" objective (Section 2.1.2).

The test conditions (P_{t_2} and H_c) shown differ somewhat from the originally planned conditions. The impact pressure (P_{t_2}) was adjusted in the course of the testing to attempt to produce transitional flows. Although the impact pressures for Run 005 and 006 were initially intended to be somewhat higher, the highly turbulent character of the flow on Run 004 indicated that pressure reduction was required to obtain transitional flow over carbon phenolic models. The results for Run 006, in particular, were relatively unsatisfying, characterized by massive delamination due to in-depth charring. This problem may have been compounded by the lower than anticipated bulk enthalpy resulting from modifications to the arc heater to obtain improved cooling and reduced erosion of the front electrode. Details of the determination of the enthalpy and pressure calibrations are discussed in Section 3.5.

Details of the model failure on Run 004 and the curative steps taken are presented in the discussion of the test models (Section 2.4). Because of the uncertainty in the survival of the ATJ-S models with the silica phenolic holders, a solid ATJ-S model was fabricated by Southern Research Institute on an extremely short turn-around. This model was mounted on strut 3 of Run 007 to act
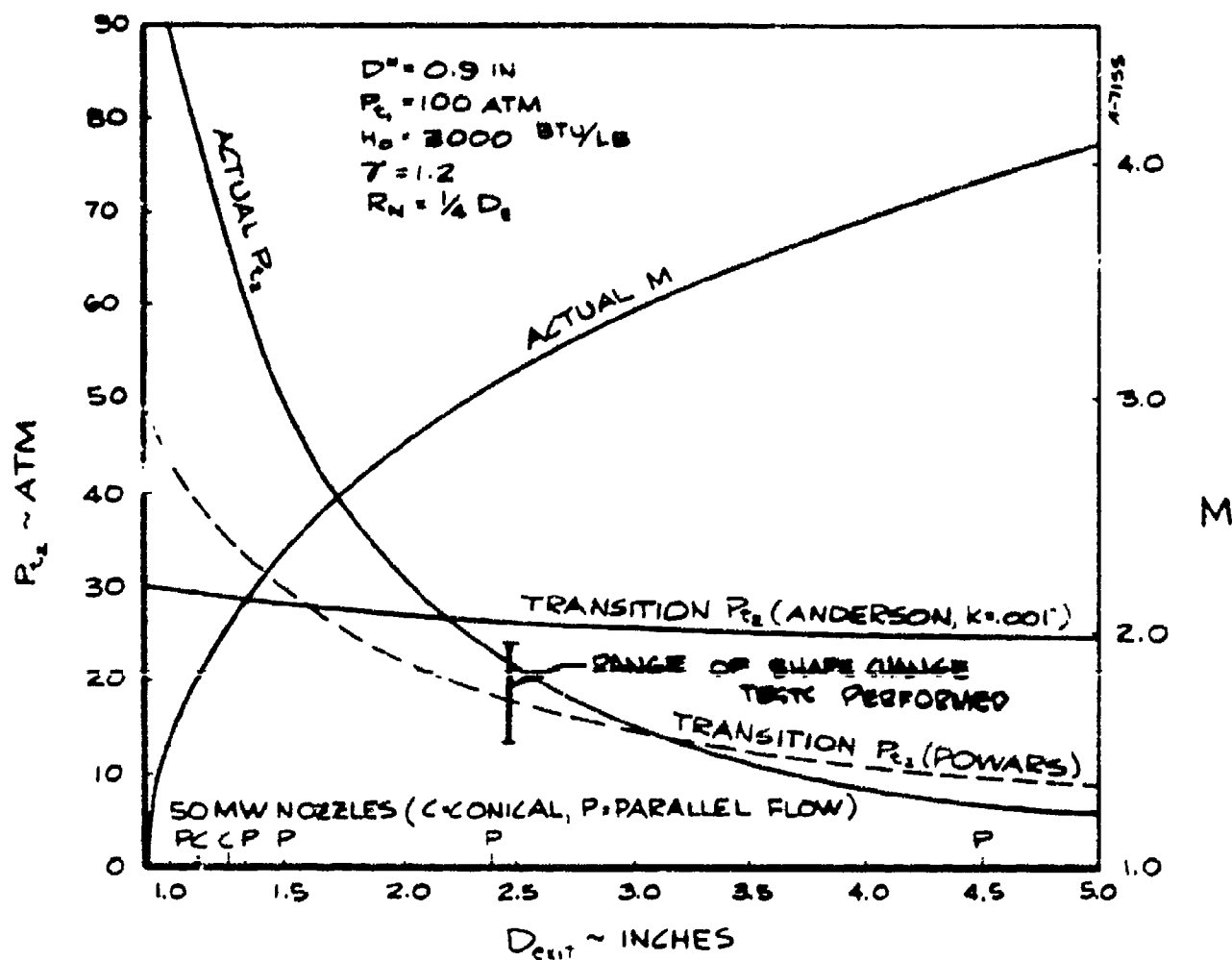
Figure 2-3. Mach Number/Impact Pressure Tradeoff

NOTE: Predicted values are from Reference 2 and are calculated for 3000 Btu/lbm enthalpy whereas actual results are approximately 2000 Btu/lbm due to changes in arc operation.

TABLE 2-1

TEST MATRIX AS ACTUALLY RUN

RTM-52-①	NOZZLE D*/D_e	P_c (psig)	P_t₂② (atm)	H_B (Btu/lbm)	est H_C③ (Btu/lbm)	MODEL OR STRUT NO.					PRIMARY PURPOSE
						1	2	3	4	5	
004	0.9"/2.39"	1674.	25.	1754.	2190.	ATJ-S, H_w=.625"/8" Brake at 9 sec	CP, R_N=.625"/8" 25 sec	δ_stag, R_N=.75" 25 in/sec	P_δ=.75", R_N=20 in/sec	δ_stag=.25", R_N=20 in/sec	Shape Change
005	0.9"/2.39"	1050.	16.	1924.	2100.	CP, R_N=.625"/8" 25 sec	CP, 30°/8°Biconic 25 sec	—			Shape Change
006	0.9"/2.39"	900.	14.	1853.	1960.	CP, R_N=.5"/cyl 15 sec	CP, R_N=.25"/cyl 10 sec	MOD-III, R_N=.75"/cyl 15 sec			Transition
007	0.9"/2.39"	1665.	25.	1878.	2350.	ATJ-S, R_N=.625"/8" 25 sec	ATJ-S, 30°/8°Biconic 25 sec	ATJ-S (Solid), R_N=.625"/8" 20 sec			Shape Change
008	0.9"/1.49"	1077.	35.	1923.	2100.	ATJ-S, R_N=.2"/cyl 4 sec	ATJ-S, R_N=.4"/cyl 4 sec	MOD-III, R_N=.2"/cyl 4 sec	P_δ=.5", R_N=25 in/sec		Transition
009	0.9"/1.49"	982.	32.	2014.	2160.	ATJ-S, Flat, R_cyl=.3" 4 sec	ATJ-S, R_N=.3"/cyl 4 sec	MOD-III, R_N=.3"/cyl 4 sec			Transition

NOTES:
① RTM-52-001 through 003 were check-out runs; no ablation data but provided calibration data.
② P_t₂/P_c derived from pressure calibration data.
③ All tests run at flat enthalpy profile for uniformity and maximum R_B; K_C/H_B estimated from calibration data.

as a backup in case of further model failures. All models for Run 007 survived the exposure, making this model basically redundant; thus elaborate data reduction was not performed for this model.

2.3 TEST EQUIPMENT

The pertinent test equipment is described in this section. This includes the arc heater unit and associated instrumentation. The ablative models are described in Section 2.4.

The tests were conducted in the RENT (reentry nosetip) test leg of the Air Force Flight Dynamics Laboratory 50 MW arc heater facility. The $D^* = 0.90$ inch, $D_e = 2.393$ inch contoured nozzle was used for Runs 001 through 007 and the $D^* = 0.90$ inch, $D_e = 1.493$ inch contoured nozzle was used for Runs 008 and 009. Details regarding the facility hardware, data acquisition systems, operating procedures, etc., are contained in Reference 9 and will not be discussed further.

The facility servo-controlled axial drive system was utilized for all tests. The model stagnation points were maintained 0.15 inch downstream of the nozzle exit for Runs 008 and 009. The model standoff distance for all other runs was 0.10 inch. Slight position variations occurred for the initial few milliseconds of the test since the system is turned off while the model surface temperature is too low to activate the positioner sensors. The model axial position was recorded to enable computation of the ablation rate. This is compared to recession rates obtained from movie data in Section 3.2.

Photographic coverage was provided by four cameras as sketched in Figure 2-4. The lens sizes, camera speeds, film type and exposure were as indicated in the pretest plan. The north and south Photosonics cameras provided high speed, high resolution shape change and recession information. Because of the visibility of the tungsten reference marks in the north camera and difficulty in reading timing marks on the south camera, film from the north camera was used consistently for the data reduction. The cameras mounted directly above provided backup recession data from the top-view Locam and documentary coverage from the overview Locam. An overhead TV monitor provided real time coverage of the model performance.

Three Thermogage optical pyrometers were used for this test series. The positions and basic specifications (including wavelength sensitivity and target size) of these instruments are indicated in Figure 2-4. All instruments "looked" at the model in a direction normal to the model centerline with the line-of-sight positioned 0.1 inches back from the stagnation point (assuming the model

SOUTH PHOTOSONICS CAMERA
(RECESSION & SHAPE CHANGE)

TOP LOCAM - RECESSION
TOP OVERVIEW - DOCUMENTARY
TV - MONITOR

NORTH PHOTOSONICS CAMERA
(PRIMARY CAMERA FOR RECESSION AND SHAPE CHANGE)

A-GIER

NOZZLE EXIT
(JET COMING OUT OF PAGE)

MODELS

STING SYSTEM

12"

12"

THERMOGAGE PYROMETERS
SILICON SENSORS; .9 μ
<1/32" SPOT DIA

① ③ } ALIGNED .1" BACK OF STAGNATION POINT

② ALIGNED .625" BACK OF STAG
FOR RUNS 004-007, .25" BACK
FOR RUNS 008 & 009

Figure 2-4. Schematic of Test Equipment Configuration

position was maintained as specified) for two pyrometers and .625 inches (for Runs 004 through 007) or .25 inches (for Runs 008 and 009) from the stagnation point for the third. The pyrometer data was recorded on the high speed digital data system and the oscillograph, as per usual practice. Detailed pyrometer data reduction is presented in Section 3.3.

Heat flux calorimeter models were used in this test series as indicated in the test matrix, Table 2-1. All heat flux models utilized null point calorimeter slugs and were swept across the jet as described in Reference 10. The instruments used were of two types:

- $\dot{q}_{STAG}$ was an Aerotherm calorimeter model with a 0.25 R_N and one null point slug located at the stagnation point. This model was used in all runs.

- $\dot{q}_\theta$ was an Aerotherm calorimeter model with a 0.75 R_N and six null point slugs mounted at various locations along the streamwise length. This model was utilized in Runs 002 through 005 only.

The reduced heat flux data is presented in Section 3.5.

All runs included the exposure of pressure models as indicated in Table 2-1. A pressure model with a 0.75" R_N and multiple ports (at the stagnation point, 20°, 30° and 40°) was swept through the stream for Runs 001 through 007. A model with a 0.5" R_N and four pressure ports was used on Runs 008 and 009. Reduced pressure data is also presented in Section 3.5.
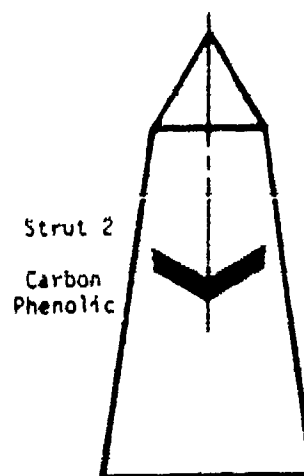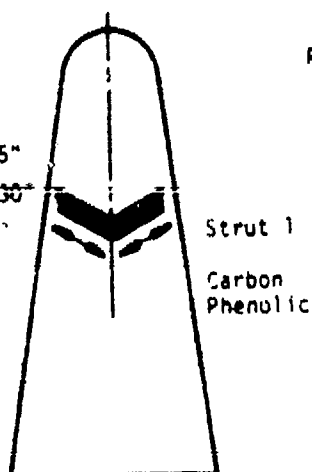
2.4 MODELS

This test series included exposure of 17 ablative models. Included in the testing were inverted dixie cup carbon phenolic, ATJ-S graphite, and Mod IIIa carbon/carbon models falling generally into two classes. The large models (four ATJ-S and three carbon phenolic) were for the shape change testing. The smaller and more varied geometry models (two carbon phenolic, four ATJ-S and four Mod III) were to observe material and nose radius effects on transition. Figure 2-5 sketches the configurations tested in the shape change portion while Figure 2-6 shows model configurations used for the transition testing. All models except the first one performed in a satisfactory manner allowing collection of the high quality shape change data desired. Two model design problems arose which did impact the experimental operation. These were (1) the catastrophic shape change model failure, and (2) breakage of the silica phenolic holders for the transition models.

The graphite shape change models utilized a composite design to limit heating of the steel strut during the long exposure times. If an integral design of ATJ-S were used for these models, the high thermal conductivity of the

RTN 52-004

Strut 1

ATJ-S
Composite

Strut 2
Carbon Phenolic
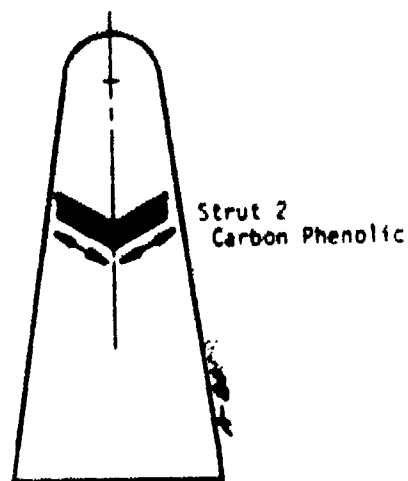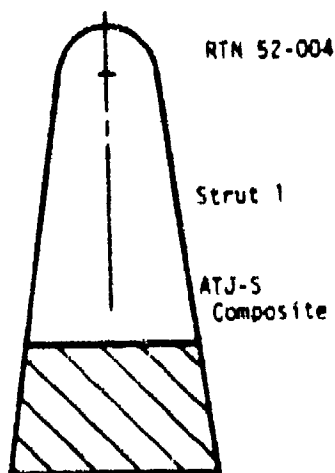
PTN 52-005

Shape Change Models
R_N(Sphere Cones) = 0.625"
Cone Half Angle (Biconics) = 30°
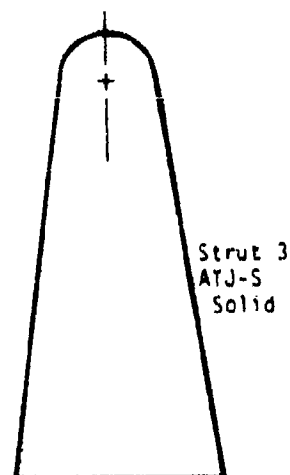Frustrum Half Angle = 8°
Model Length = 6"

Strut 1
Carbon
Phenolic

Strut 2
Carbon
Phenolic

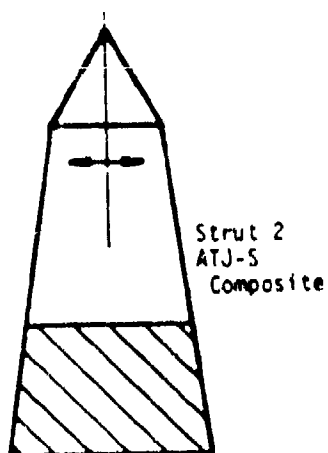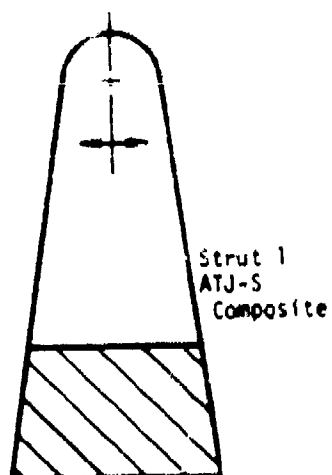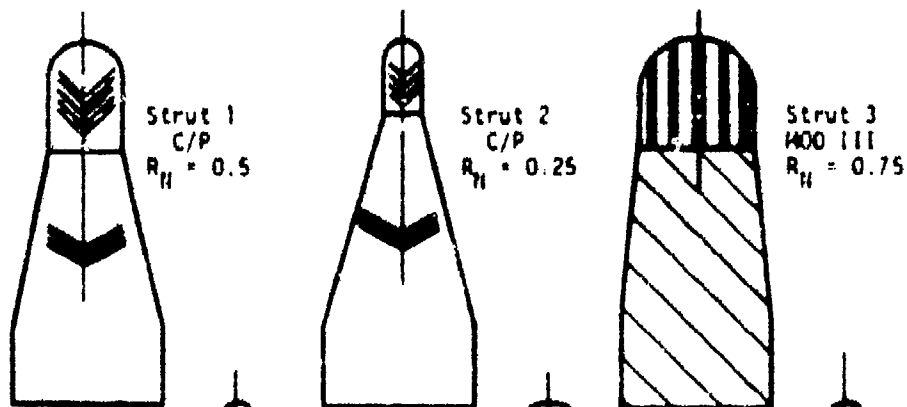RTN 52-007

Strut 1
ATJ-S
Composite

Strut 2
ATJ-S
Composite

Strut 3
ATJ-S
Solid

Figure 2-5. Shape Change Models

RTM 52-006

Strut 1
C/P
$R_N = 0.5$

Strut 2
C/P
$R_N = 0.25$

Strut 3
MOD III
$R_N = 0.75$

RTM 52-008

Strut 1
ATJ-S
$R_N = 0.2$

Strut 2
ATJ-S
$R_N = 0.4$

Strut 3
MOD III
$R_N = 0.2$

RTM 52-009

Strut 1
ATJ-S
$R_N = 0.3$

Strut 2
ATJ-S
$R_N = 0.3$

Strut 3
MOD III
$R_N = 0.3$

RTM 52-010

Strut 3
MOD III
45° Biconic
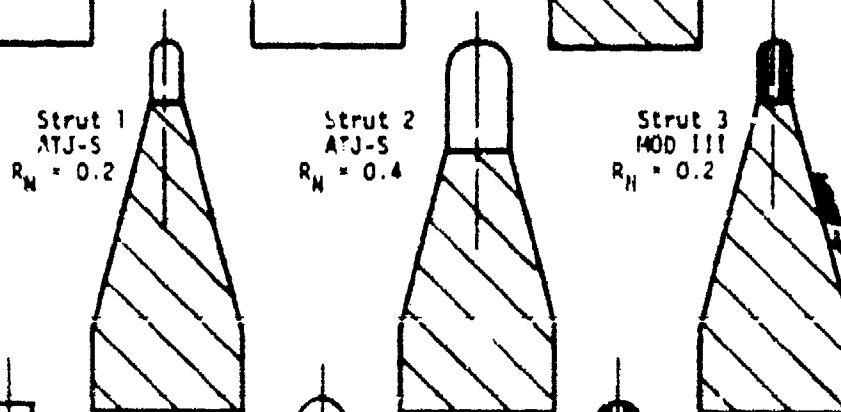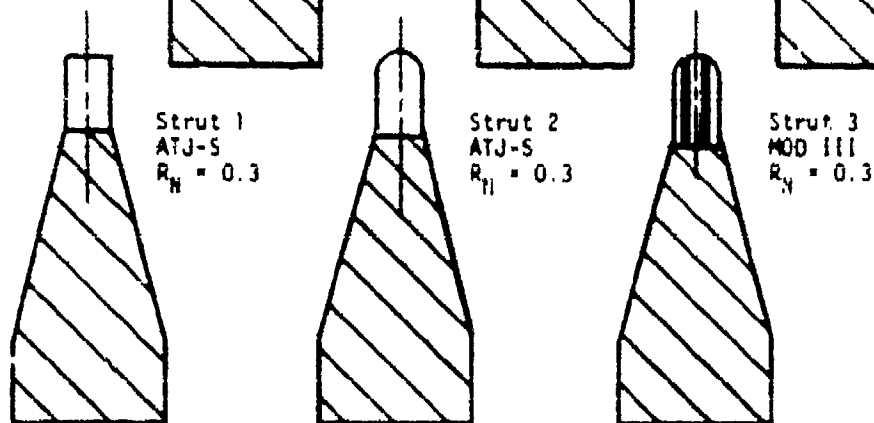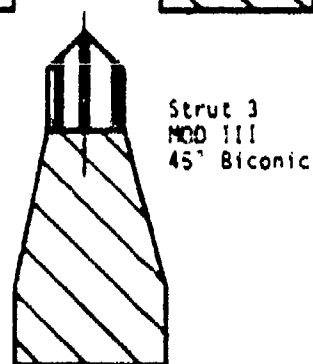
Figure 2-6. Transition Models

graphite would result in potentially critical temperatures at the steel mounting interface. To prevent this an insert of relatively low conductivity silica phenolic was used as shown in Figure 2-7a. The graphite nosetip was bonded to the insert with a commercial epoxy in addition to being retained by a 1-D carbon/carbon cross-pin. The first model of this design failed approximately nine seconds into its exposure. The failure occurred in the skirt region, indicative of an incompatibility between the graphite and the insert. After examination of the model, it was speculated that the failure was due to volatilization of the epoxy bonding without sufficient venting to allow the gas to escape. The resulting pressure rise then fractured the graphite, causing failure. To prevent this gas buildup, the remaining models of this design were drilled as shown in Figure 2-7b to provide pressure relief of the vaporized adhesive. In addition, a solid model was fabricated at Southern Research for incorporation as a backup. For this model, a slightly reduced exposure time (20 seconds) was specified to lessen the possibility of damage. Both of the remaining ATJ-S models and the backup model were tested on Run 007, which was a rather spectacular run because of the 70 second total exposure time for the three ablative models. All three models survived although the first model cracked severely in the skirt region on exit. Tentative confirmation of the bond volatization hypothesis was provided by films of the run, which showed dark spots around the holes apparently attributable to jets of outgas products.

The second problem, breaking of the transition model holder, while not serious, was irritating since the models would bounce around the facility possibly sustaining additional damage. This breakage was caused by the severe side loading to which models are exposed as they are removed from the high pressure jet, in conjunction with the fact that the silica phenolic model holders are weakened due to charring while in the jet. This is a common problem in 50 MW testing when silica phenolic or carbon phenolic model holders are used. Only the Mod III model on Run 9 survived although only the first model on Run 8 was not recovered. The one model where it was impossible to discern post-exposure chipping from ablation was the flat face model which appeared to behave anomalously.

The use of tungsten pins to provide reference marks for the recession measurements was highly successful. The pins are especially valuable as opposed to holes because they quickly heat up and provide a bright spot even at early times. Where feasible, it appears desirable to have the pins as far forward as possible to appear in the field of view for all cameras.
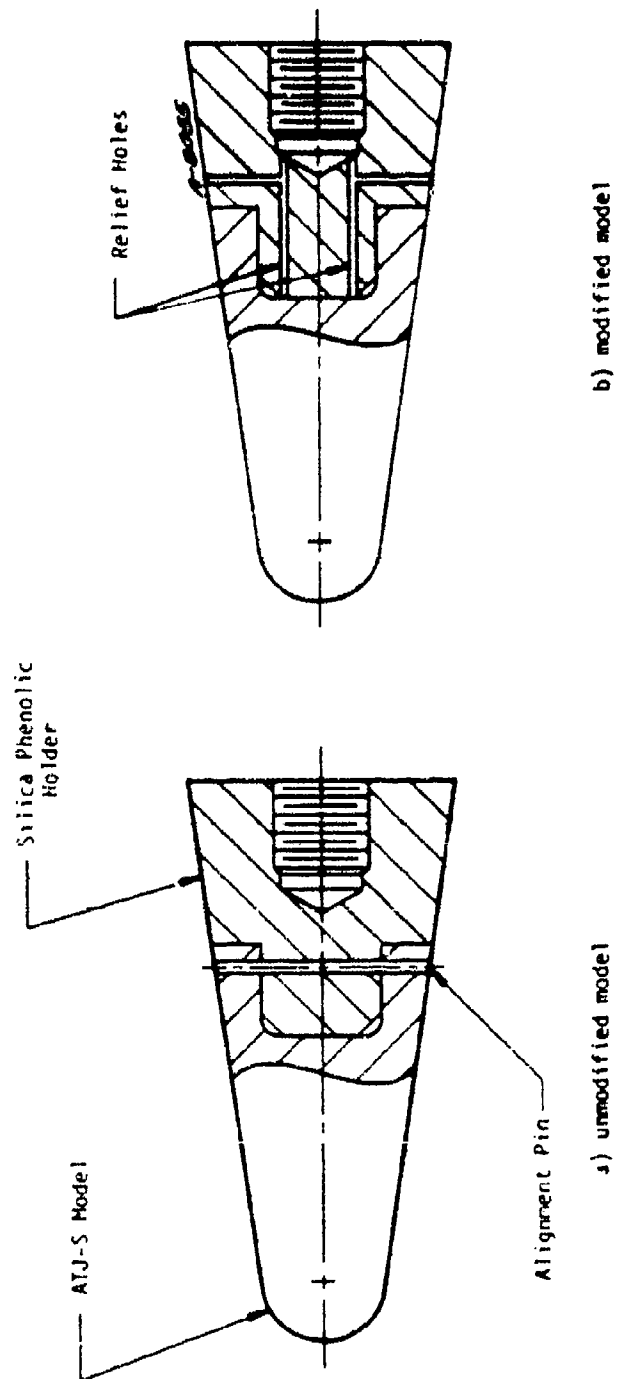
Relief Holes

Silica Phenolic
Holder

ATJ-S Model

Alignment Pin

a) unmodified model

b) modified model

Figure 2-7. Volatilization Relief

2-15

SECTION 3

RESULTS

The data obtained in the course of this test series are summarized in this section. The primary data source for both the shape change and transition tests is the high speed photography. Both the model shape change profiles (Section 3.1) and stagnation point recession histories (Section 3.2) are deduced from this film data. Since the model is advanced axially to compensate for ablation (as discussed in Section 3.2), the model axial position read-out also provides data relative to the model recession history. The reduced pyrometer data is presented in Section 3.3, although surface temperature measurement was not a primary objective of this test series. Post-test photographs of the models are included as Section 3.4. Reduced pressure and heat flux calibration data is presented in Section 3.5.

3.1 SHAPE CHANGE DATA

Ablative model shape change histories as traced from the movie film data and techniques utilized in reducing this data are presented in this section. As discussed in Section 2.2, the first three runs were used to correct a model axial positioner malfunction and provided only pressure and heat flux data. The shape change histories for Runs 004 through 009 are shown in Figures 3-1 through 3-6.

The model shape change histories were obtained through the following procedure: The movie film was projected onto a screen (using a L & W Photo Optical Data Analyzer Model 224-A) and the initial model shape was traced on a sheet of paper so as to accommodate the entire model. For the initial profile, care was taken to establish a reference point on the advancing model or strut which would be visible throughout the entire test for successive shape change profiles. The reference mark was generally the tungsten pin mounted on the model as discussed in Section 2.4. Time increments were selected to provide from 10 to 15 profiles over the test duration.

The film data was synchronized in time to the high speed digital data which was recorded, and later printed, at millisecond intervals. This same time scale is exposed in a coded form on the edge of the movie film corresponding to each frame. The "zero time" was taken as the time when the model first
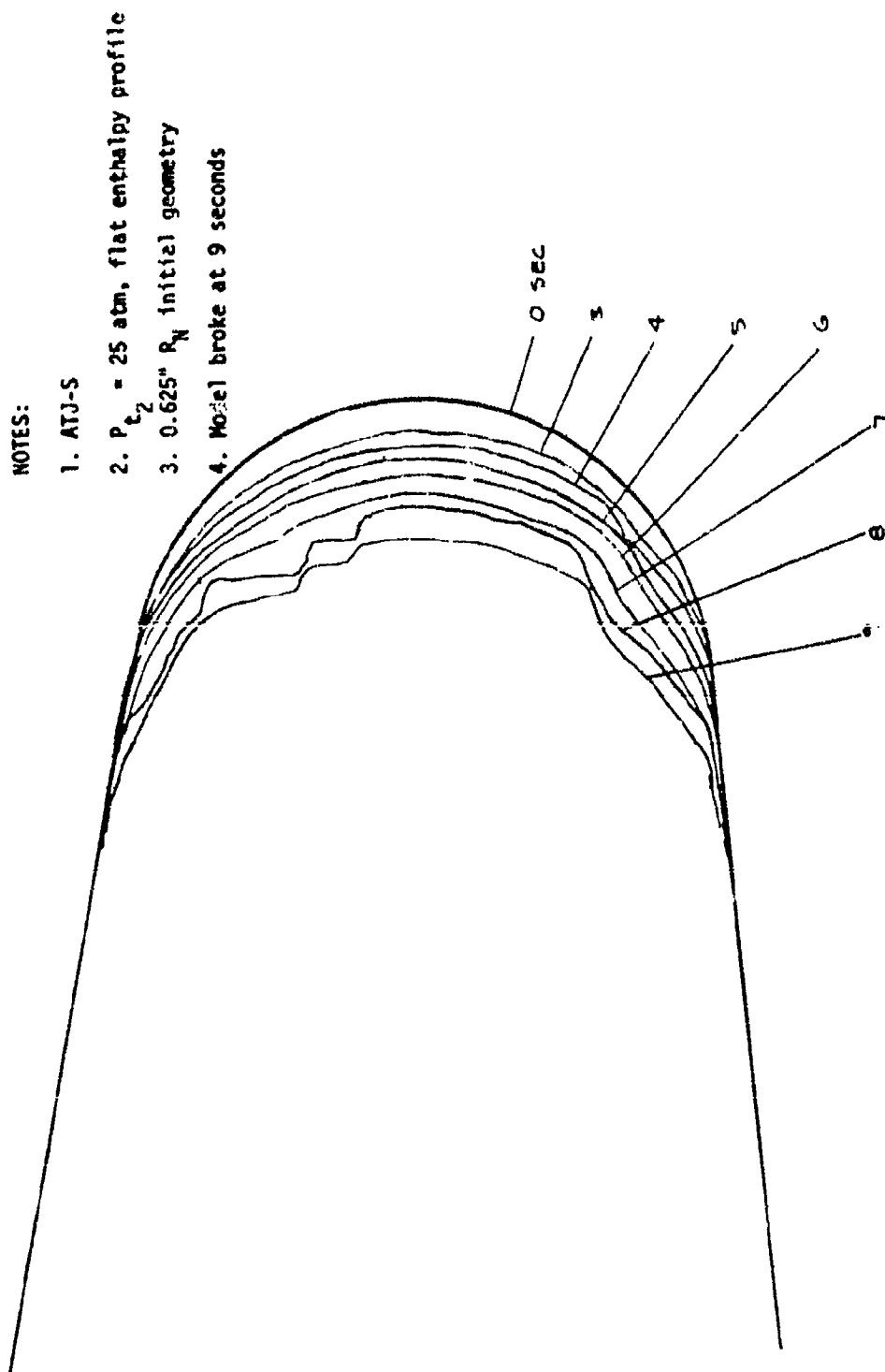
3-1

NOTES:

1. ATJ-S
2. P_{e_2} = 25 atm, flat enthalpy profile
3. 0.625" R_N initial geometry
4. Model broke at 9 seconds

0 SEC
3
4
5
6
7
8

Figure 3-1a. Ablated Shape Contours, RTN 004, Strut 1

3-2

NOTES:

1. Carbon phenolic

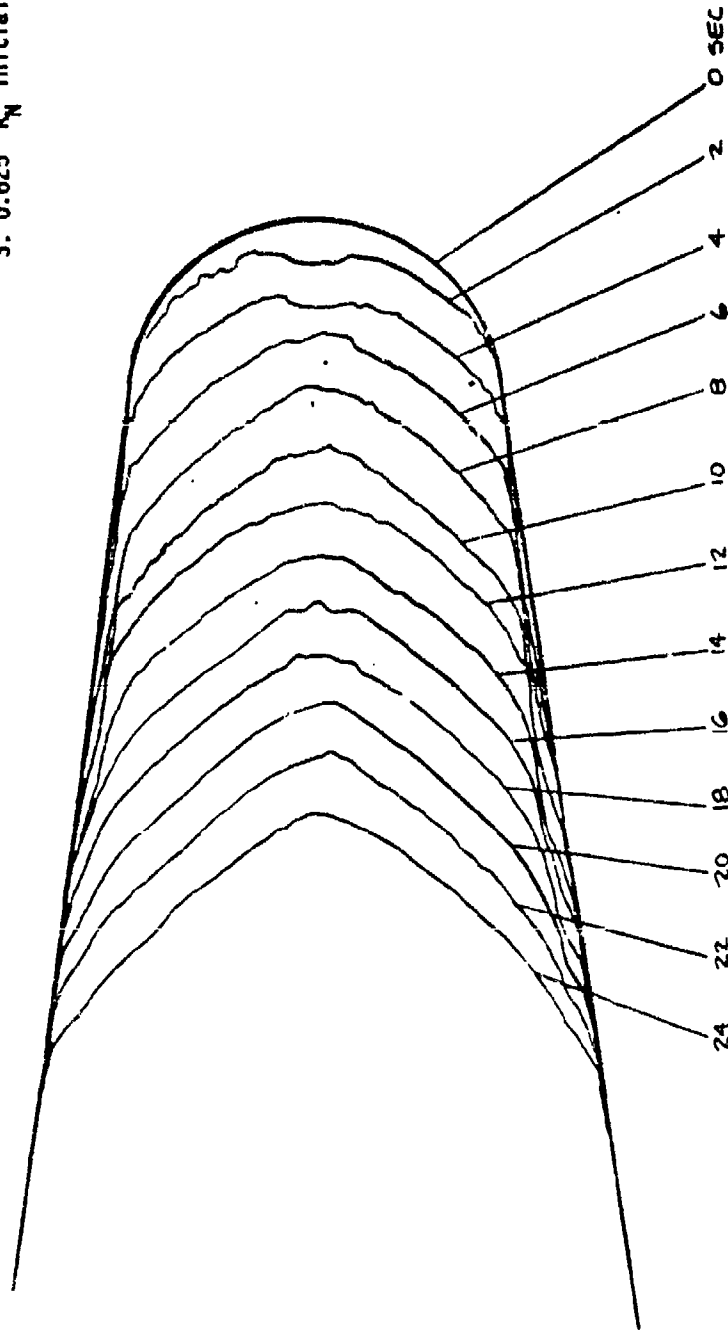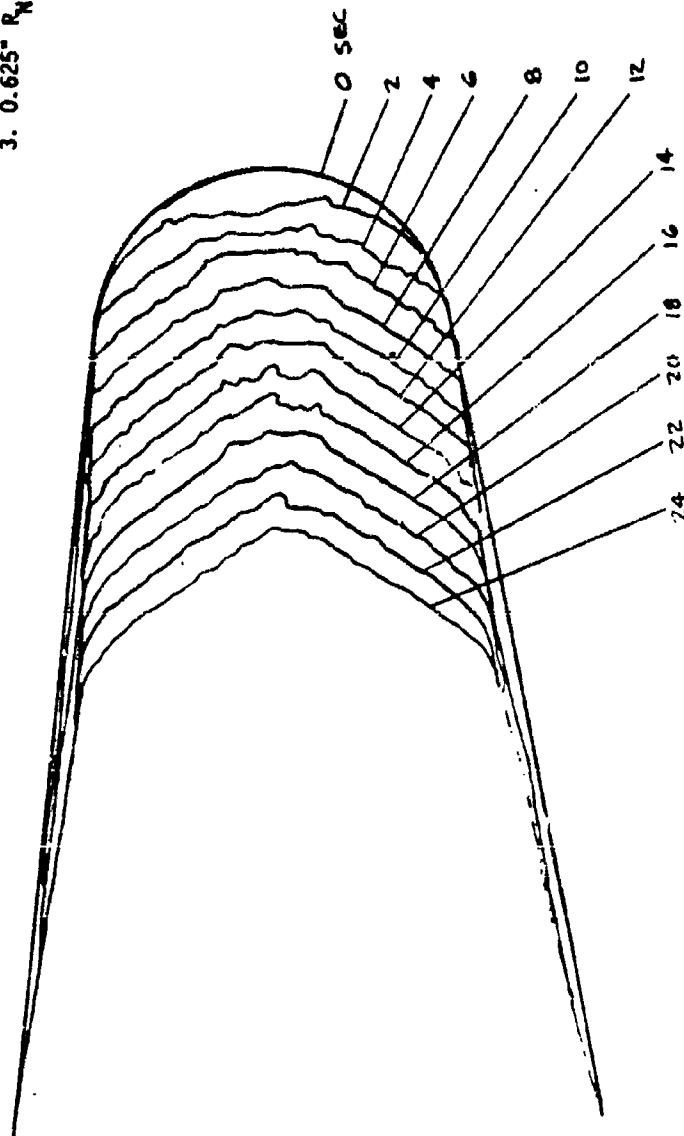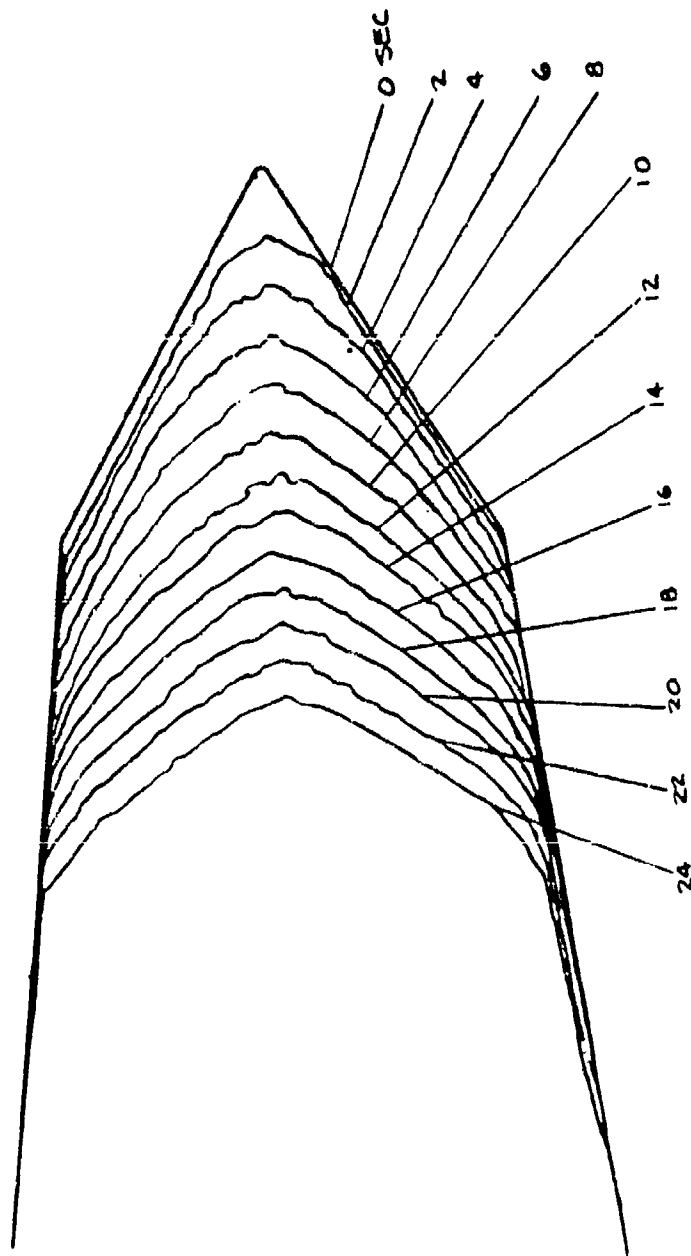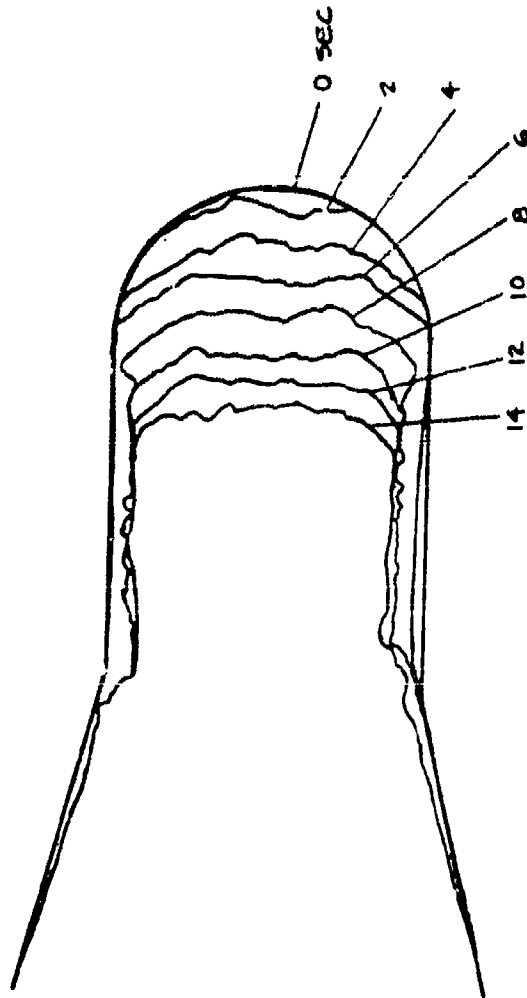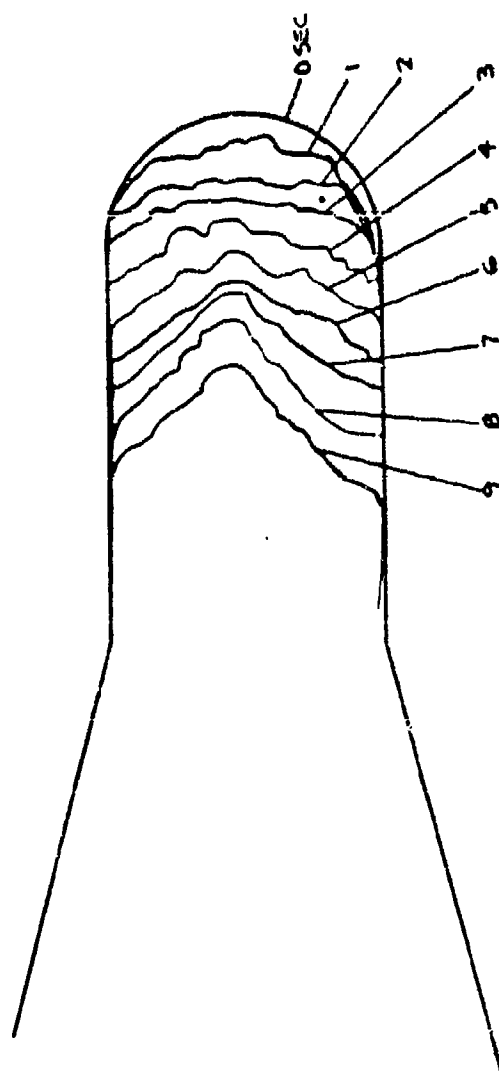2. P_{t_2} = 25 atm, flat enthalpy profile

3. 0.625" R_N initial geometry

Figure 3-1b. Ablated Shape Contours, RTM 004, Strut 2

NOTES:

1. Carbon phenolic

2. P_{t_2} = 16 atm, flat enthalpy profile

3. 0.625" R_N initial geometry

0 sec
2
4
6
8
10
12
14
16
18
20
22
24

Figure 3-2a. Ablated Shape Contours., RTN 005, Strut 1

NOTES:

1. Carbon phenolic

2. $P_{t_2} = 16$ atm, flat enthalpy profile
3. $30°/8°$ initial geometry

O SEC
2
4
6
8
10
12
14
16
18
20
22
24

Figure 3-2b. Ablated Shape Contours, RTN 005, Strut 2

NOTES:

1. Carbon phenolic

2. P_{t_2} = 14 atm, flat enthalpy profile

3. 0.5" R_N initial geometry

4. Model experienced massive delamination

Figure 3-3a. Ablated Shape Contours, RTN 006, Strut 1

NOTES:

1. Carbon phenolic

2. P_{t_2} = 14 atm, flat enthalpy profile

3. 0.25" R_N initial geometry
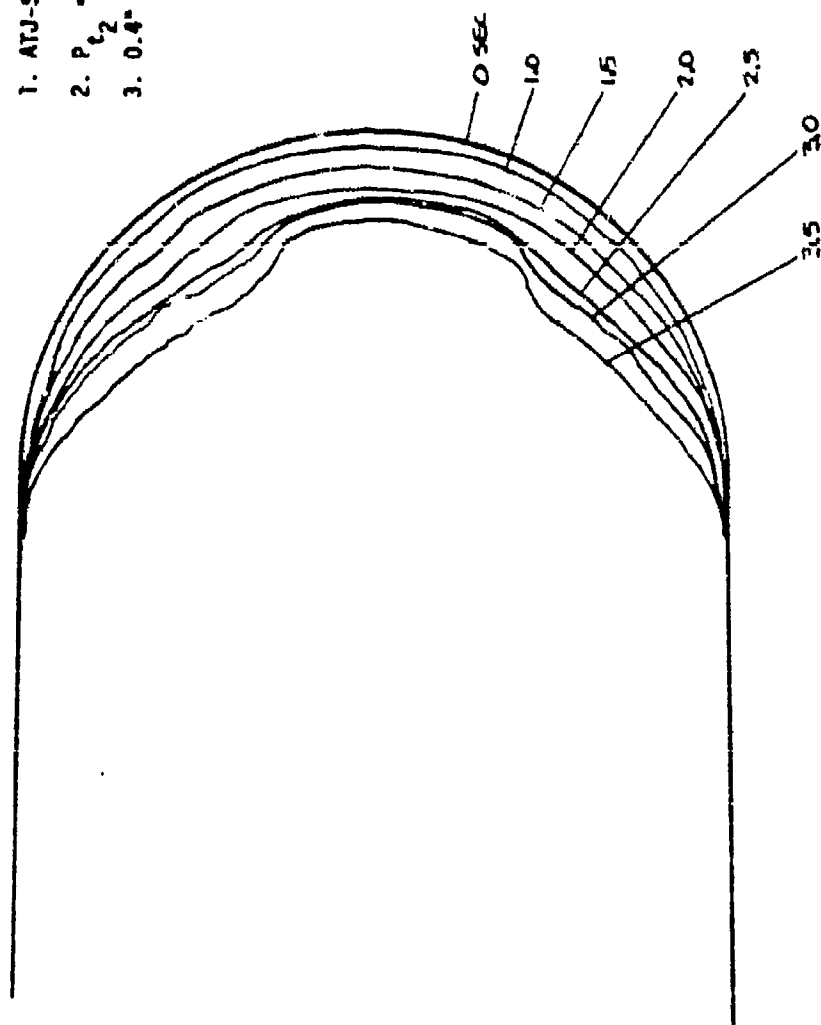

Figure 3-3b. Ablated Shape Contours, RTN 006, Strut 2

NOTES:

1. Mod III carbon/carbon

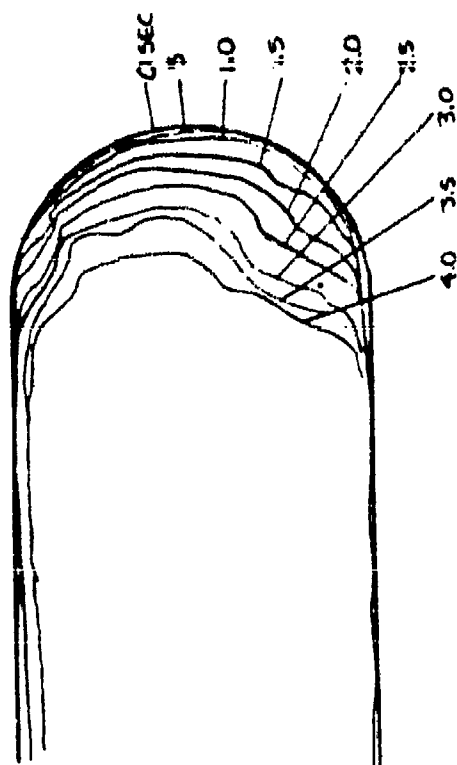2. P_{t_2} = 14 atm, flat enthalpy profile

3. 0.75" R_N initial geometry

0 sec
4
6
8
10
12
14
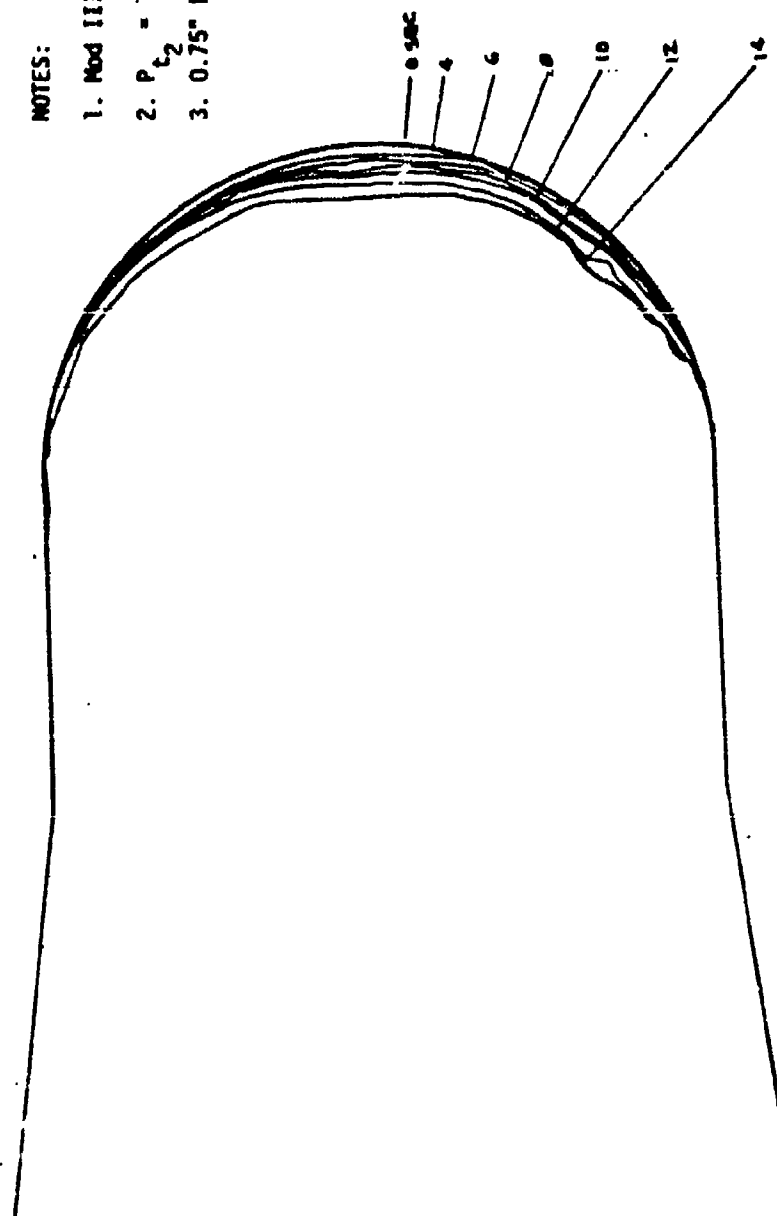
Figure 3-3c. Ablated Shape Contours, RTN 006, Strut 3

NOTES:

1. ATJ-S

2. P_{t_2} = 25 atm, flat enthalpy profile

3. 0.625" R_N initial geometry
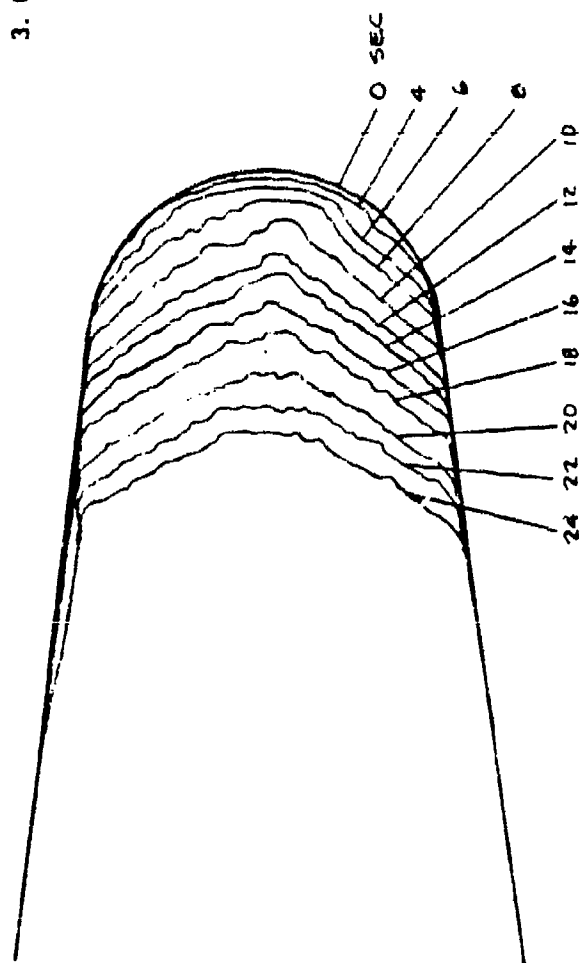
Figure 3-4a. Ablated Shape Contours, RTN 007, Strut 1

NOTES:

1. A⁻J-S

2. P_{t_2} = 25 atm, flat enthalpy profile

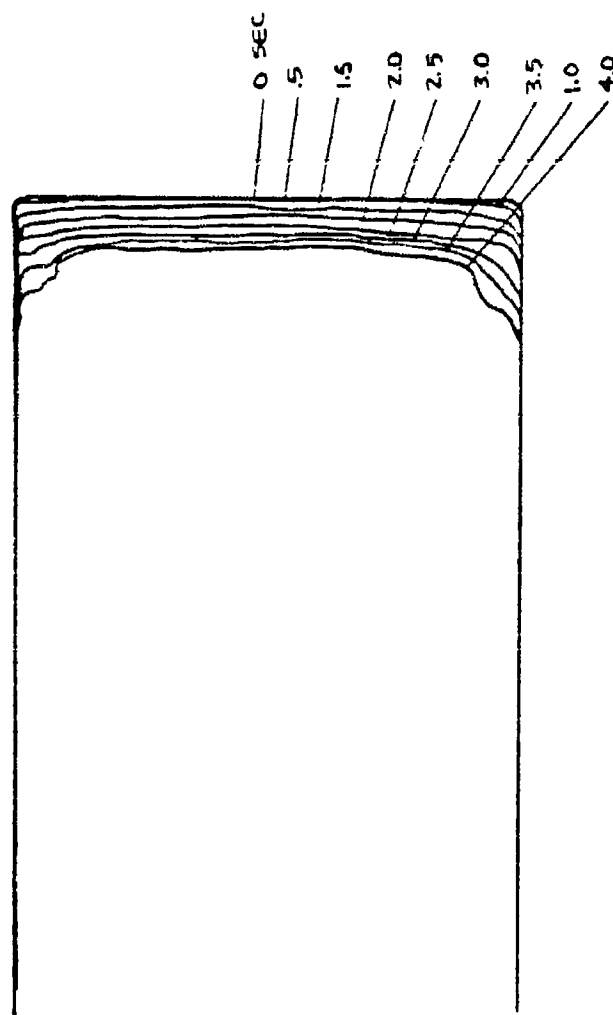3. 30°/8° initial geometry

O SEC
2
4
6
8
10
12
14
16
18
20
22
24
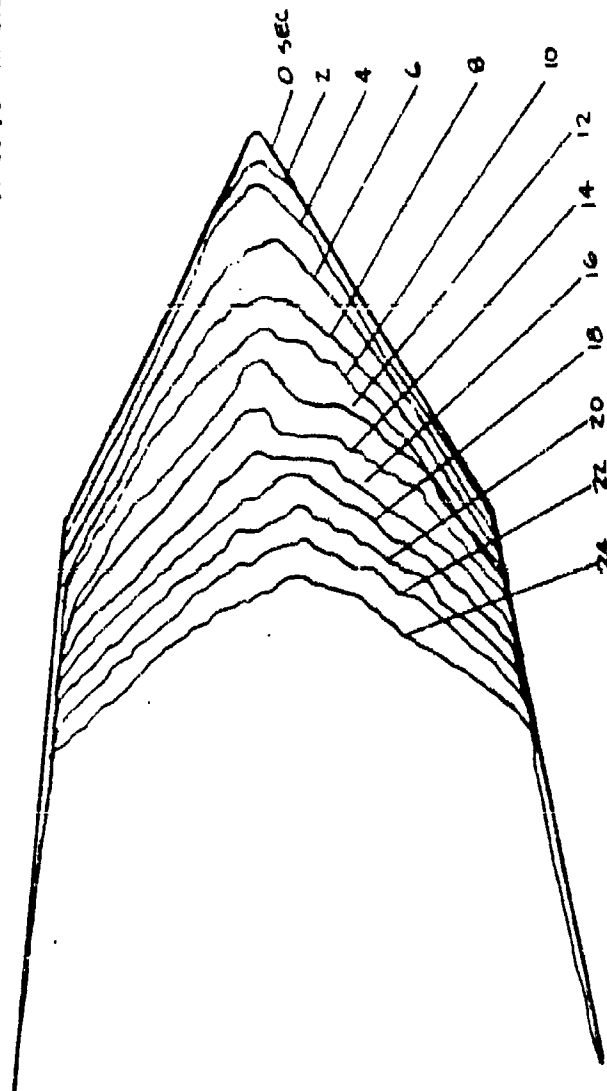
Figure 3-4b. Ablated Shape Contours, RTN 007, Strut 2

NOTES:

1. ATJ-S

2. P_{t_2} = 35 atm, flat enthalpy profile

3. 0.4" R_N initial geometry
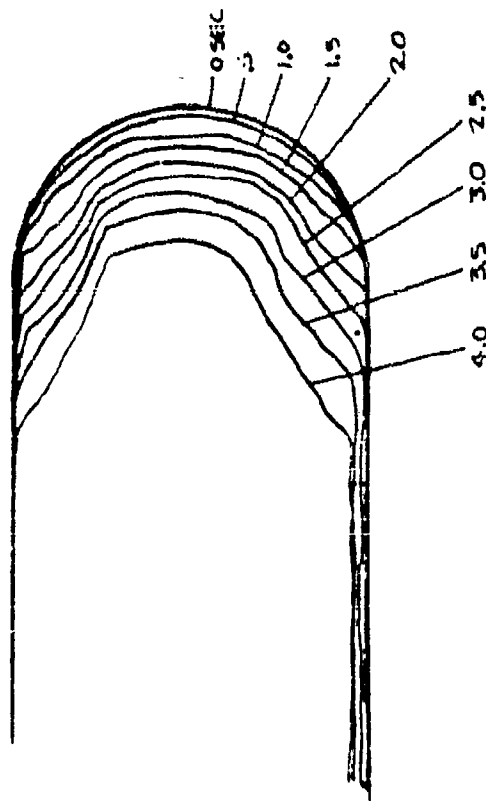
Figure 3-5a. Ablated Shape Contours, RIM 008, Strut 1

NOTES:

1. ATJ-S

2. P_{t_2} = 35 atm, flat enthalpy profile
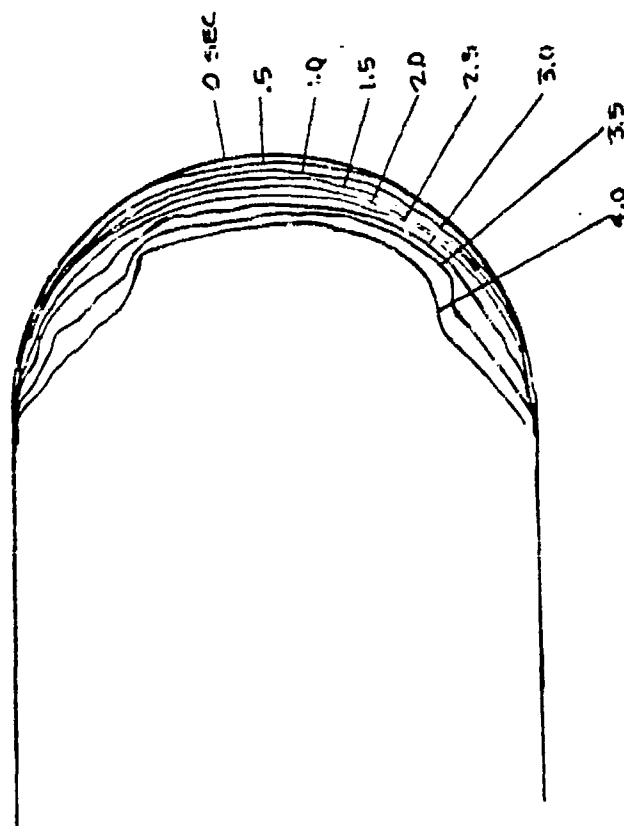
3. 0.4" R_N initial geometry

0 SEC
1.0
1.5
2.0
2.5
3.0
3.5

Figure 3-5b. Ablated Shape Contours, RTN 008, Strut 2

NOTES:

1. Mod III carbon/carbon

2. P_{t_2} = 35 atm, flat enthalpy profile

3. 0.2" R_N initial geometry

Figure 3-5c. Ablated Shape Contours, R'N 008, Strut 3

NOTES:

1. ATJ-S

2. P_{t_2} = 32 atm, flat enthalpy profile
3. Flat, R_{cyl} = 0.3" initial geometry

O SEC
.5
1.5
2.0
2.5
3.0
3.5
1.0
4.0

Figure 3-6a. Ablated Shape Contours, FTN 009, Strut 1

NOTES:

1. ATJ-S

2. P_{t_2} = 32 atm, flat enthalpy profile

3. 0.3" R_N initial geometry

0 SEC
.5
1.0
1.5
2.0
2.5
3.0
3.5
4.0

Figure 3-6b. Ablated Shape Contours, RTN 009, Strut 2

3-15

NOTES:

1. Mo; III carbon/carbon

2. P_{t_2} = 32 atm, flat enthalpy profile

3. 0.3" R_N initial geometry

0 SEC
.5
1.0
1.5
2.0
2.5
3.0
3.5
4.0
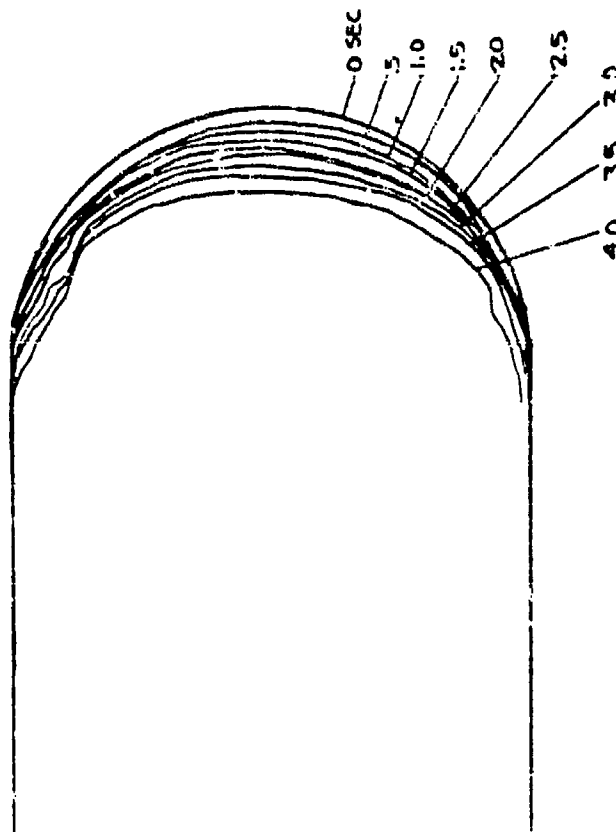
Figure 3-6c.   Ablated Shape Contours, RTN 009, Strut 3

crossed the jet centerline on the way into the jet (the models slightly over-shoot the jet centerline for a few milliseconds due to the elasticity of the model sting system as the carriage is locked into place).

In general, film from the north Photosonics camera was used for these contours. The split filter used with this camera usually resulted in the clearest indication of both the model contours and the reference marks.

Figures 3-1 through 3-6 are a reasonable reconstruction of the model shape change histories; however, they are not precise as the images were not exceptionally distinct for many films. In addition to the uncertainties associated with the translation of the film images to the shape contours, there are certainly optical and photographic distortions. The shape change contours were not corrected for any of these uncertainties since the extent of each is not known. These figures do not show microsurface roughness but are indicative of macrosurface roughness.

No shape change results are presented for Run 007, strut 3 since the backup model mentioned in Section 2.4 did not have any reference marks and thus obtaining definitive shape change contours would be difficult.

3.2   SURFACE RECESSION DATA

Stagnation point surface recession histories were deduced from available data for all ablative models on Runs 004 through 009, and these data are plotted in Figures 3-7 through 3-12. Methods used to reduce the film data and model positioner data are discussed in this section.

3.2.1 Recession from Movie Film Data

This data was obtained from the shape change contours shown in Figures 3-1 through 3-6 by measuring the distance between successive contours. By measuring reference distances on the shape change plots and comparing them to the known actual geometry, a scale factor may be determined to convert recession measurements to actual inches. The recession measurements were synchronized with time by recording the "time" on the film tracing and subtracting the "zero time" discussed in Section 3.1. The stagnation point recession data are shown in Figures 3-7 through 3-12.

3.2.2 Recession from Model Positioner Data

The RENT facility utilizes a servo-controlled strut drive system to maintain the tip of the ablating model at the same position relative to the nozzle exit throughout the run. The positioner data output through the run is stored
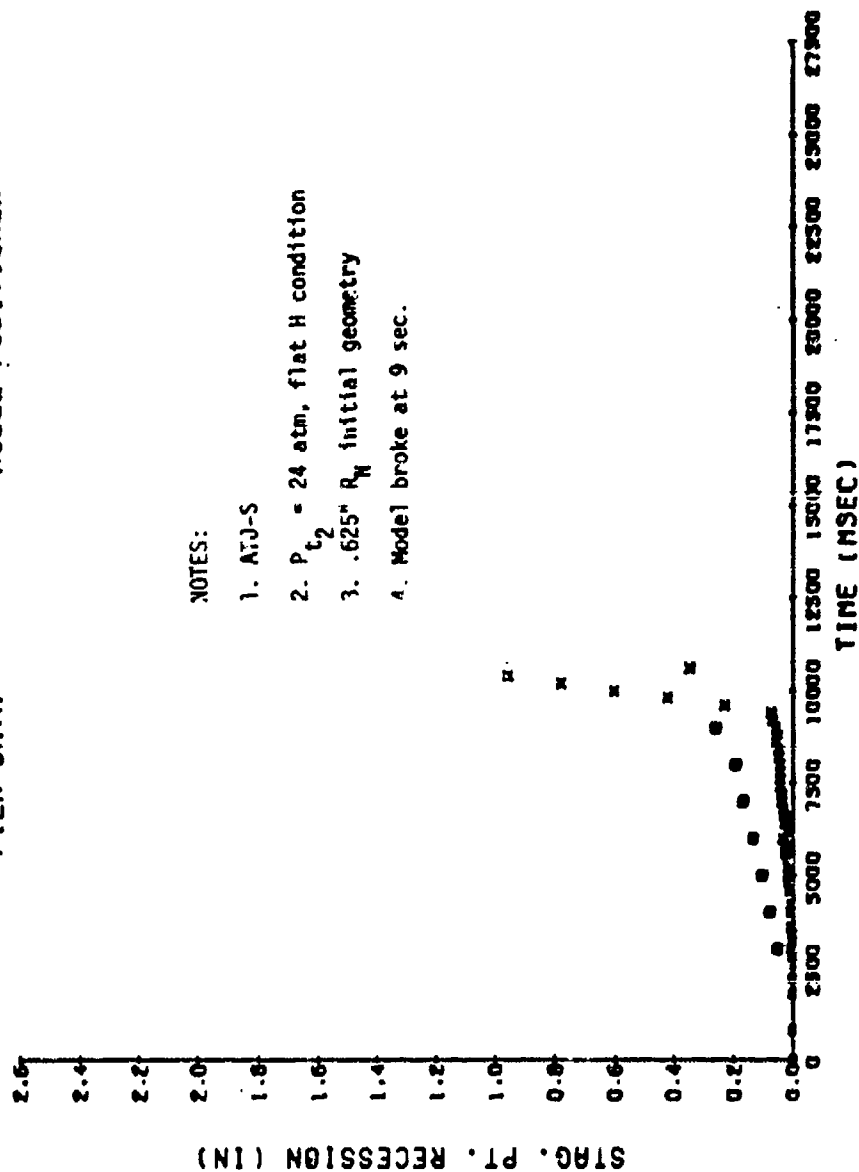
3-17

Figure 3-7a. Reduced Model Surface Recession Data

RECESSION DATA, 50MW RTN-004, STING 2

• FILM DATA
× MODEL POSITIONER

NOTES:

1. Carbon phenolic
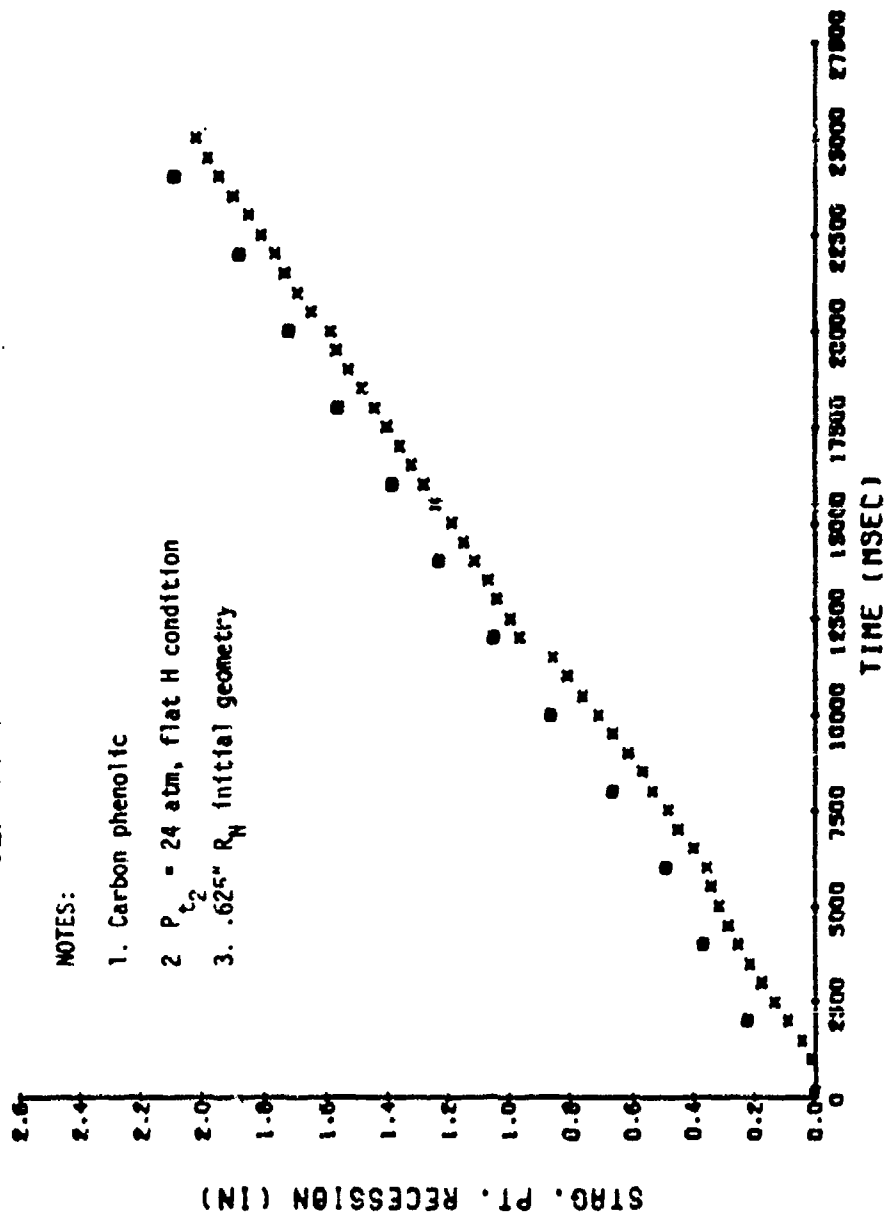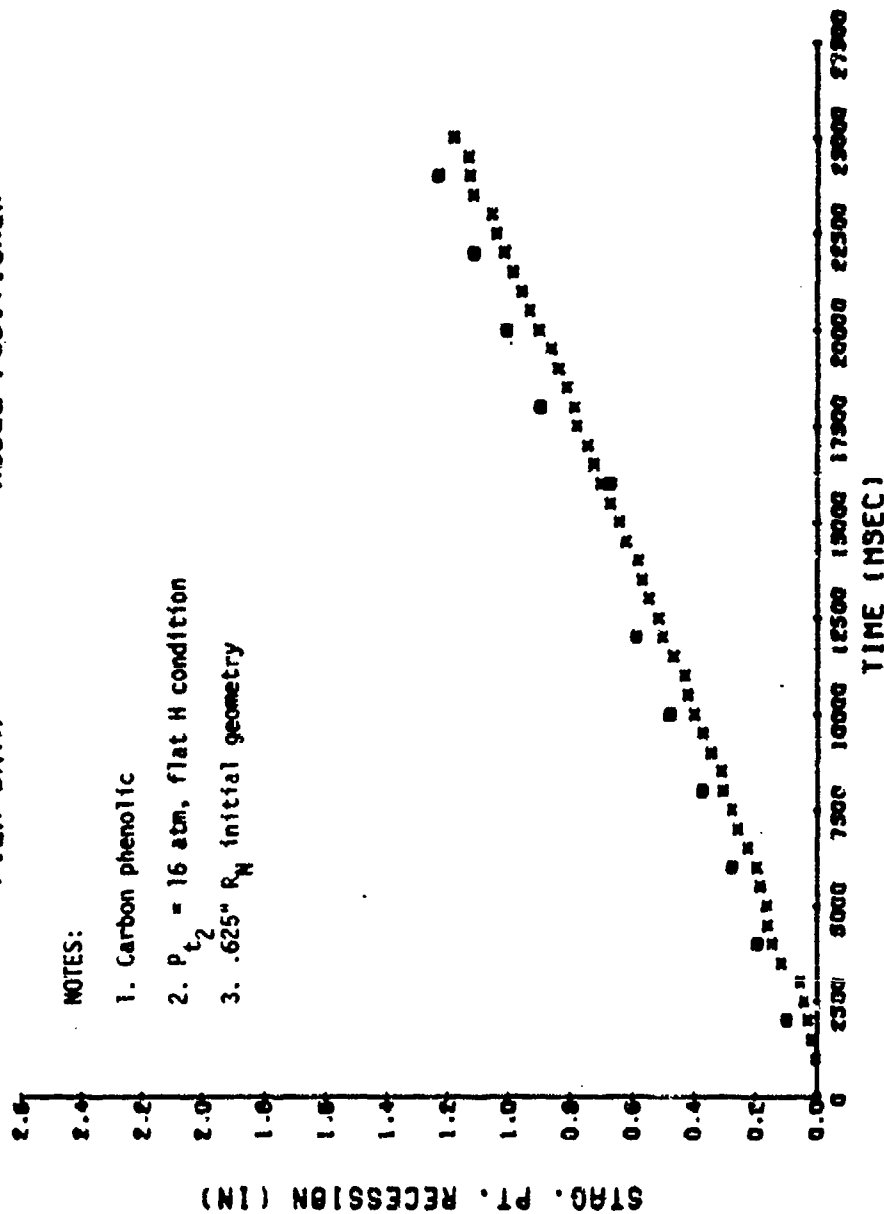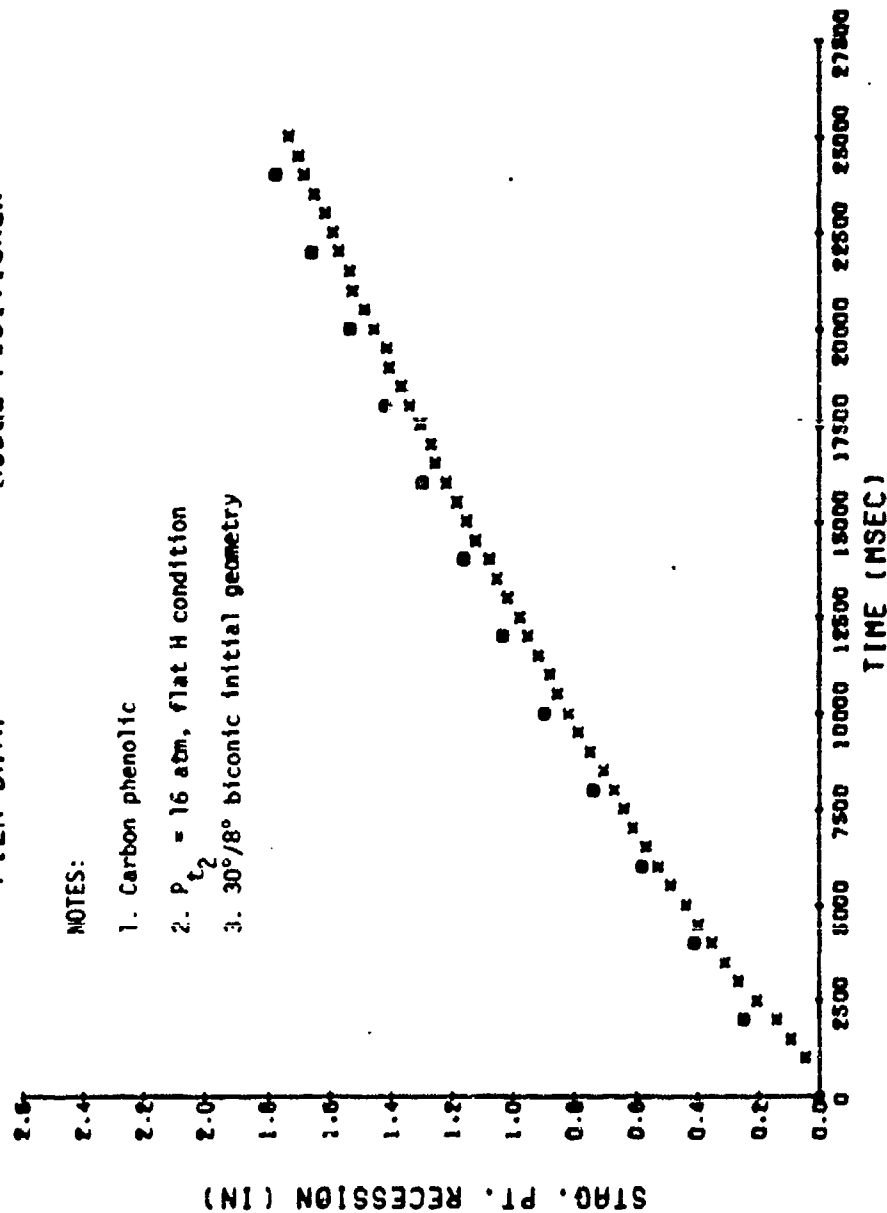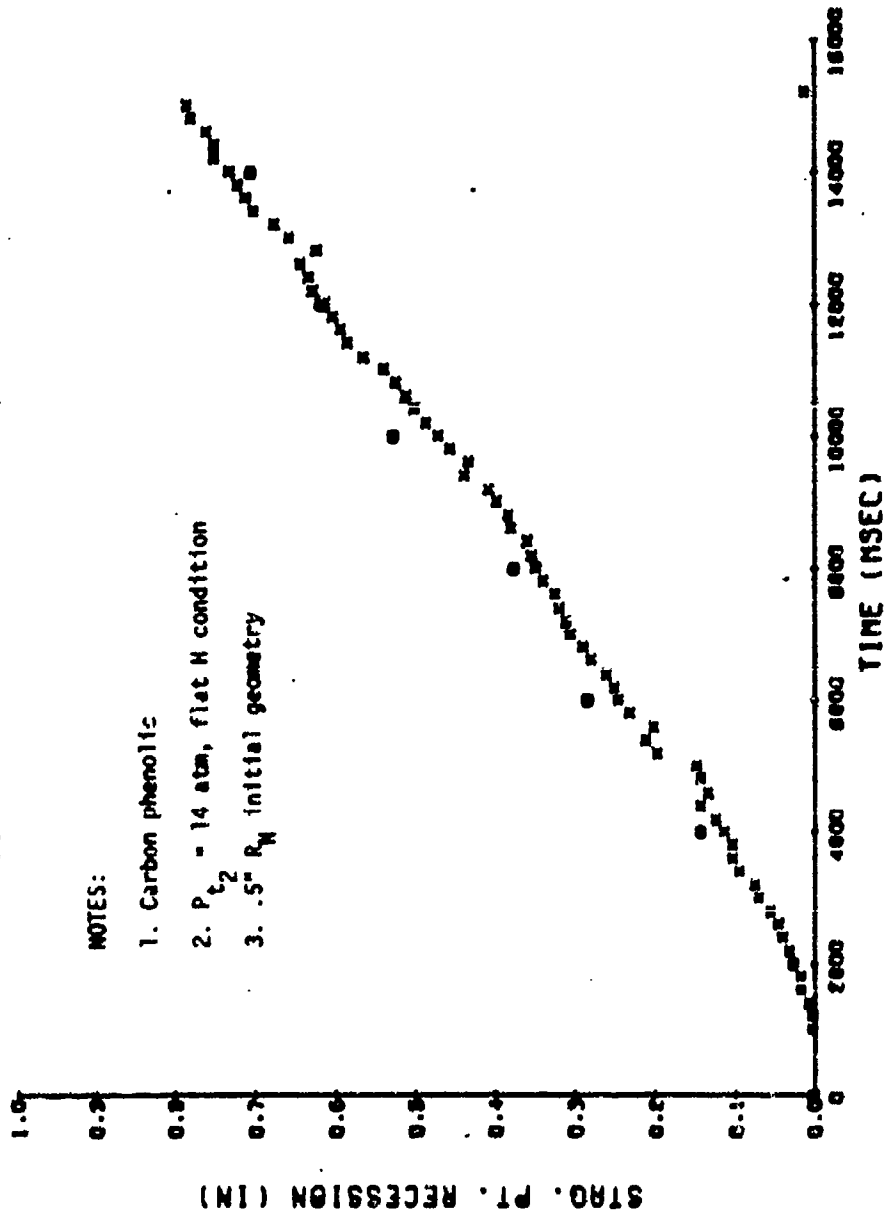
2. P_{t_2} = 24 atm, flat H condition

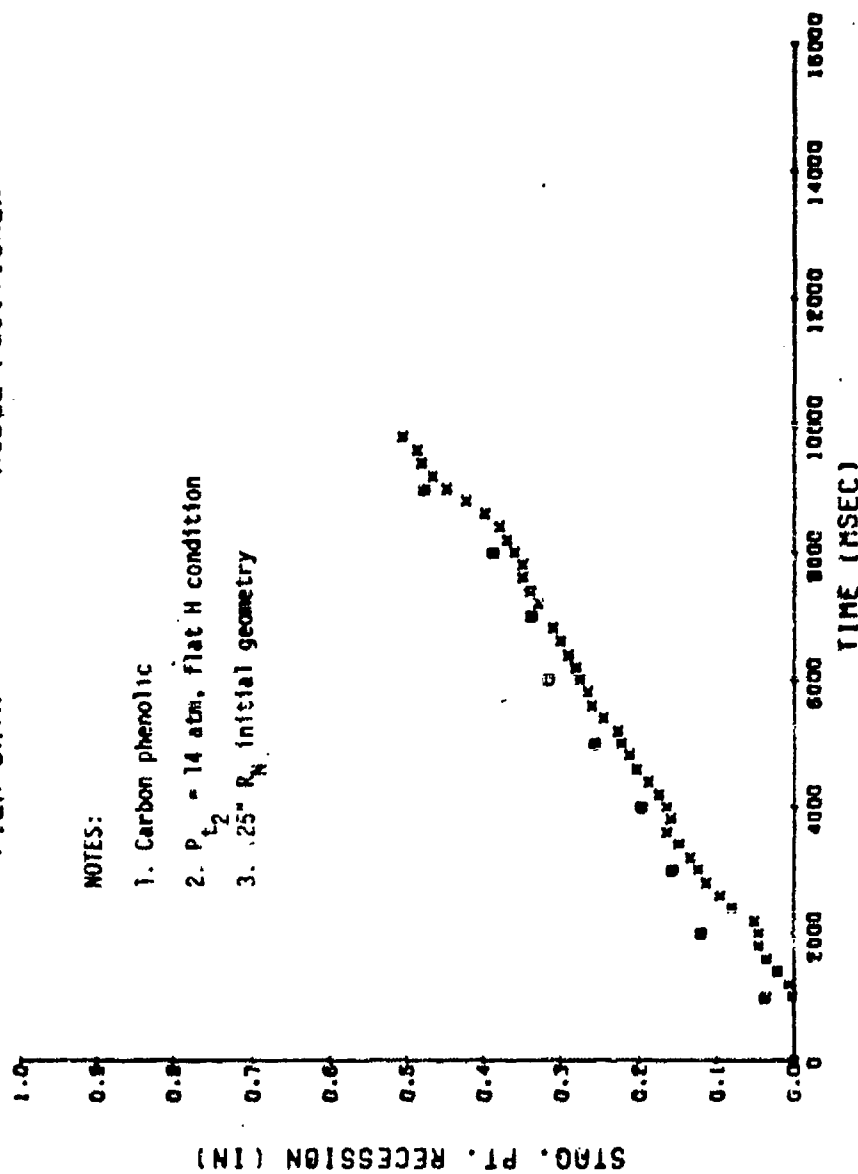3. .625" R_N initial geometry

Figure 3-7b. Reduced Model Surface Recession Data

RECESSION DATA. 50MW RTN-005. STING 1
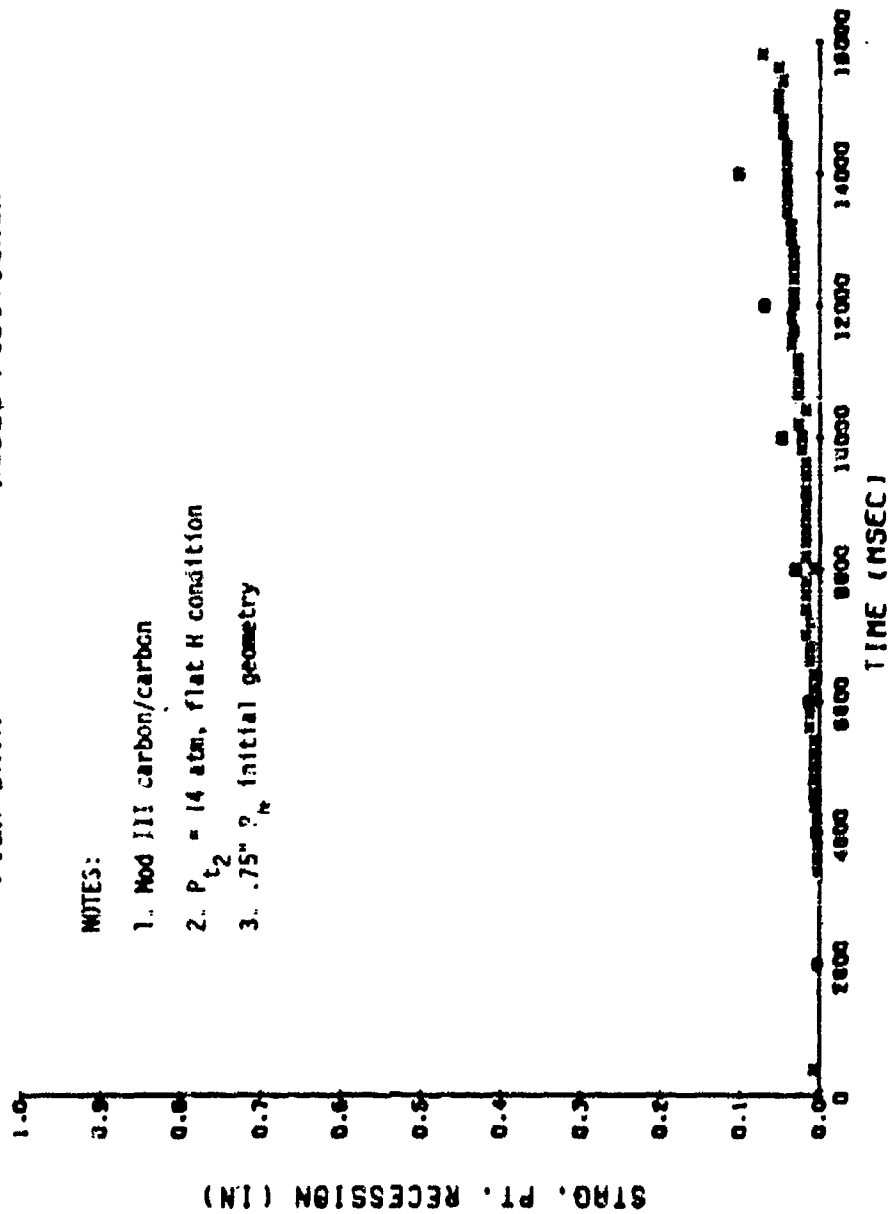
*FILM DATA
*MODEL POSITIONER

NOTES:

1. Carbon phenolic
2. P_{t_2} = 16 atm, flat H condition
3. .625" R_N initial geometry

STAG. PT. RECESSION (IN)

TIME (MSEC)

Figure 3-8a. Reduced Model Surface Recession Data

RECESSION DATA. 50MW RTN-005. STING 2
● FILM DATA   × MODEL POSITIONER

NOTES:

1. Carbon phenolic

2. P_{t_2} = 16 atm, flat H condition

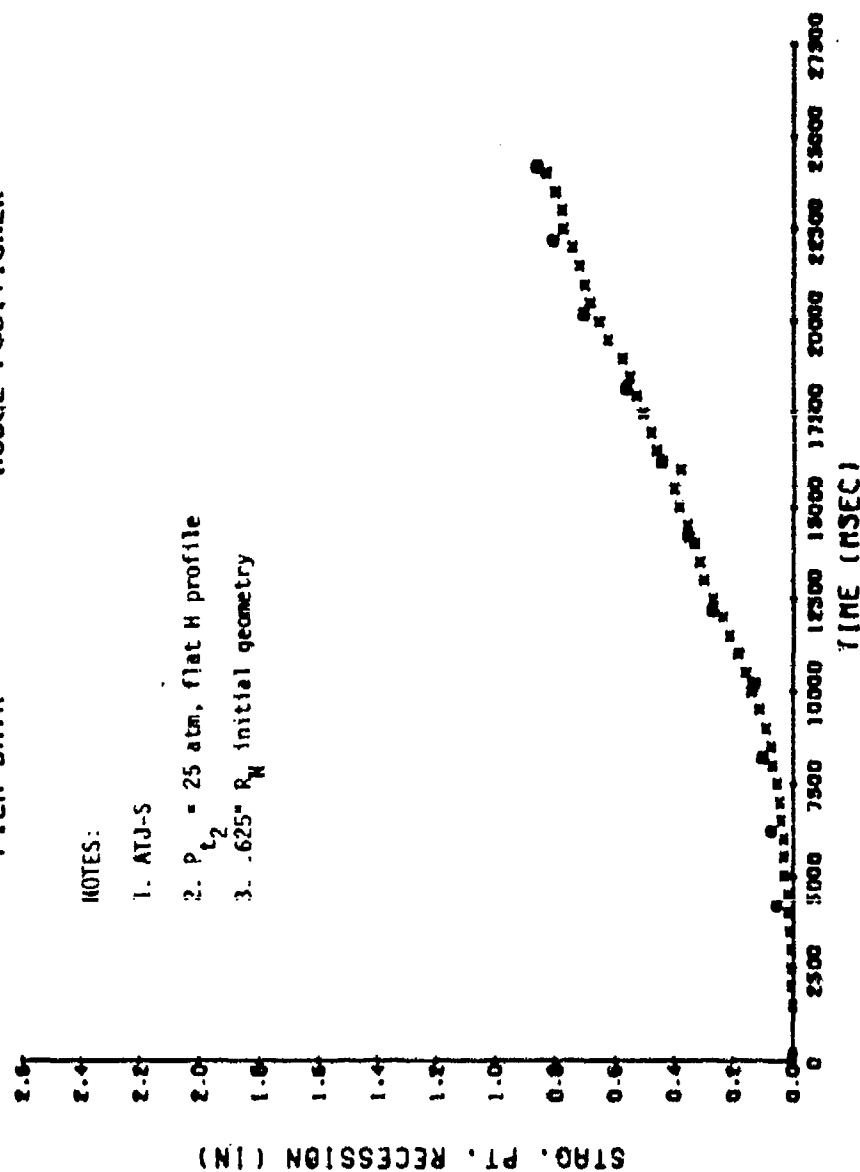3. 30°/8° biconic initial geometry

STAG. PT. RECESSION (IN)

TIME (MSEC)

Figure 3-8b.   Reduced Model Surface Recession Data

RECESSION DATA. 50MW RTN-006. STING 1

■FILM DATA   ■MODEL. POSITIONER

NOTES:

1. Carbon phenolic

2. P_{t_2} = 14 atm, flat H condition

3. .5" R_N initial geometry

STAG. PT. RECESSION (IN)

TIME (MSEC)

Figure 3-9a. Reduced Model Surface Recession Data

RECESSION DATA. 50MW RTN-006. STING 2
*FILM DATA
*MODEL POSITIONER

NOTES:
1. Carbon phenolic
2. $P_{t_2} = 14$ atm, flat H condition
3. .25" R_N initial geometry

STAG. PT. RECESSION (IN)

TIME (MSEC)

Figure 3-9b. Reduced Model Surface Recession Data

RECESSION DATA. SOMW RTN-006. STING 3
=FILM DATA   =MODEL POSITIONER

NOTES:

1. Mod III carbon/carbon

2. P_{t_2} = 14 atm, flat H condition

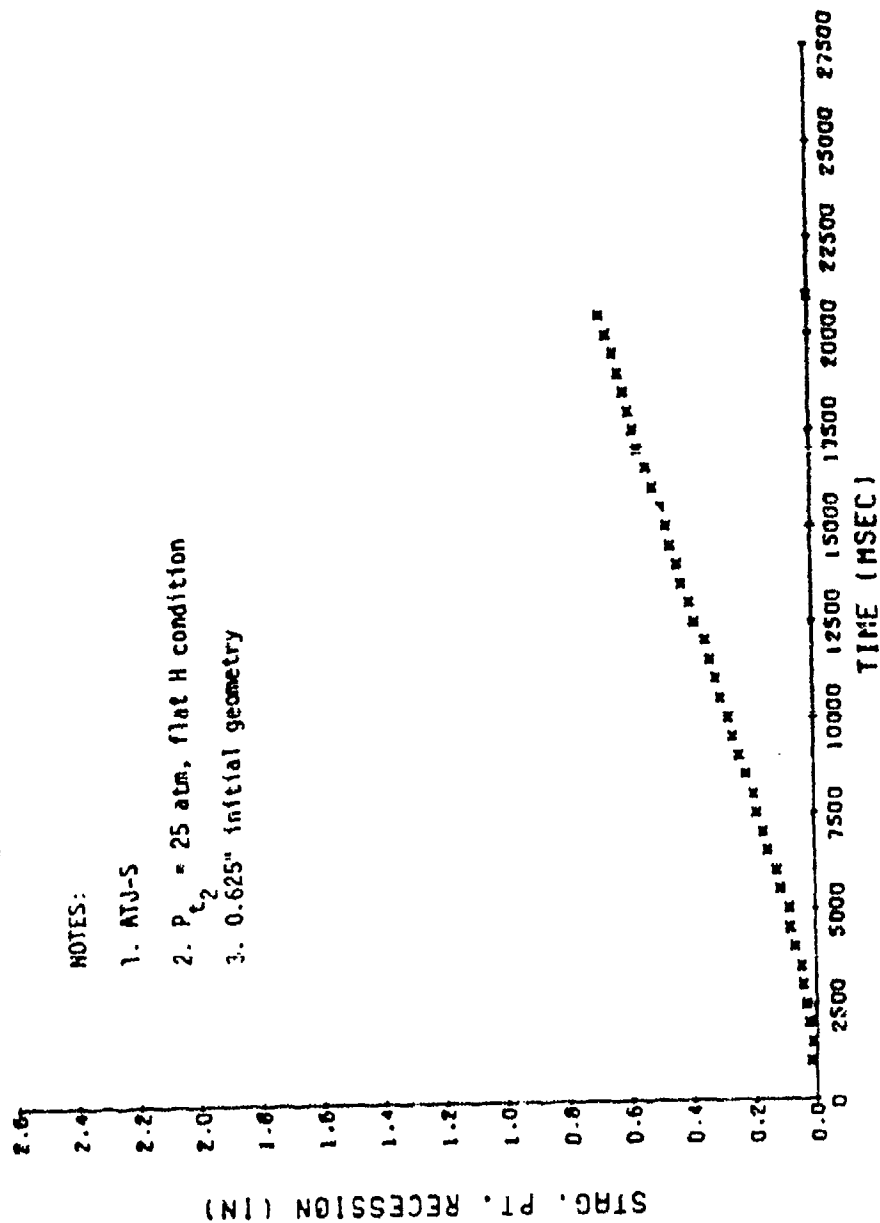3. .75" P_{t_2} initial geometry

STAG. PT. RECESSION (IN)

TIME (MSEC)

Figure 3-9c. Reduced Model Surface Recession Data

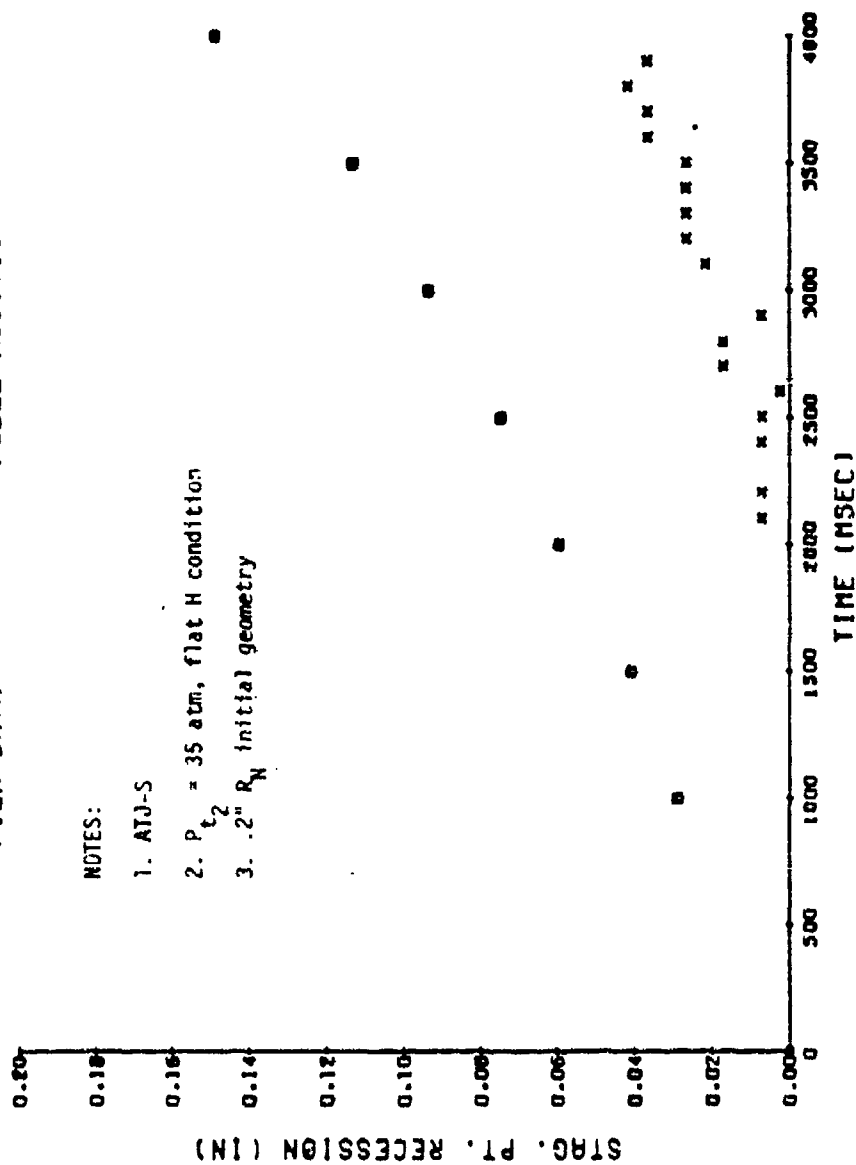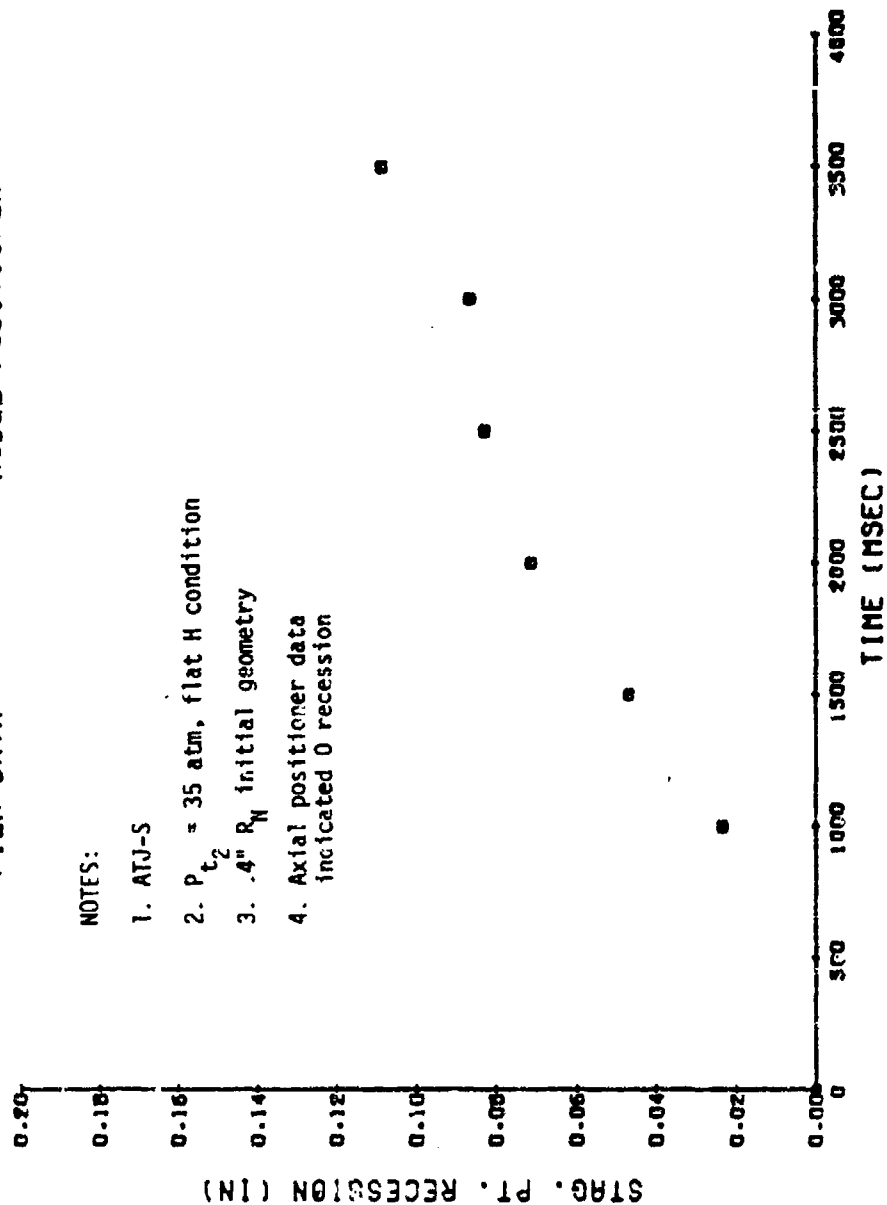RECESSION DATA. 50MW RTN-007. STING 1

■FILM DATA   ×MODEL POSITIONER

NOTES:

1. ATJ-S

2. P_{t_2} = 25 atm, flat H profile

3. .625" R_N initial geometry

Figure 3-10a. Reduced Model Surface Recession Data

STAG. PT. RECESSION (IN)

TIME (MSEC)

RECESSION DATA. 50MW RTN-007. STING 2

=FILM DATA
=MODEL POSITIONER

NOTES:

1. ATJ-S

2. P_{t_2} = 25 atm, flat H condition

3. 30°/8° biconic initial geometry
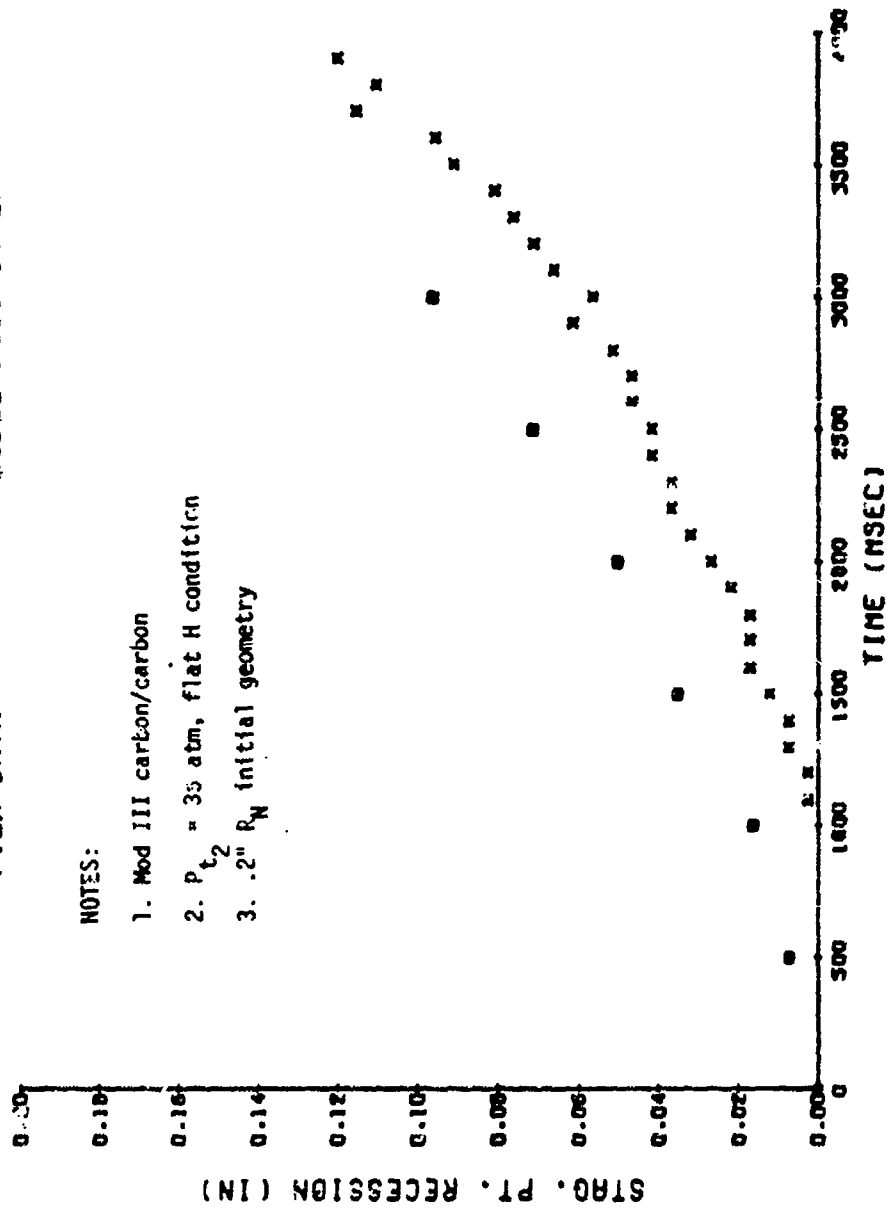

TIME (MSEC)

STAG. PT. RECESSION (IN)
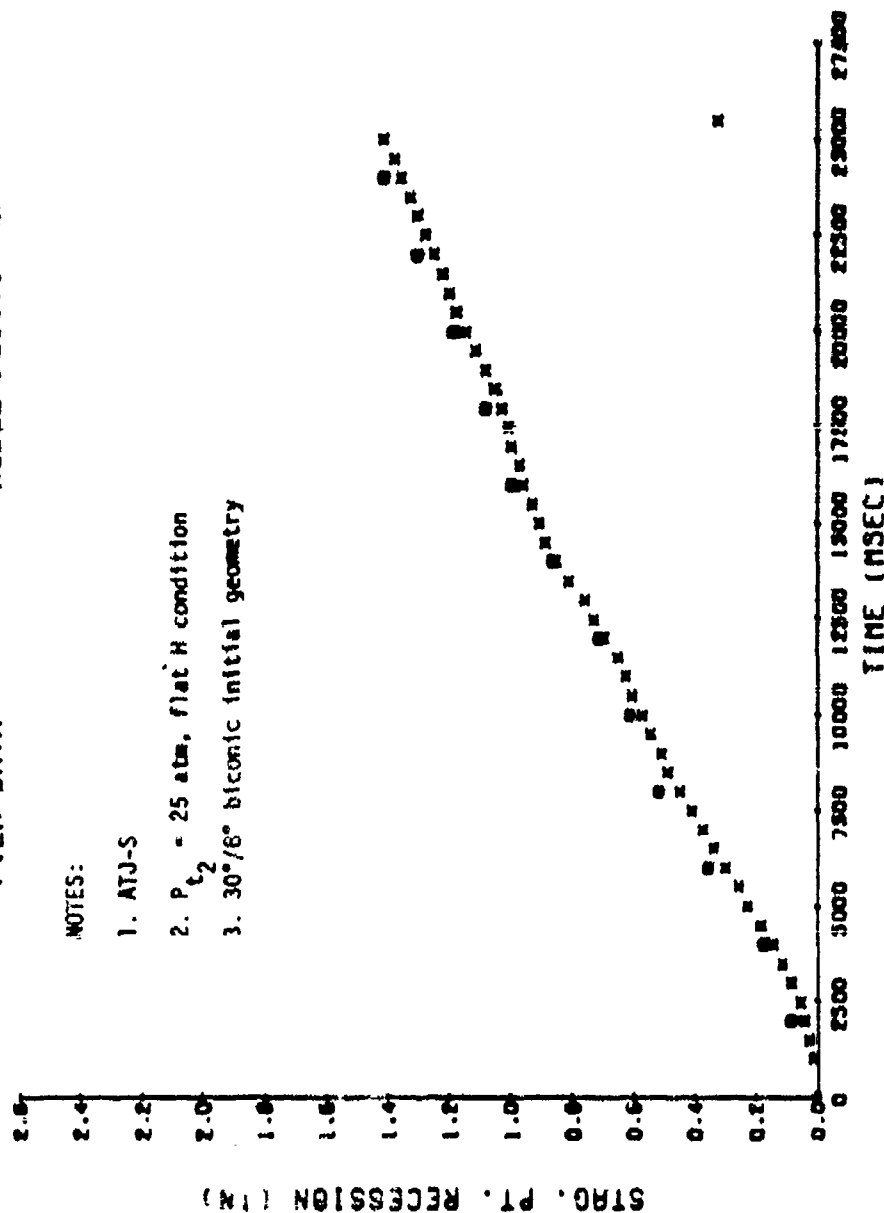
Figure 3-10b. Reduced Model Surface Recession Data

RECESSION DATA. 50MW RTN-007. STING 3

● FILM DATA
× MODEL POSITIONER

NOTES:

1. ATJ-S

2. P_{t_2} = 25 atm, flat H condition

3. 0.625" initial geometry

STAG. PT. RECESSION (IN)

TIME (MSEC)

Figure 3-10c. Reduced Model Surface Recession Data

RECESSION DATA. 50MW RTN-008. STING 1

* FILM DATA   * MODEL POSITIONER

NOTES:

1. ATJ-S

2. P_{t_2} = 35 atm, flat H condition

3. .2" R_N initial geometry

STAG. PT. RECESSION (IN)

0.20 0.18 0.16 0.14 0.12 0.10 0.08 0.06 0.04 0.02 0.00

TIME (MSEC)

0   500   1000   1500   2000   2500   3000   3500   4000

Figure 3-11a. Reduced Model Surface Recession Data

3-28

RECESSION DATA. 50MW RTN-008. STING 2

•FILM DATA   ✱MODEL POSITIONER

NOTES:

1. ATJ-S

2. P_{t_2} = 35 atm, flat H condition

3. .4" R_N initial geometry

4. Axial positioner data
   indicated 0 recession

STAG. PT. RECESSION (IN)

0.20
0.18
0.16
0.14
0.12
0.10
0.08
0.06
0.04
0.02
0.00

0   500   1000   1500   2000   2500   3000   3500   4000

TIME (MSEC)

Figure 3-11b.   Reduced Model Surface Recession Data

3-29

Figure 3-11c. Reduced Model Surface Recession Data

RECESSION DATA. 50MW RTN-009. STING 1

■ FILM DATA   ■ MODEL POSITIONER

NOTES:
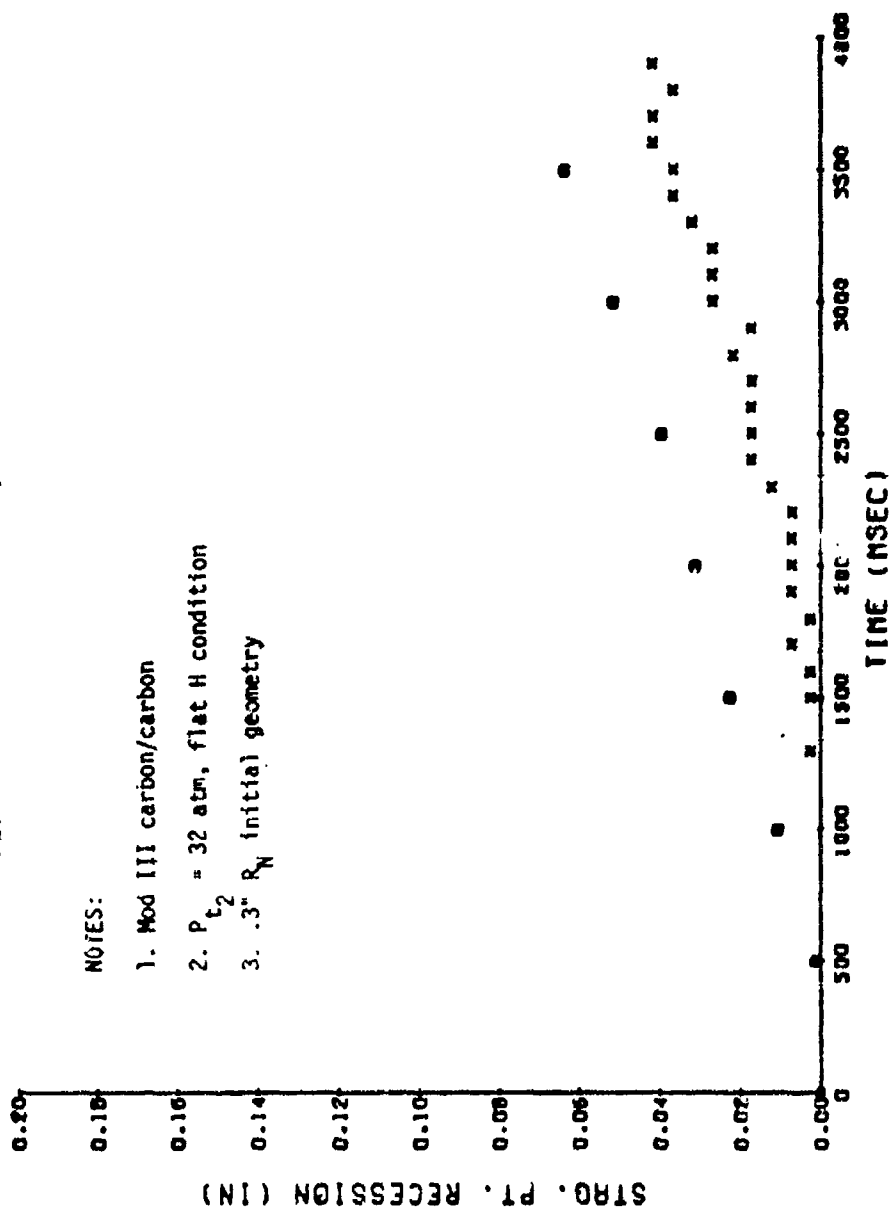
1. ATJ-S

2. P_{t_2} = 32 atm, flat H condition

3. Flat, .2" R_{cyl} initial geometry
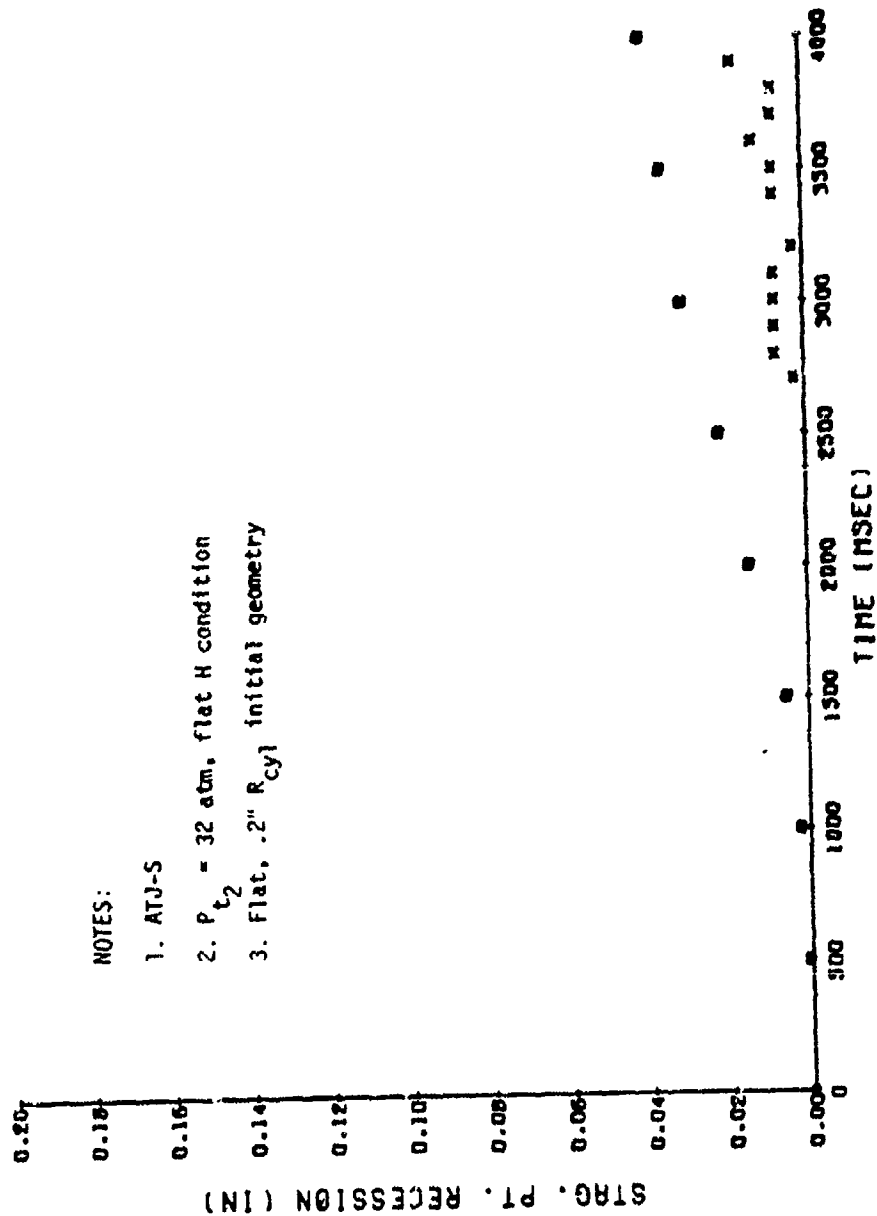
Figure 3-12a.   Reduced Model Surface Recession Data

RECESSION DATA. 50MW RTN-009. STING 2

● FILM DATA
■ MODEL POSITIONER

NOTES:

1. ATJ-S

2. P_{t_2} = 32 atm, flat H condition

3. .3" R_N initial geometry

STAG. PT. RECESSION (IN)

TIME (MSEC)
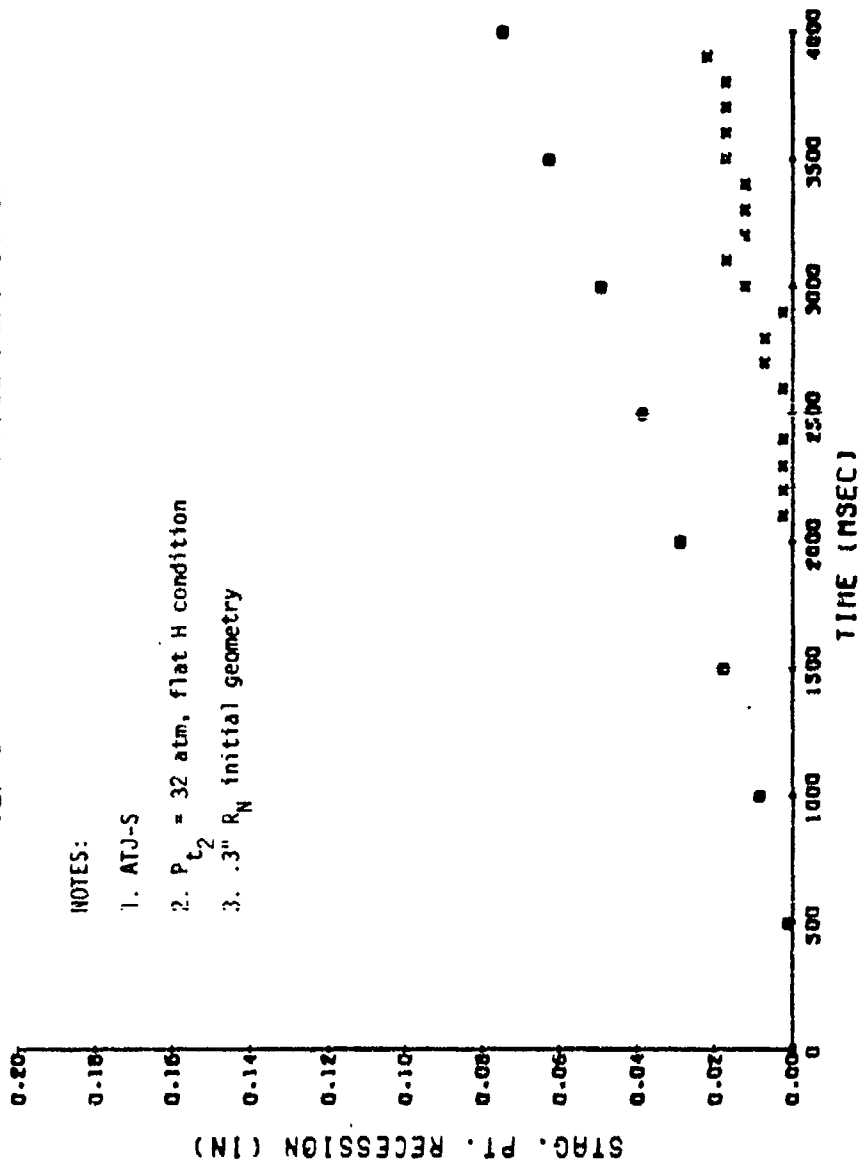
Figure 3-12b. Reduced Model Surface Recession Data

Figure 3-12c. Reduced Model Surface Recession Data

on the high speed data tape and can be reduced to provide a check of the optical recession results. Axial position information is read from the tape at intervals of either 100 or 500 milliseconds depending on run length. The model recession data is obtained by differencing the initial positioner reading and the subsequent output which is susceptible to two potential problems. The first problem, which is relatively minor, is that slight variations appear in maintaining the nominal (0.10 or 0.15 inch) standoff from the nozzle exit. The second problem, which is more serious, is the initial behavior of the model. The model location is determined by the signals from a pair of closely spaced pyrometers actuated by the radiation from the hot model. The initial tendency when the cold model is inserted in the stream is for the positioner system to attempt to move the model up into the nozzle exit. To prevent this the model is locked into position for the interval while it is heating. The result in the data is an initial period of no recession followed by a short interval of exaggerated recession when the positioner is unlocked and it attempts to compensate for the ablation that has occurred. This error is not substantial on the shape change runs (Runs 005 through 007, Figures 3-7 through 3-10) where exposure times are relatively long; however, on the transition tests (Runs 008 and 009, Figures 3-11 and 3-12) this error coupled with the increased optical and positioner errors associated with the small size of these models resulted in significant discrepancies between the film and positioner data at least in absolute magnitude. In most cases the slopes of the two curves, the recession rate, are quite similar, which is the parameter of actual interest. When differences exist the film data is more likely to be correct.

3.3   SURFACE TEMPERATURE DATA

Measurements of the surface temperature of ablating models provide the basis for a more quantitative understanding of the physics responsible for the total ablation response of the particular material being tested (cf., Reference 11). However, measurement of the model surface temperature in a high pressure arc such as the 50 MW RENT facility is difficult for reasons such as less-than-optimum view angles available, the small target size required, high temperature capability and fast response requirements, errors due to shock layer and boundary layer radiation, etc. Application of the instrumentation and the resulting surface temperature data is presented in this section.

Three Thermogage optical pyrometers were used for surface temperature data. These instruments use a silicon photovoltaic diode detector which has a sensitivity peak of 0.9 microns. Response time is of the order 10 microseconds. The particular units used have a focal length of 12 inches, a target size of

less than 1/32 inch, and a temperature range of about 6000°R without the filter and about 8200°R with a neutral density filter.

The calibration of these was checked before and after testing since substantial drift was observed from the calibrations initially supplied with the devices. Little change was noticed between pretest and post-test calibrations. The post-test calibration was used and as may be seen gave excellent agreement for the opposed pyrometers.

The mounting configuration of the pyrometers within the facility is indicated in Figure 2-4. All viewed the models in a direction essentially perpendicular to the model centerlines. Pyrometers #1 and #3 (Thermogage #932 and 119, respectively) viewed the model at a location 0.10 inch back from the stagnation point, i.e., 0.25 inch back from the nozzle exit plane for Runs 005 and 006 and 0.20 inch back for all other runs. Pyrometer #2 (Thermogage 923) was aimed to view the model at a location along the centerline 0.625 inch back from the stagnation point for Runs 004 through 007 and 0.25 inch back for the remaining Runs 008 and 009.

The signals from all pyrometers were recorded on both the oscillograph trace and high speed digital data system. Raw digital data from the pyrometers was input to a data reduction computer program set up by Aerotherm which includes signal conversion information, the appropriate calibration curves, and machine plotted output in the form of brightness temperature vs. time.

Ablative model surface temperature histories obtained in the above described fashion are shown in Figures 3-13 through 3-18. These data are plotted in terms of brightness temperature, i.e., they presume that the emittance, ϵ, is unity. Brightness temperature, T_b, may be converted to actual temperature, T, by the formula

$$\frac{1}{T} = \frac{1}{T_b} + \frac{\lambda}{C} \ln \epsilon$$

where λ is the wavelength and C = 1.438 cm°K. There are data (e.g., Reference 12) indicating that the emittances for the graphitic materials of interest here are quite high, around $\epsilon = 0.95$. For $\lambda = .9$ microns and $\epsilon = .95$, $T_b = 6500$°R, the above formula indicates that T = 6576°R. Thus, for the graphitic models, the actual surface temperatures are probably only slightly greater than the brightness temperatures shown in Figures 3-13 through 3-18.

All results except those for Run 006, strut 3, Run 007, strut 3, Run 008, strut 3 and Run 009, strut 3 provide excellent data. Unfortunately, surface
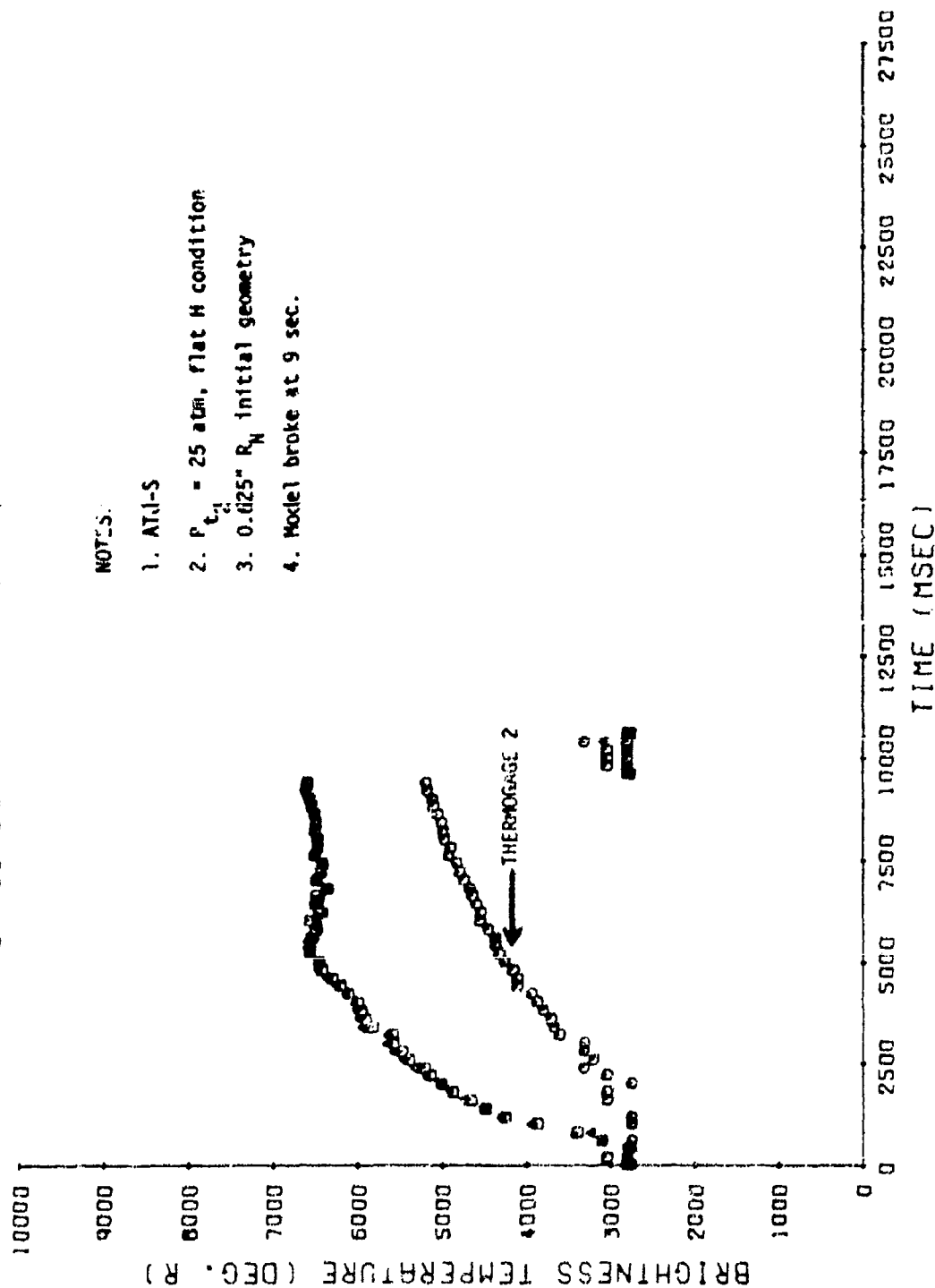
Figure 3-13e. Reduced Pyrometer Data

PYRO DATA - 50MW RTN-004, STING 2

□ THERMOGAGE1 ⊙ THERMOGAGE2 ▲ THERMOGAGE3

NOTES:

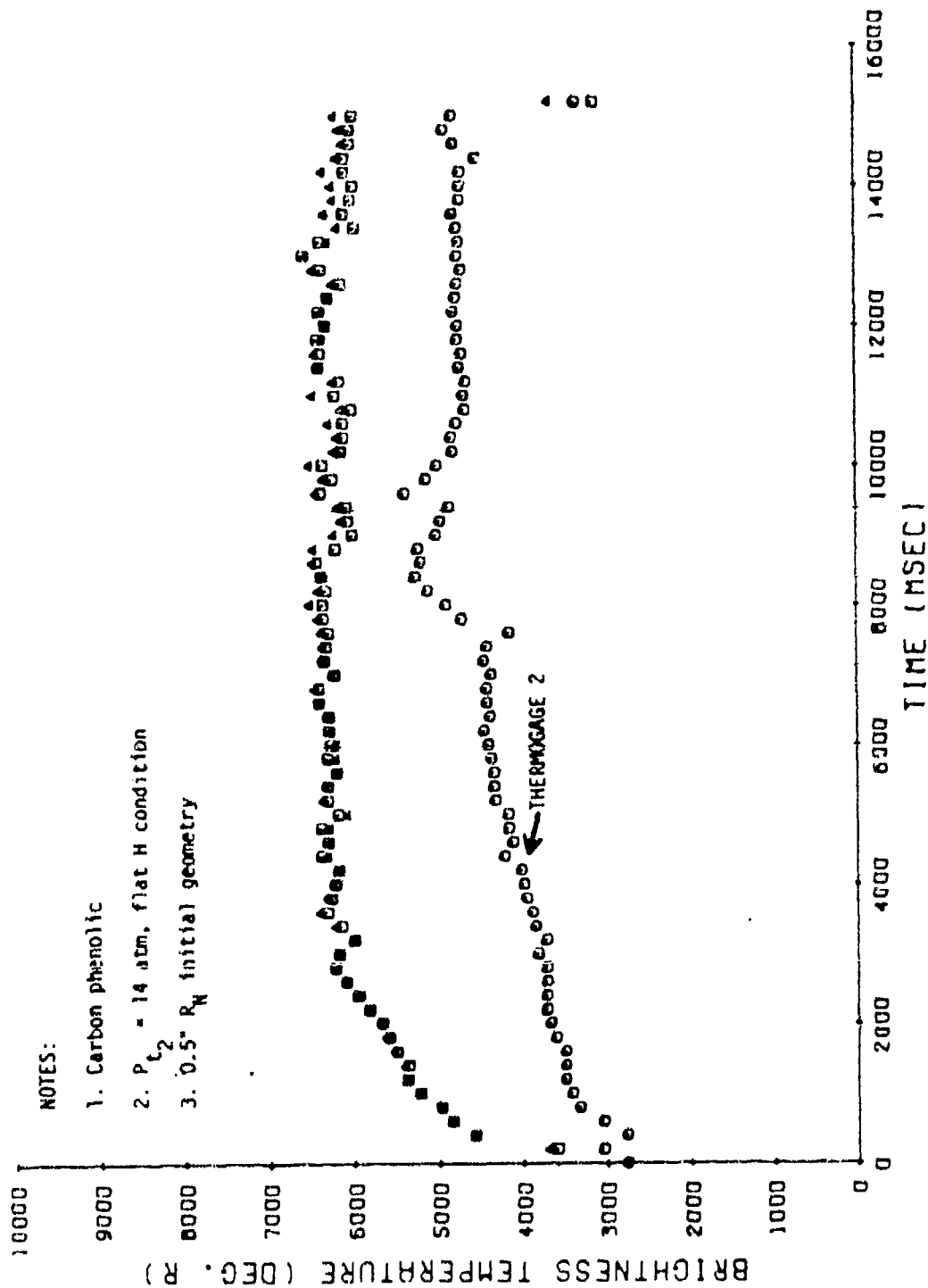1. Carbon phenolic

2. P_{t_2} = 25 atm, Flat H condition

3. 0.625" R_N Initial geometry

THERMOGAGE 2

BRIGHTNESS TEMPERATURE (DEG. R)

TIME (MSEC)
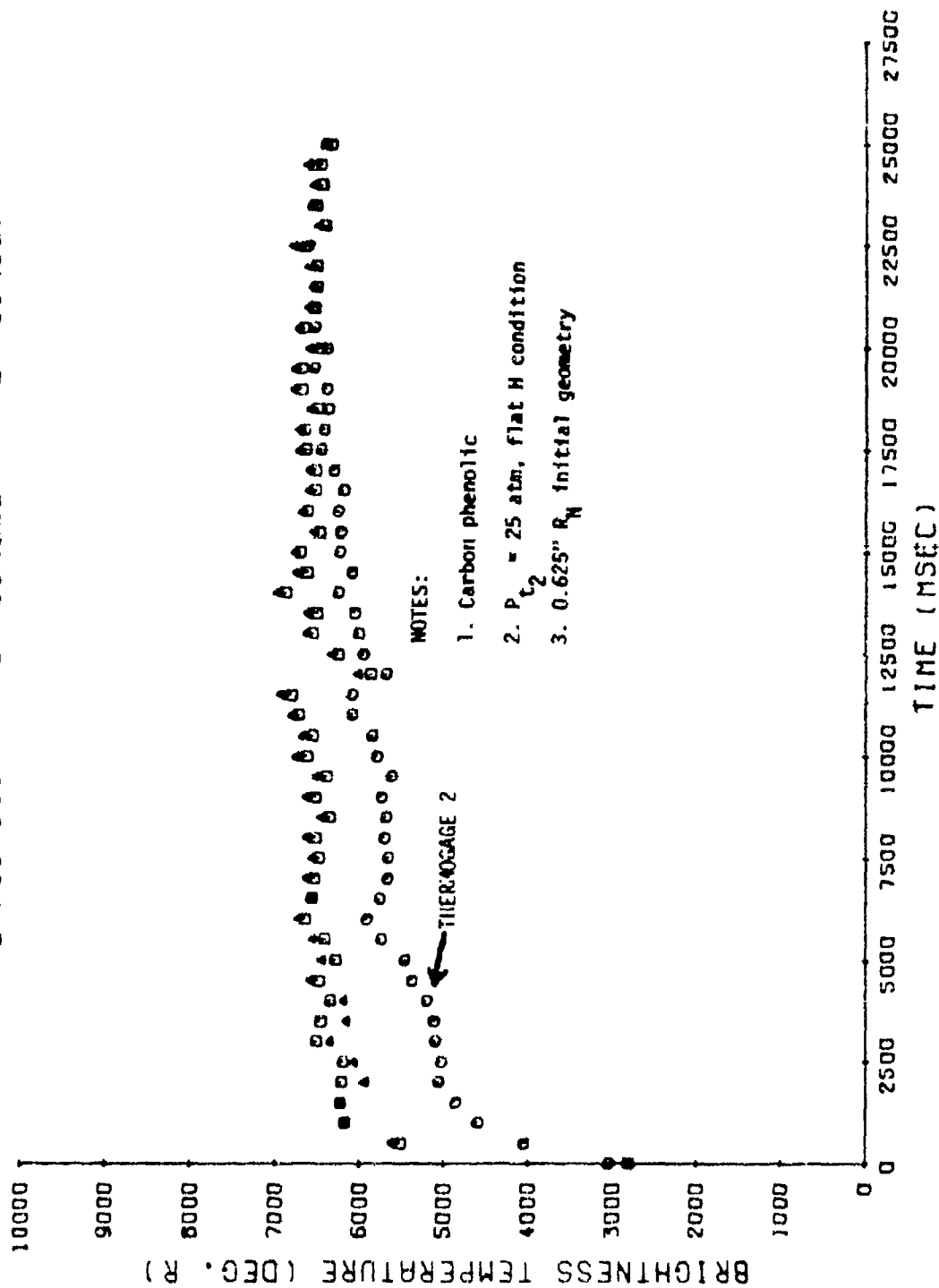
Figure 3-13b. Reduced Pyrometer Data

PYRO DATA - 50MW RTN-005, STING 1

□ THERMOGAGE1 ▪ THERMOGAGE2 ▲ THERMOGAGE3

NOTES:

1. Carbon phenolic

2. P_{t_2} = 16 atm, flat H condition

3. 0.625" R_N initial geometry
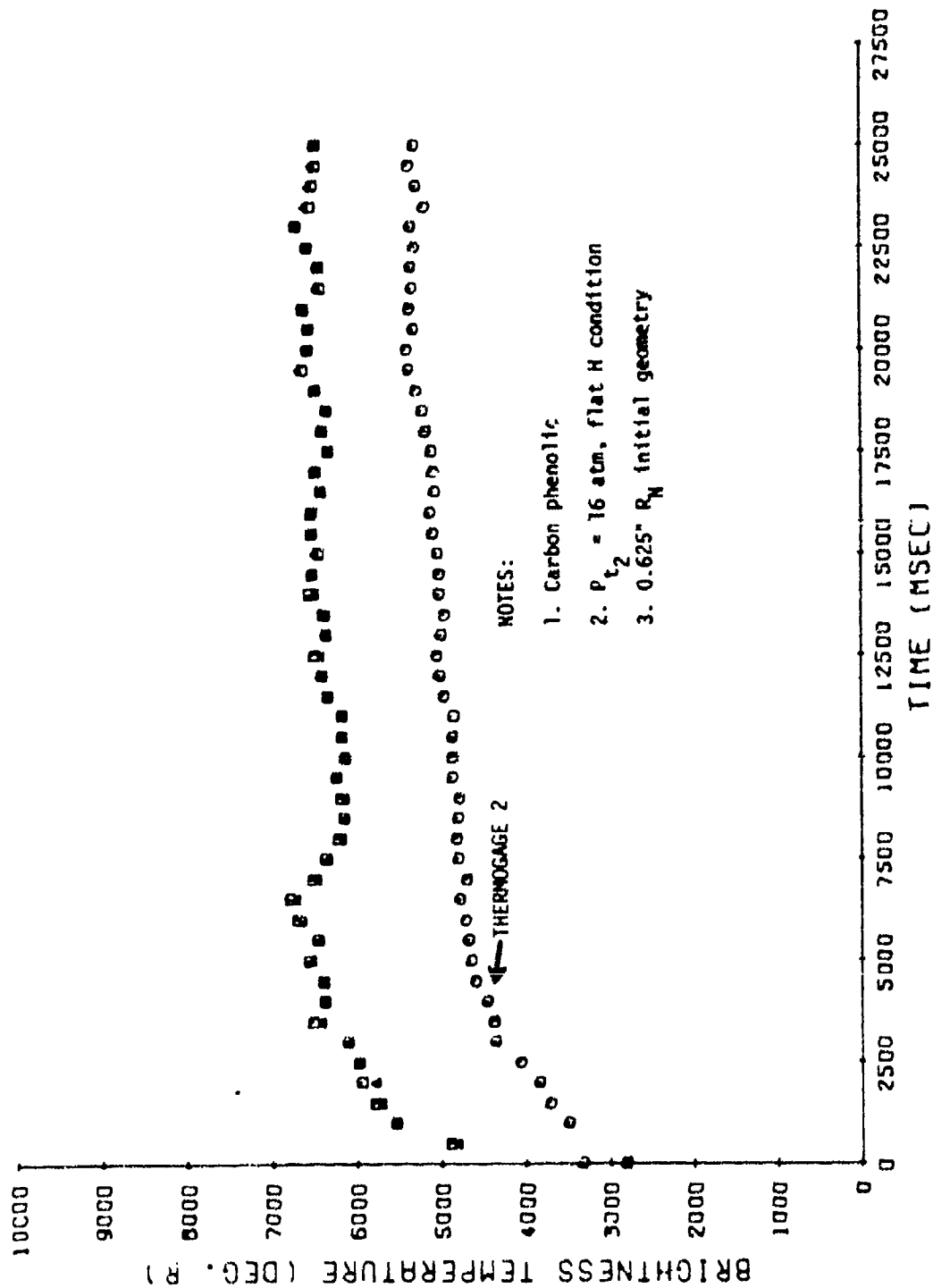
Figure 3-14a. Reduced Pyrometer Data

PYRO DATA - 50MW RTN-005, STING 2

● THERMOGAGE1 ● THERMOGAGE2 ▲ THERMOGAGE3

NOTES

1. Carbon phenolic

2. P_{t_2} = 16 atm, flat H condition

3. 30°/8° biconic initial geometry

THERMOGASE 2

BRIGHTNESS TEMPERATURE (DEG. R)

TIME (MSEC)
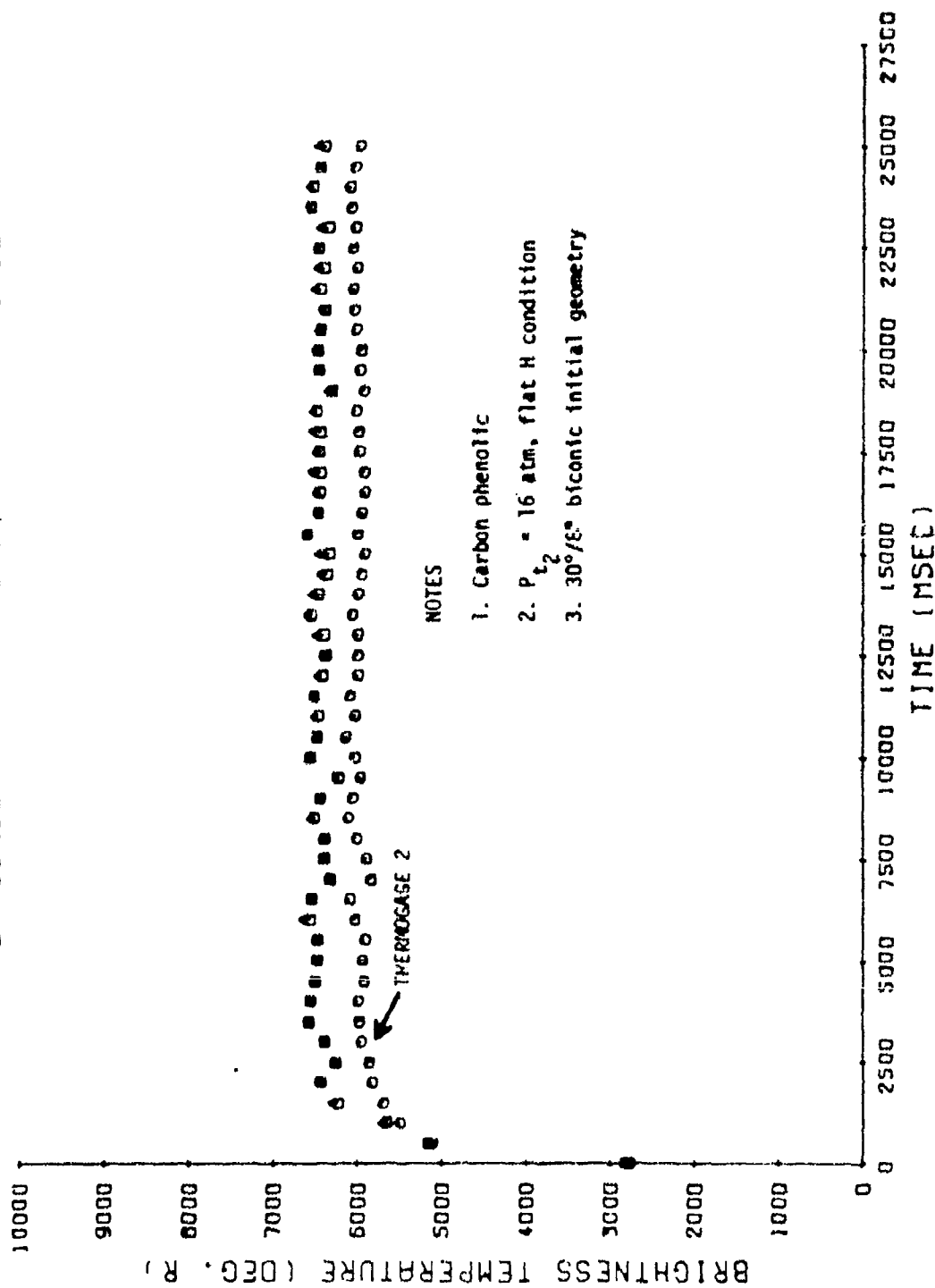
Figure 3-14b.   Reduced Pyrometer Data

PYRO DATA - 50MW RTN-006. STING 1

□ THERMOGAGE1   ⊙ THERMOGAGE2   ▲ THERMOGAGE3

NOTES:

1. Carbon phenolic

2. P_{t_2} = 14 atm, flat H condition

3. 0.5" R_N initial geometry

THERMOGAGE 2

Figure 3-15a. Reduced Pyrometer Data
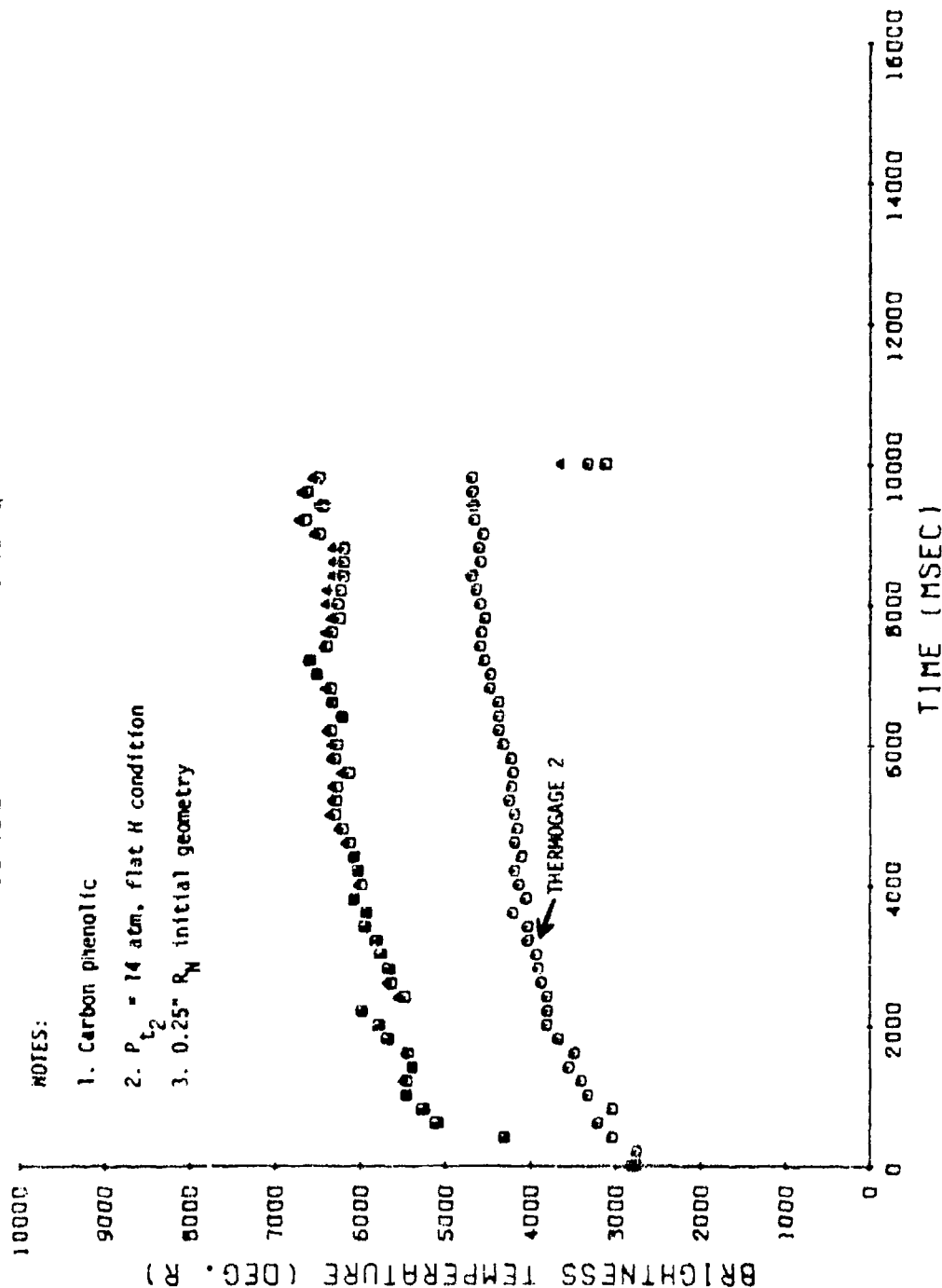
Figure 3-15b. Reduced Pyrometer Data

PYRO DATA - 50MW RTN-007, STING 1

□ THERMOGAGE1 ⊙ THERMOGAGE2 ▲ THERMOGAGE3

NOTES:

1. ATJ-S

2. P_{t_2} = 25 atm, flat H condition

3. 0.625" R_N initial geometry
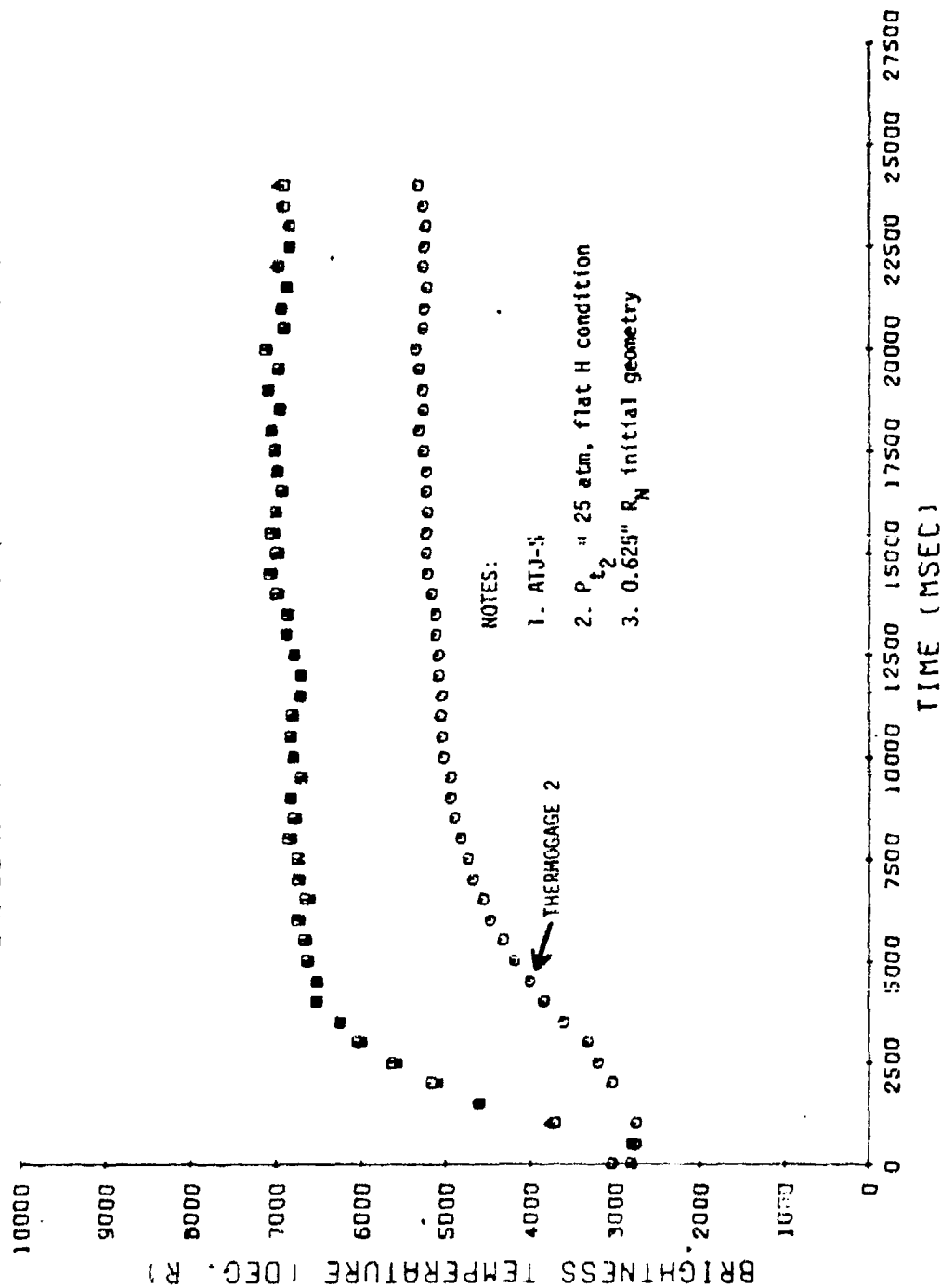
THERMOGAGE 2

Figure 3-16a. Reduced Pyrometer Data
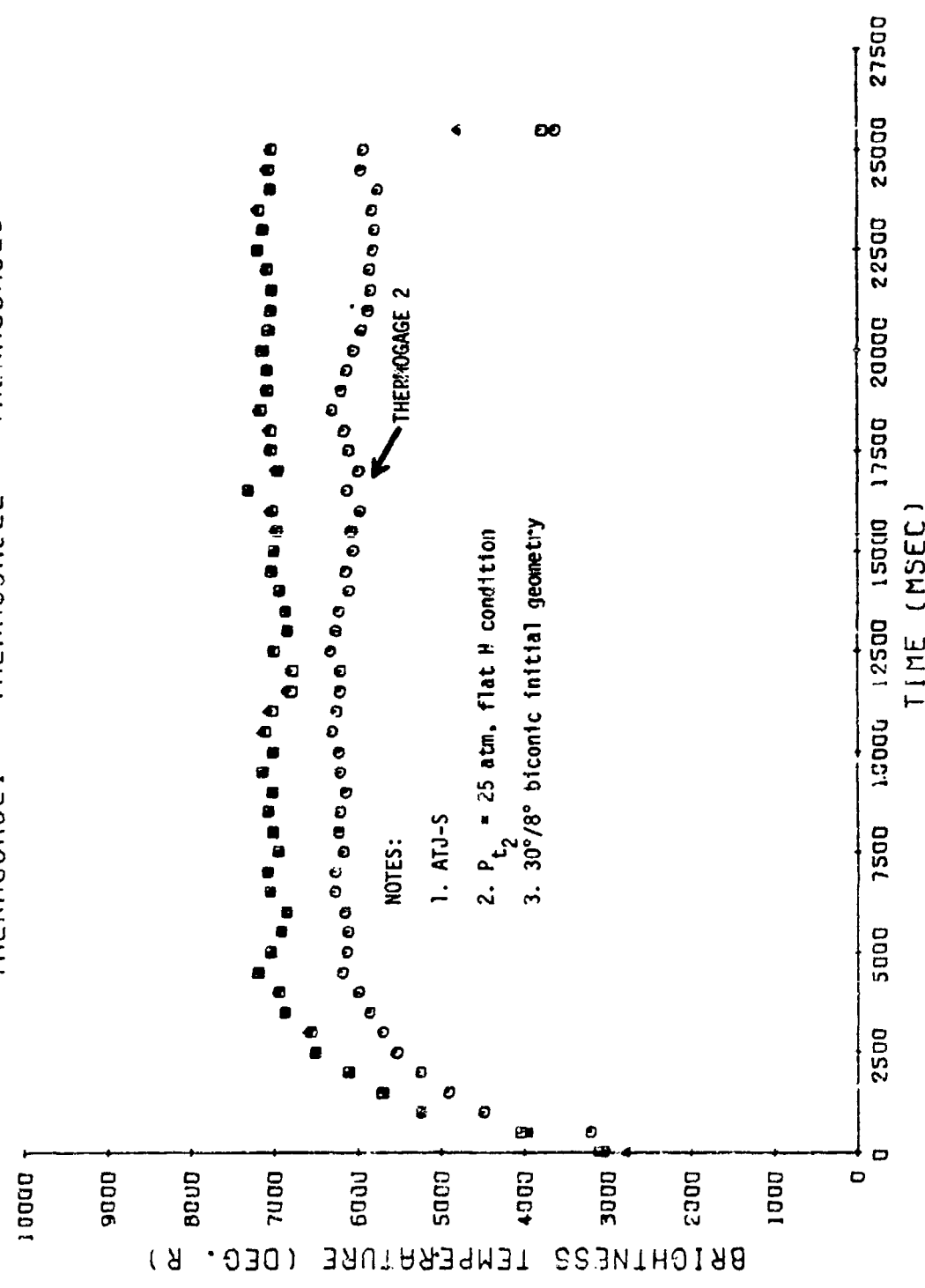
Figure 3-16b. Reduced Pyrometer Data

Figure 3-17a. Reduced Pyrometer Data

PYRO DATA - 50MV RTN-008. S1ING
□ THERMOGAGE1   ⊙ THERMOGAGE2   ▲ THERMOGAGE3

NOTES:

1. ATJ-S

2. P_{t_2} = 35 atm, flat H condition

3. 0.2" R_N initial geometry

THERMOGAGE 2

BRIGHTNESS TEMPERATURE (DEG. R)

TIME (MSEC)
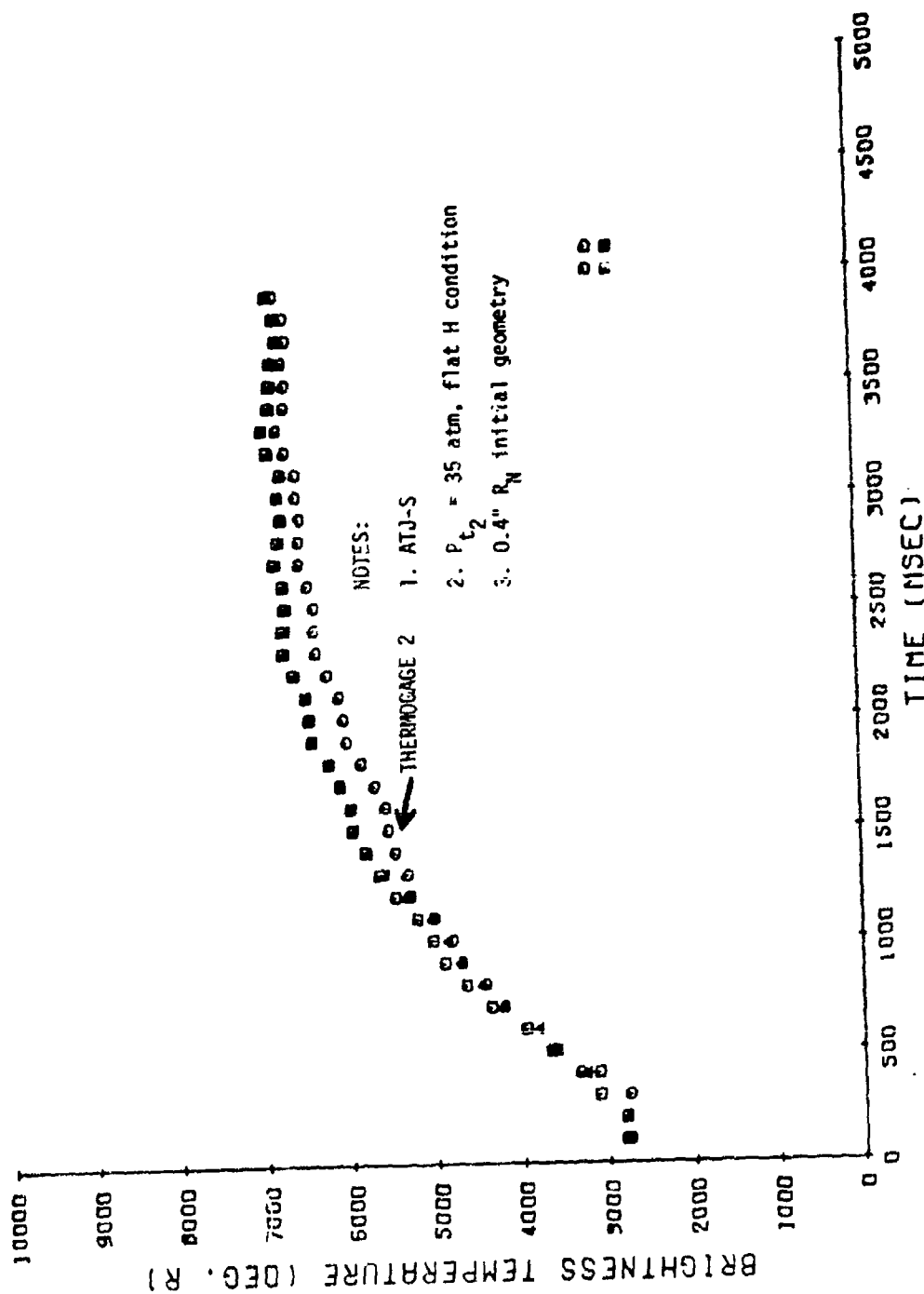
Figure 3-17b. Reduced Pyrometer Data

PYRO DATA - 50MV RTN-009. STING 1

□ THERMOGAGE1 ⊙ THERMOGAGE2 ▲ THERMOGAGE3

NOTES:

1. ATJ-S

2. P_{t_2} = 32 atm, flat H condition

3. Flat, R_{cyl} = 0.3" initial geometry

4. Early time temperatures appear to be below the lower pyrometer limits

THERMOGAGE 2

TIME (MSEC)

BRIGHTNESS TEMPERATURE (DEG. R)

10000 9000 8000 7000 6000 5000 4000 3000 2000 1000 0

0 500 1000 1500 2000 2500 3000 3500 4000 4500 500
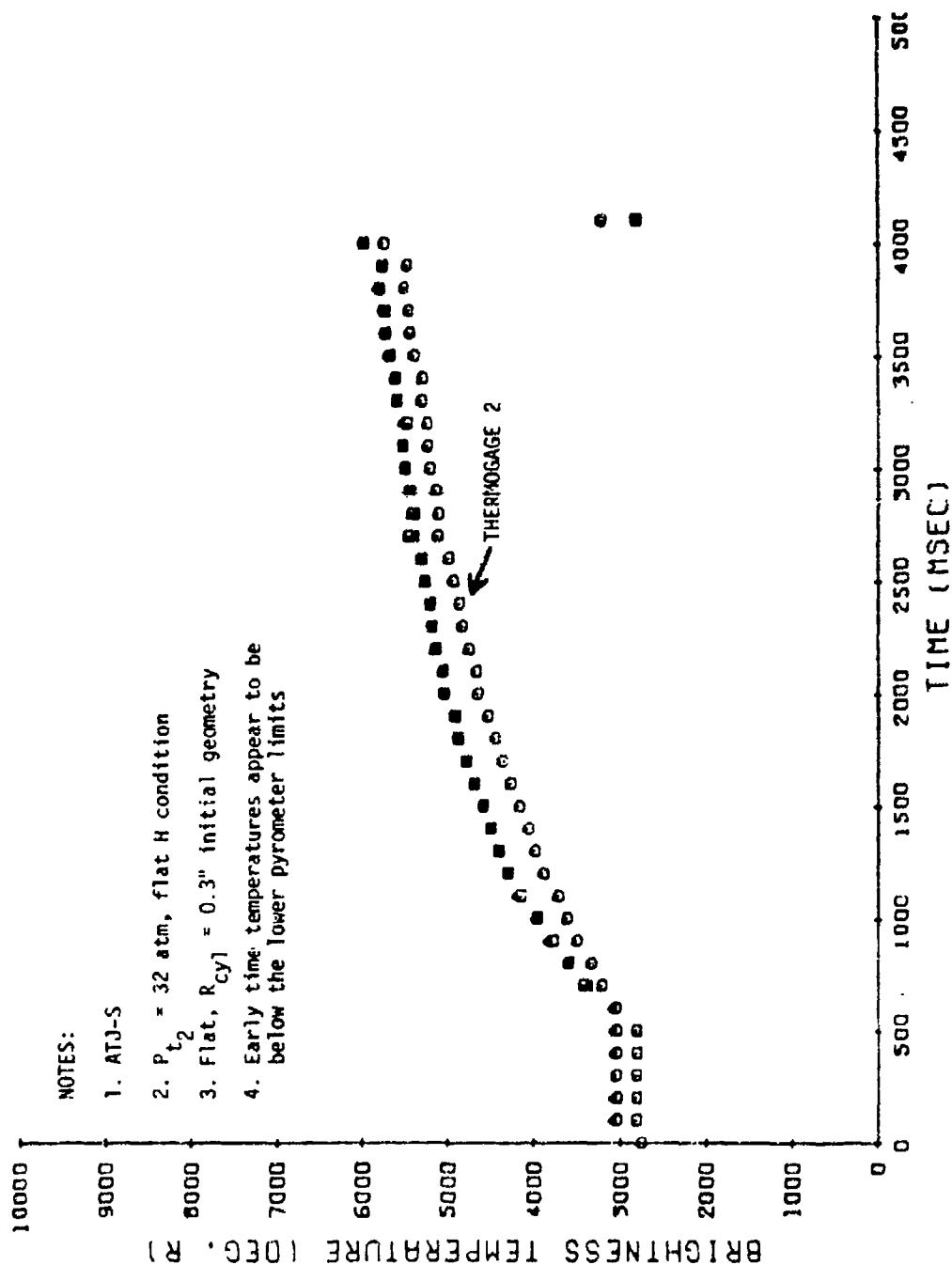
Figure 3-18a. Reduced Pyrometer Data
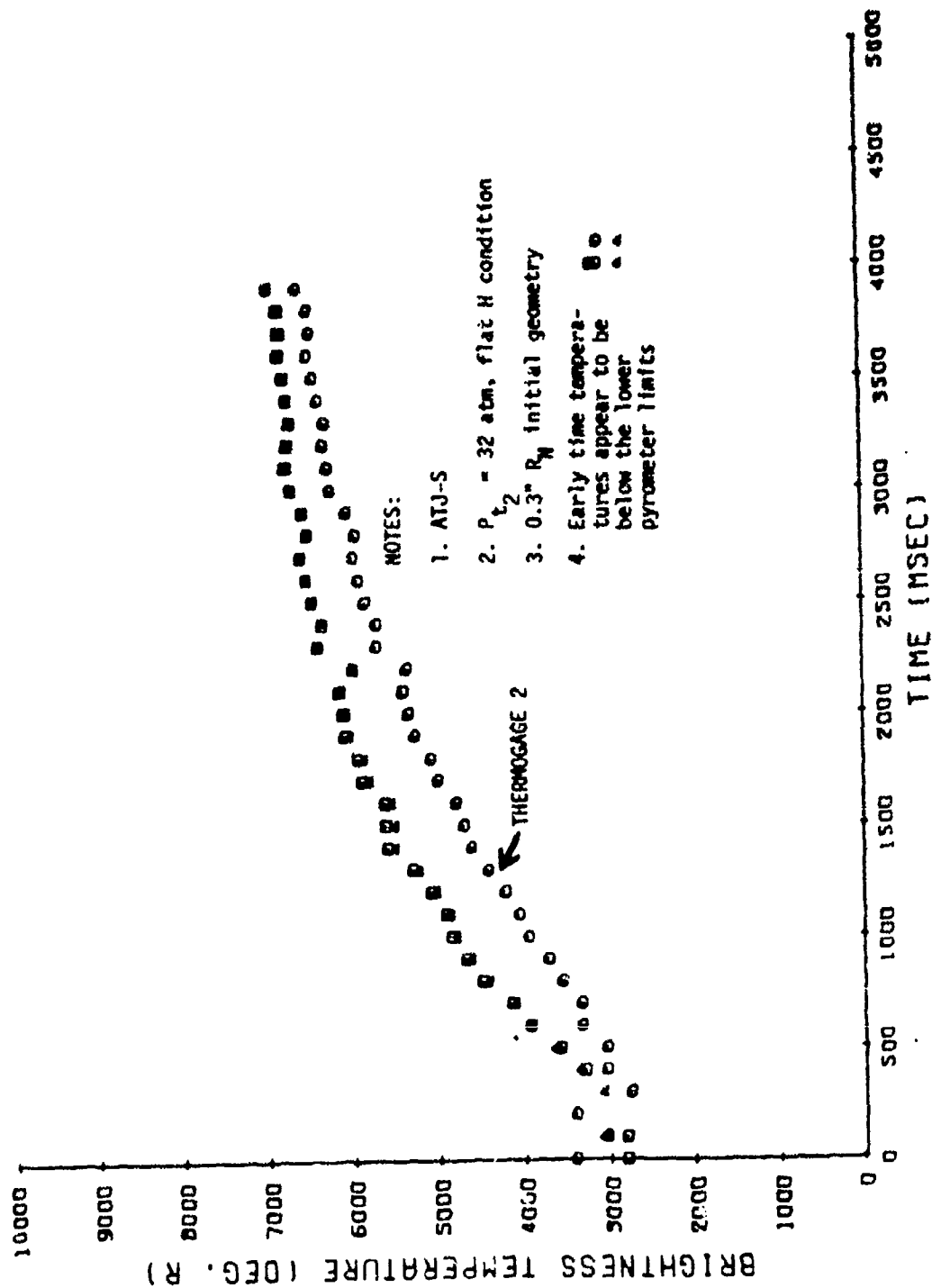
Figure 3-18b. Reduced Pyrometer Data

brightness digital data was unavailable for the above tests, possibly due to equipment malfunction or switching errors for the third strut testing.

3.4   POST-TEST PHOTOGRAPHS

Shown in Figures 3-19 through 3-25 are both profile and detail post-test photographs of the ablative models tested on this series.

3.5   CALIBRATION DATA

This test series included exposure of both pressure and heat flux probes to obtain calibrations of the arc jet conditions. The instrumentation used was described briefly in Section 2.3 and the calibration model exposure schedule is indicated in Table 2-1. The calibration measurement results are presented in Sections 3.5.1 and 3.5.2 for the pressure and heat flux data, respectively.

3.5.1   Pressure Data

Pressure data were reduced from the raw high speed digital data by AFFDL using a program which considers the transducer calibration and provides machine plotted profiles as output. Figures 3-26a through d show measured jet pressure profiles from a typical pressure model (0.75 inch R_N with ports at 0°, 20°, 30°, and 40°) exposed on a typical run (RTN-52-005) for the 2.393 inch nozzle. Figure 3-27 presents the same data for a typical run (008) with the 1.493 inch nozzle. These figures illustrate the type of data obtained with the pressure models; the pressure profile plots for other runs are not included here but are available from the present authors if required.

The pressure data was interpreted by estimating the average "plateau" level for each profile measurement (such as Figures 3-26 and 3-27). These data were then interpreted in two ways:

1.   Pressure distribution data (for pressure models with multiple ports) were compared with Newtonian theory;

2.   Stagnation point pressure measurements were normalized by chamber pressure measurements, and these ratios were compared with theoretical ratios based on the nozzle expansion ratio.

Figures 3-28 and 3-29 show the measured pressure distributions compared with the theoretical modified Newtonian approximation:

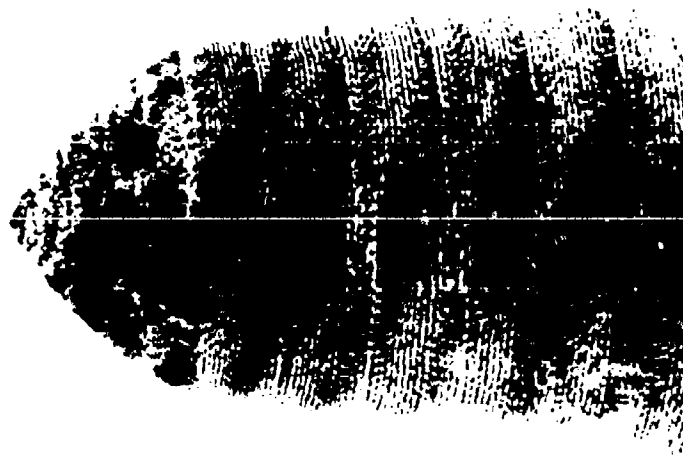$$\frac{P}{P_{t_2}} = \frac{P_e}{P_{t_2}} + \left(1 - \frac{P_e}{P_{t_2}}\right)\cos^2\theta$$
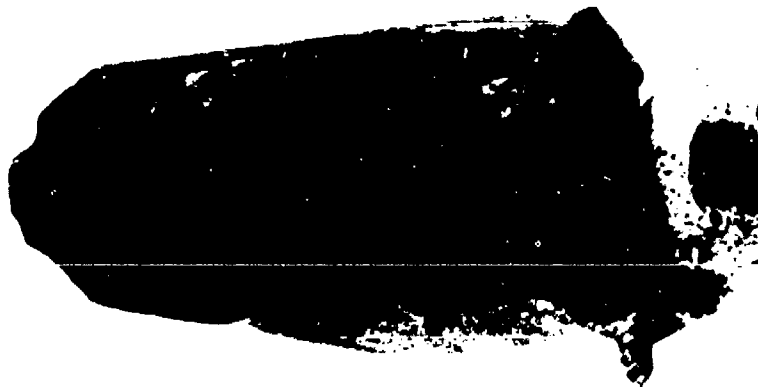
Final Ablated Shape

Surface Detail

Figure 3-19. Post-Test Photographs - Shape Change Models

a. RTN 52-004, Strut 1
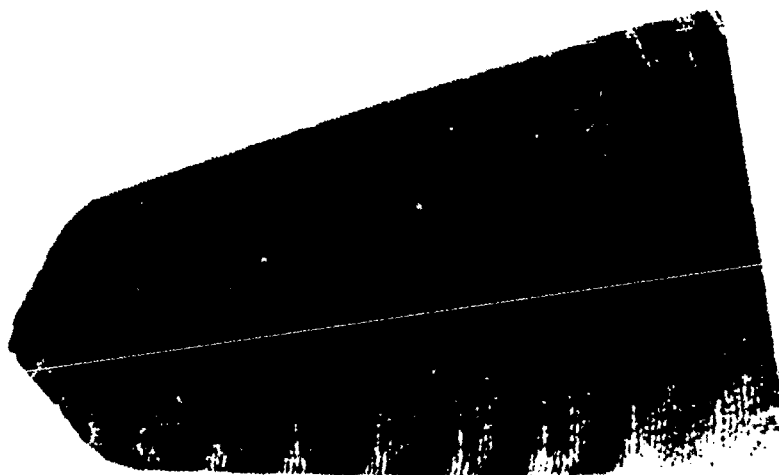(Note: Model failed after 9 seconds of exposure)

Final Ablated Shape

Surface Detail

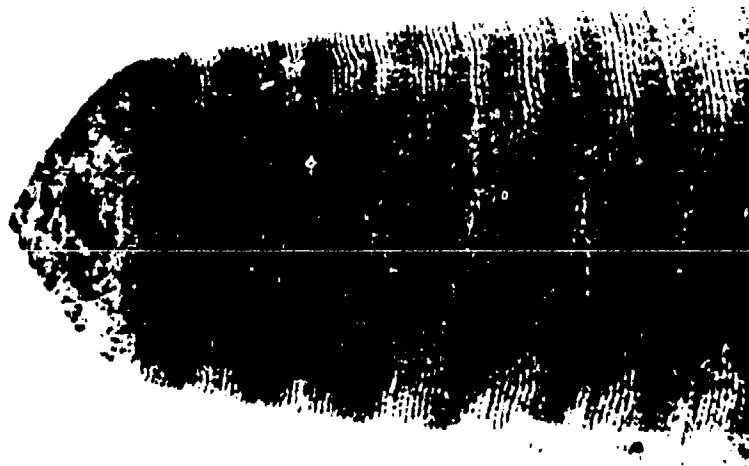Figure 3-19. Concluded

b. RTN 52-004, Strut 2

Surface Detail

Final Ablated Shape

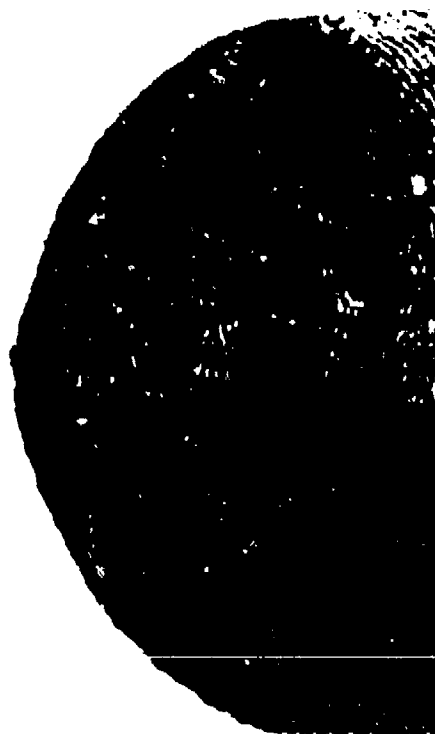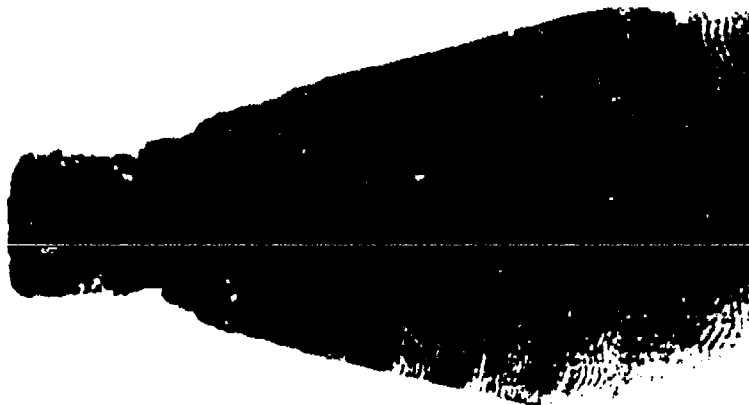Figure 3-20. Post-Test Photographs - Shape Change Models

a. RTN 52-005, Strut 1

Final Ablated Shape

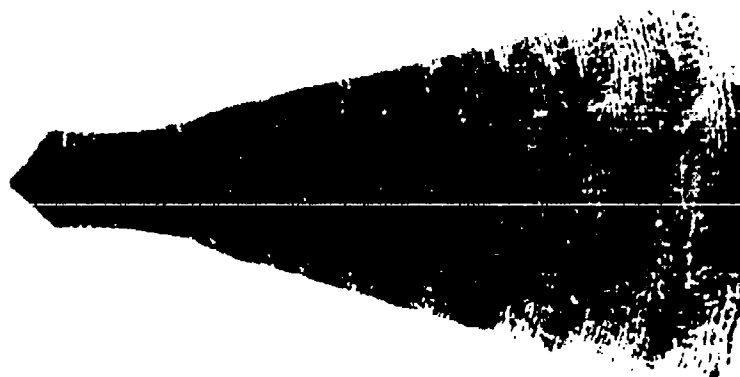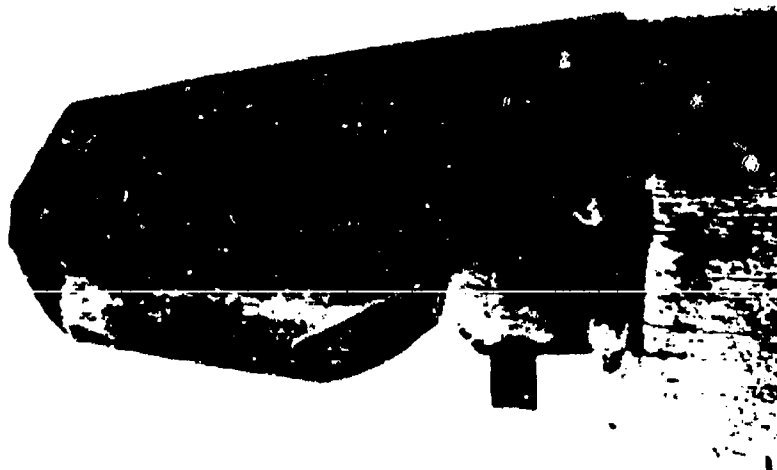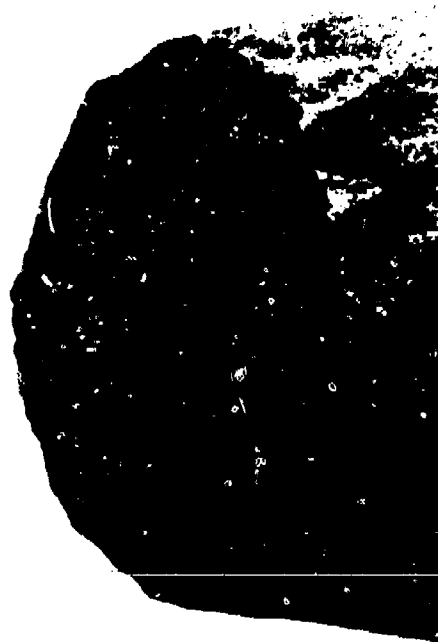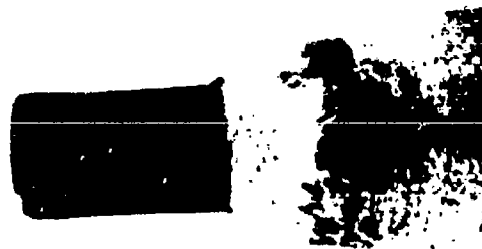Surface Detail

Figure 3-20. Concluded

b. RTN 52-005, Strut 2

Final Ablated Shape

Surface Detail

Figure 3-21. Post-Test Photographs - Transition Models

a. RTN 52-006, St..,t 1

Final Ablated Shape

Surface Detail

Figure 3-21. Continued

b. RTN 52-006, Strut 2

Surface Detail

Final Ablated Shape

Figure 3-21. Concluded

c. RTN 52-0106, Strut 3

Final Ablated Shape

Surface Detail

Figure 3-22. Post-Test Photographs - Shape Change Models

a. RTN 52-007, Strut 1

Final Ablated Shape   Surface Detail

Figure 3-22. Continued

b. RTN 52-C07, Strut 2

Figure 3-22. Post-test photographs of an ablation mode, showing ablation shape and surface character (ATJ-S graphite)

Surface Detail

Final Ablated Shape

Figure 3-23. Post-Test Photographs - Transition Models

a. RTN 52-008, Strut 2
   (Note: Model on Strut 1 was not recovered)

Surface Detail

Final Ablated Shape

Figure 3-23. Concluded

b. RTN 52-L08, Strut 3

Final Ablated Shape

Surface Detail

Figure 3-24. Post-Test Photographs - Transition Models
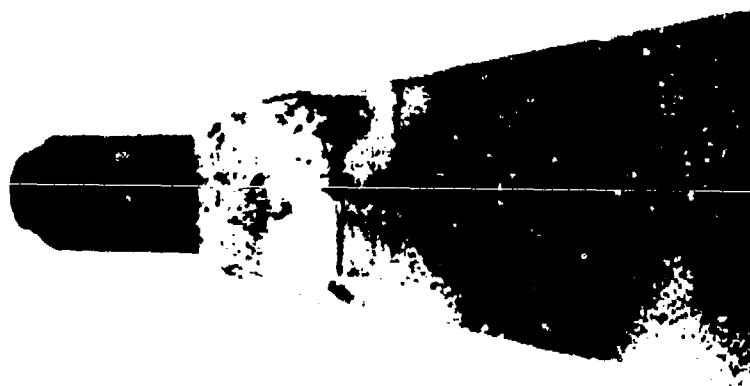
a. Run 52-009, Strut 1

Final Ablated Shape

Surface Detail

Figure 3-24. Continued

b. RTN 52-0(l9, Strut 2

Surface Detail

Final Ablated Shape

Figure 3-24. Concluded

c. RTN 52-009, Strut 3

Final Ablated Shape   Surface Detail

Figure 3-25.   Post-Test Photographs - Transition Models

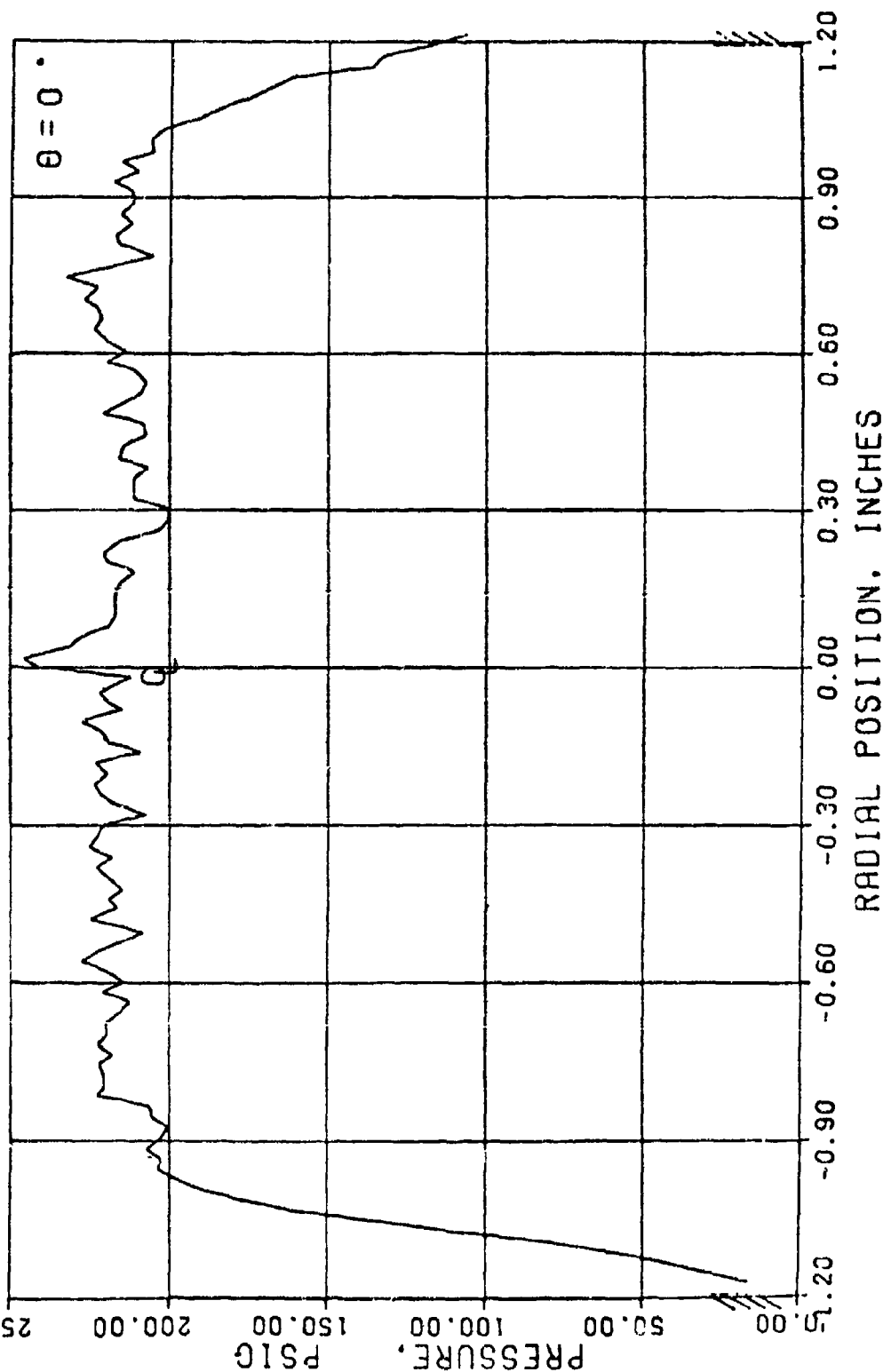RTN 52-010, Strut 3
(Tested as part of Philco-Ford Tests)

Figure 3-26a. Sample Pressure Transducer Output, 2.393 in Nozzle

Figure 3-26b. Sample Pressure Transducer Output, 2.393 in Nozzle

Figure 3-26c. Sample Pressure Transducer Output, 2.393 in Nozzle

Figure 3-26d. Sample Pressure Transducer Output, 2.393 in Nozzle

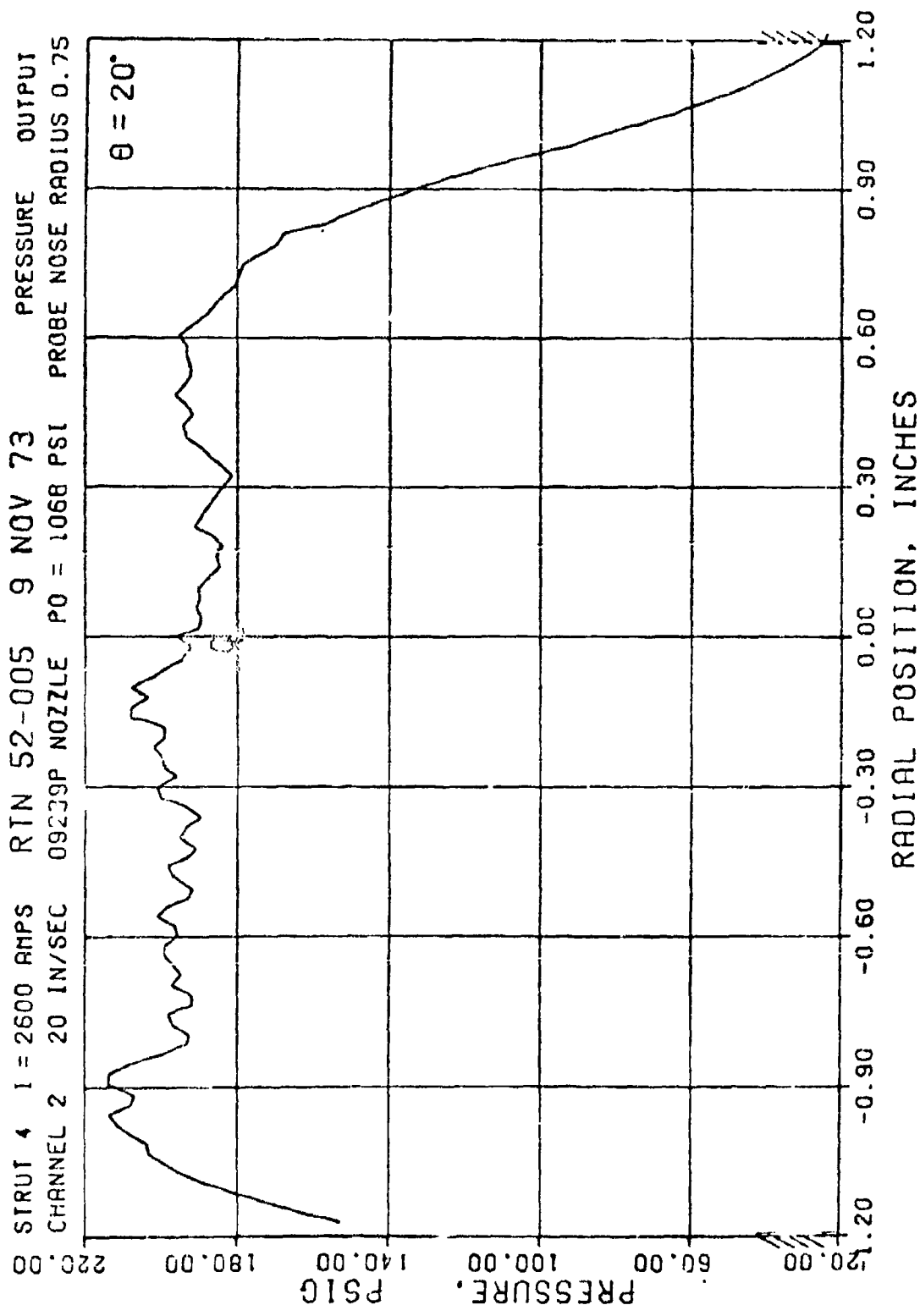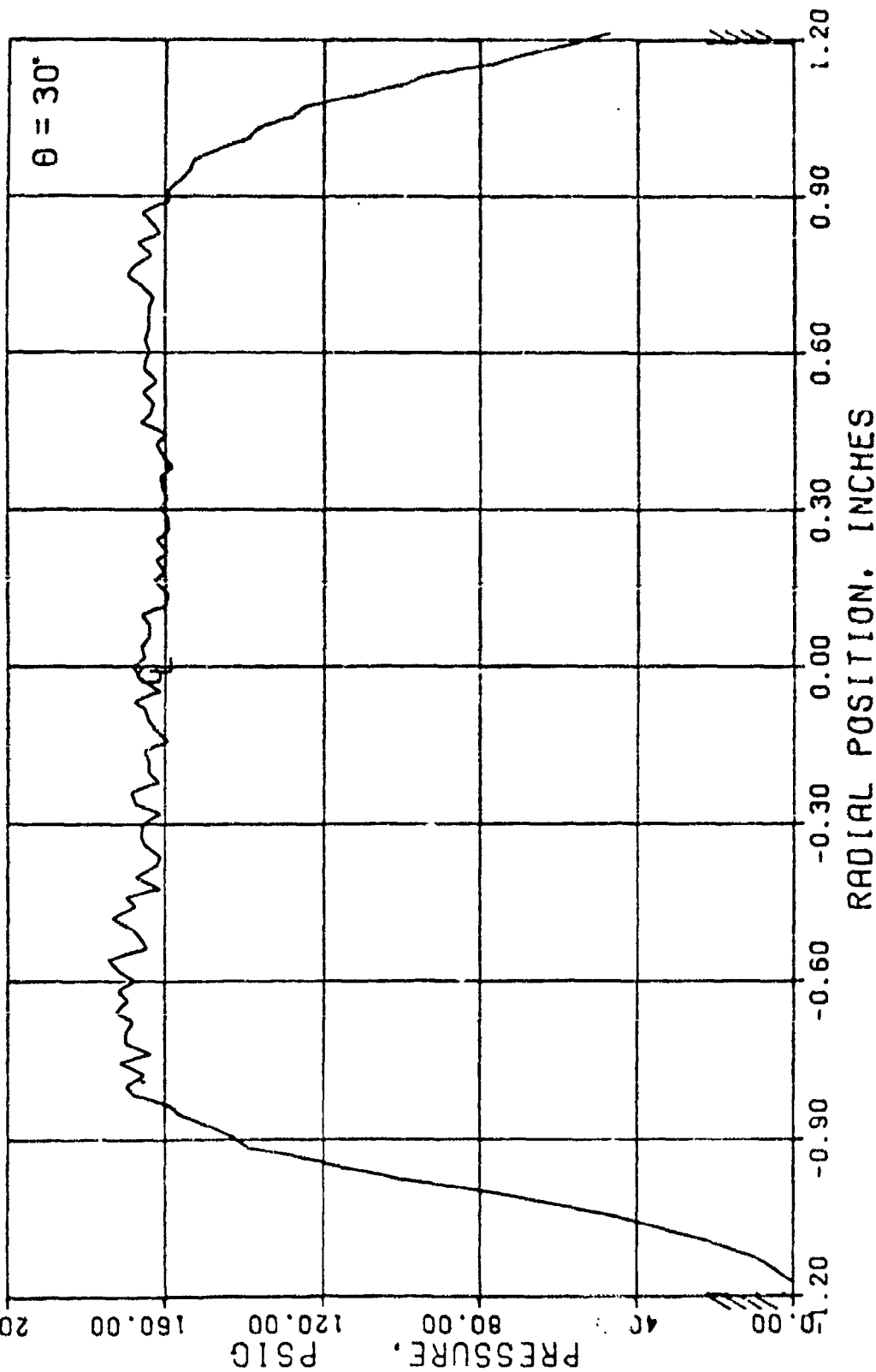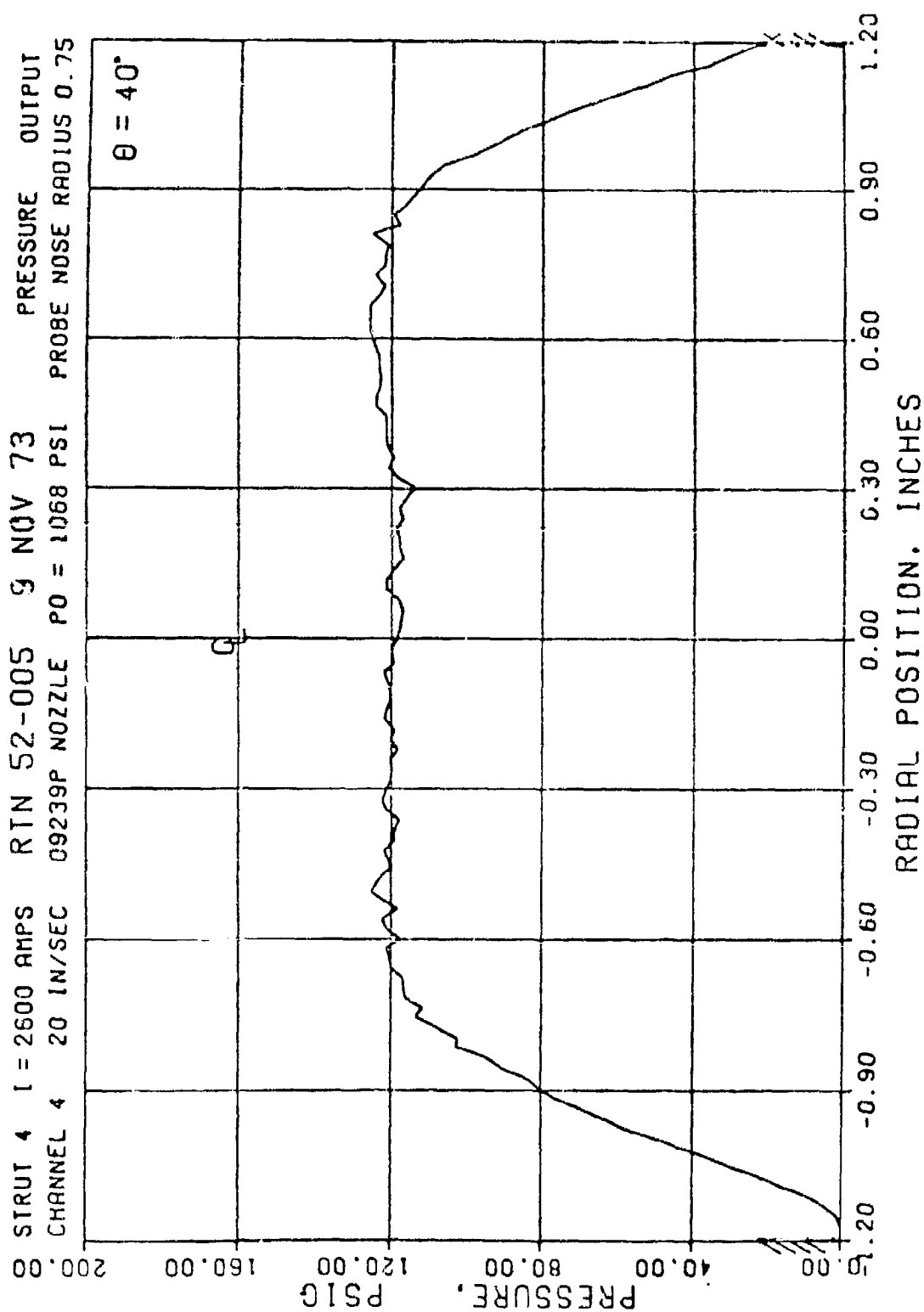Figure 3-27a. Sample Pressure Transducer Output, 1.493 in Nozzle
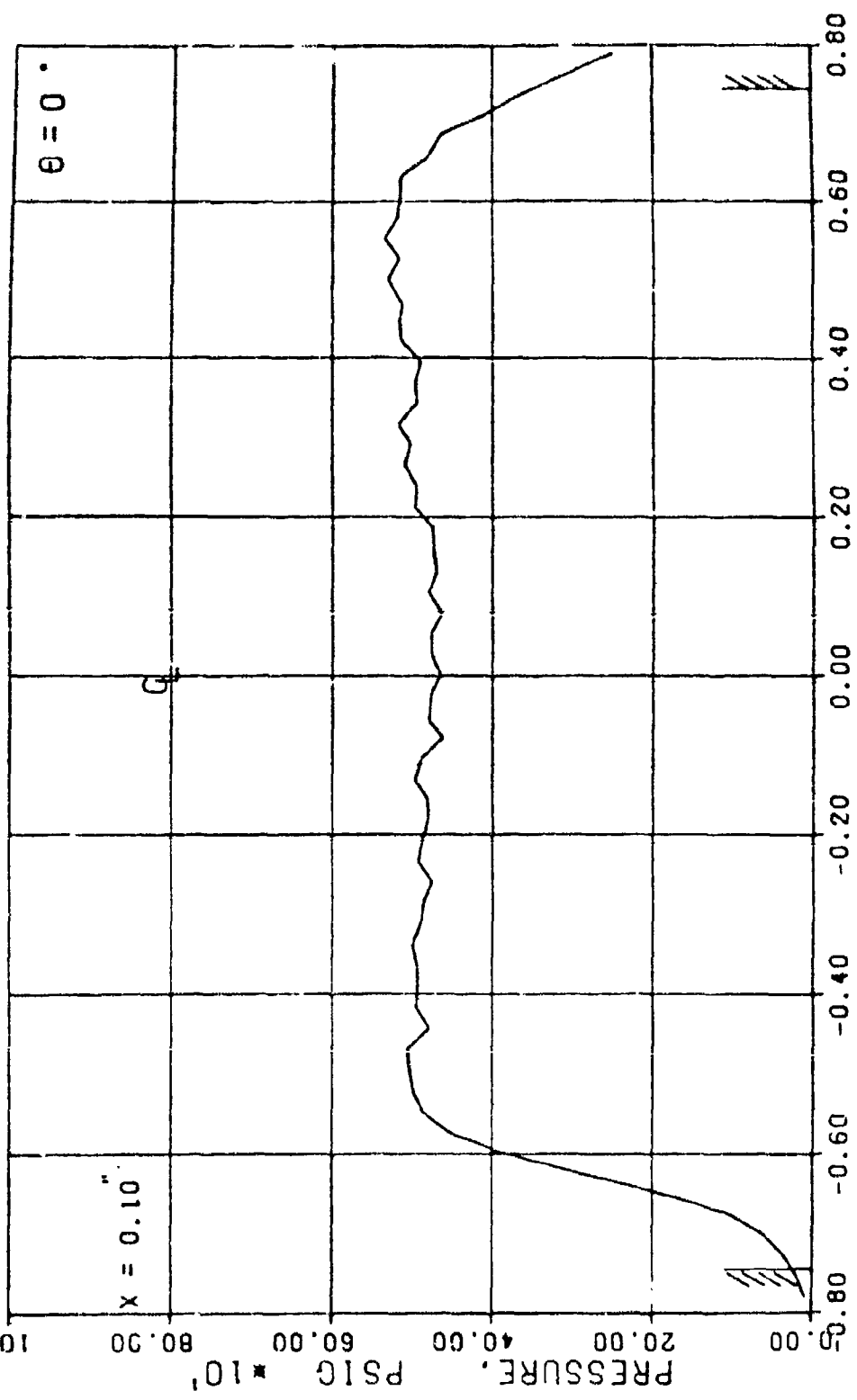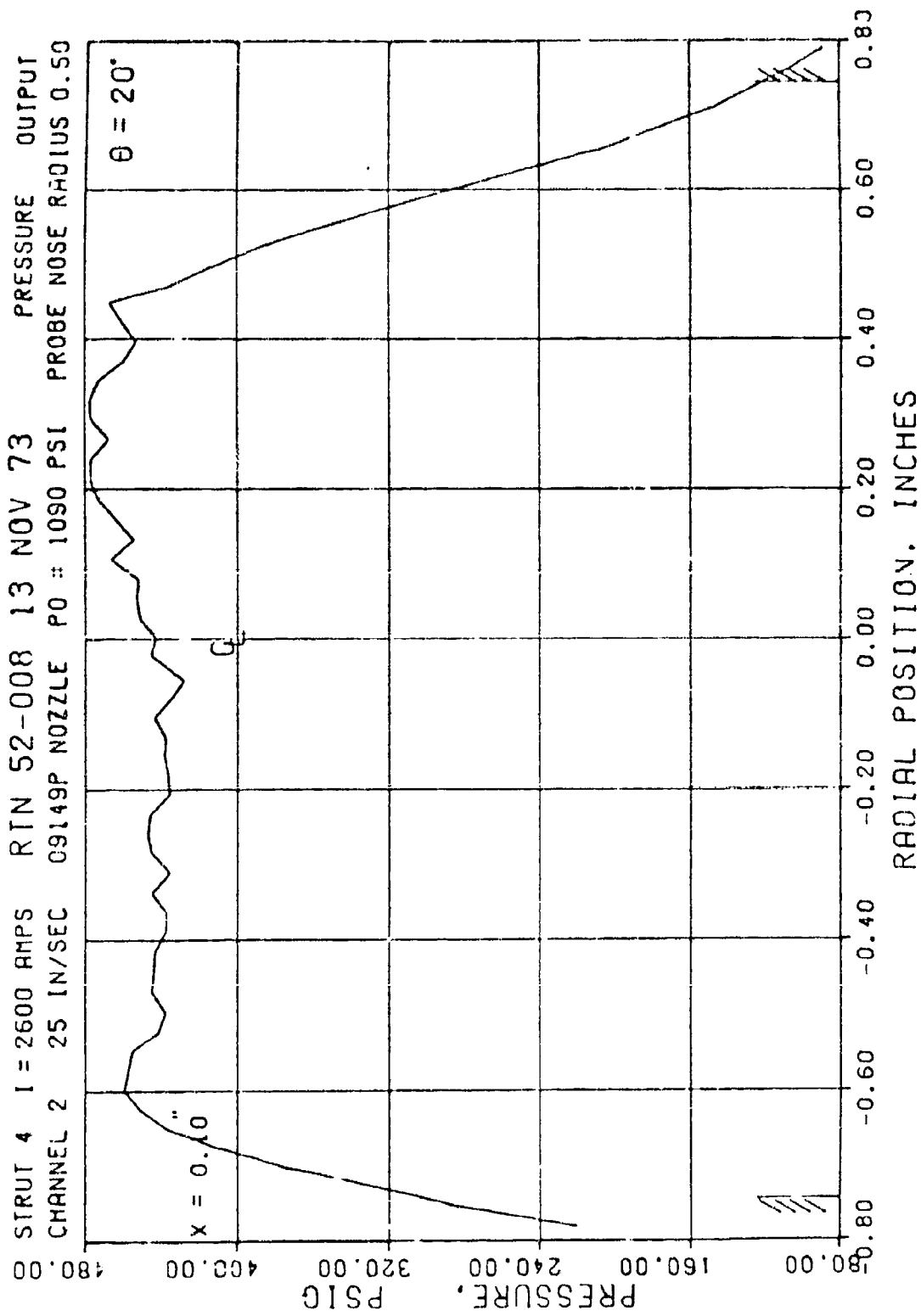
Figure 3-27b. Sample Pressure Transducer Output, 1.493 in Nozzle

STRUT 4   I = 2600 AMPS   RTN 52-008 13 NOV 73   PRESSURE OUTPUT
CHANNEL 3   25 IN/SEC   09149P NOZZLE   PO = 1090 PSI   PROBE NOSE RADIUS 0.50

θ = 30°

X = 0.10"

RADIAL POSITION, INCHES

PRESSURE, PSIG ×10¹

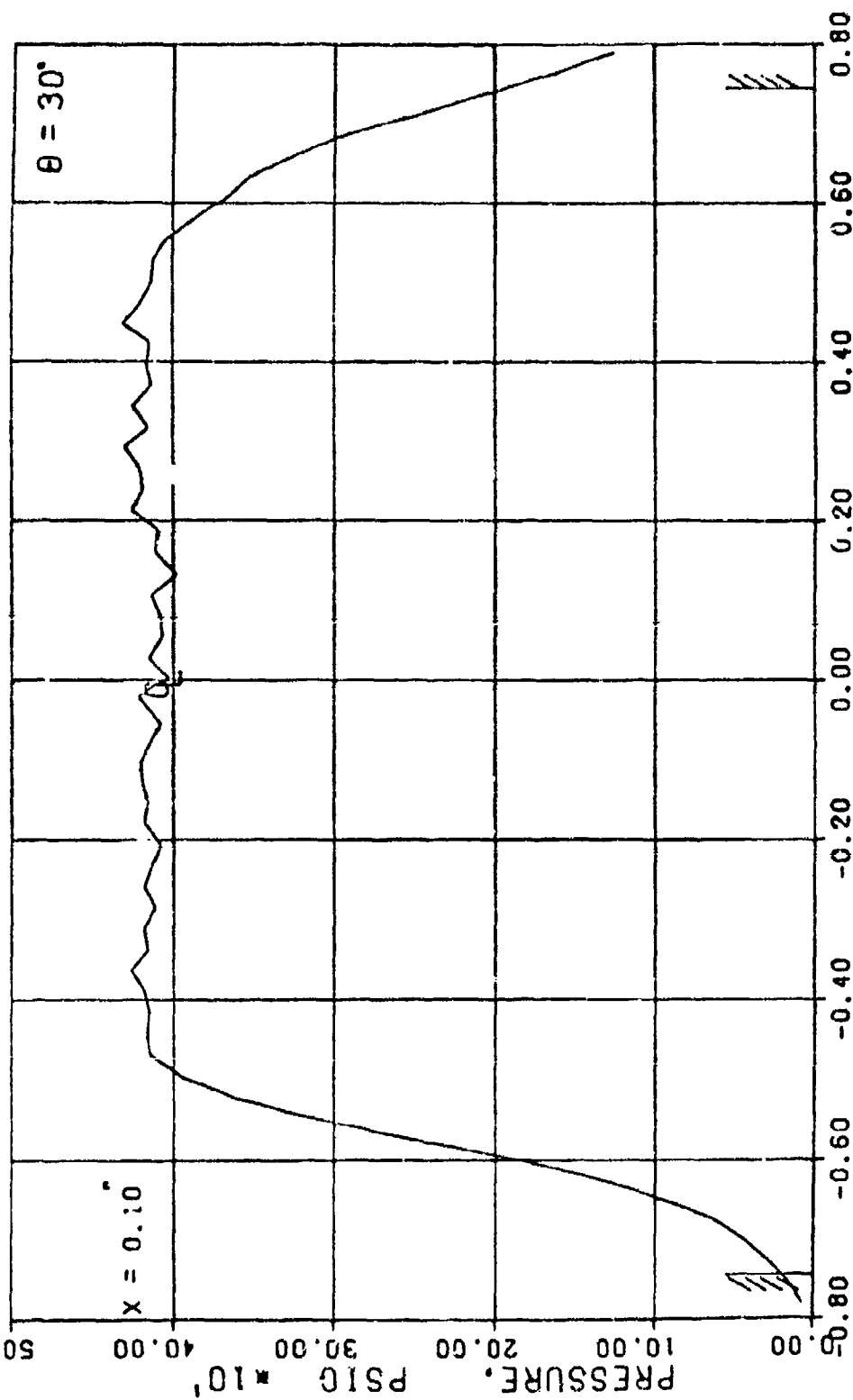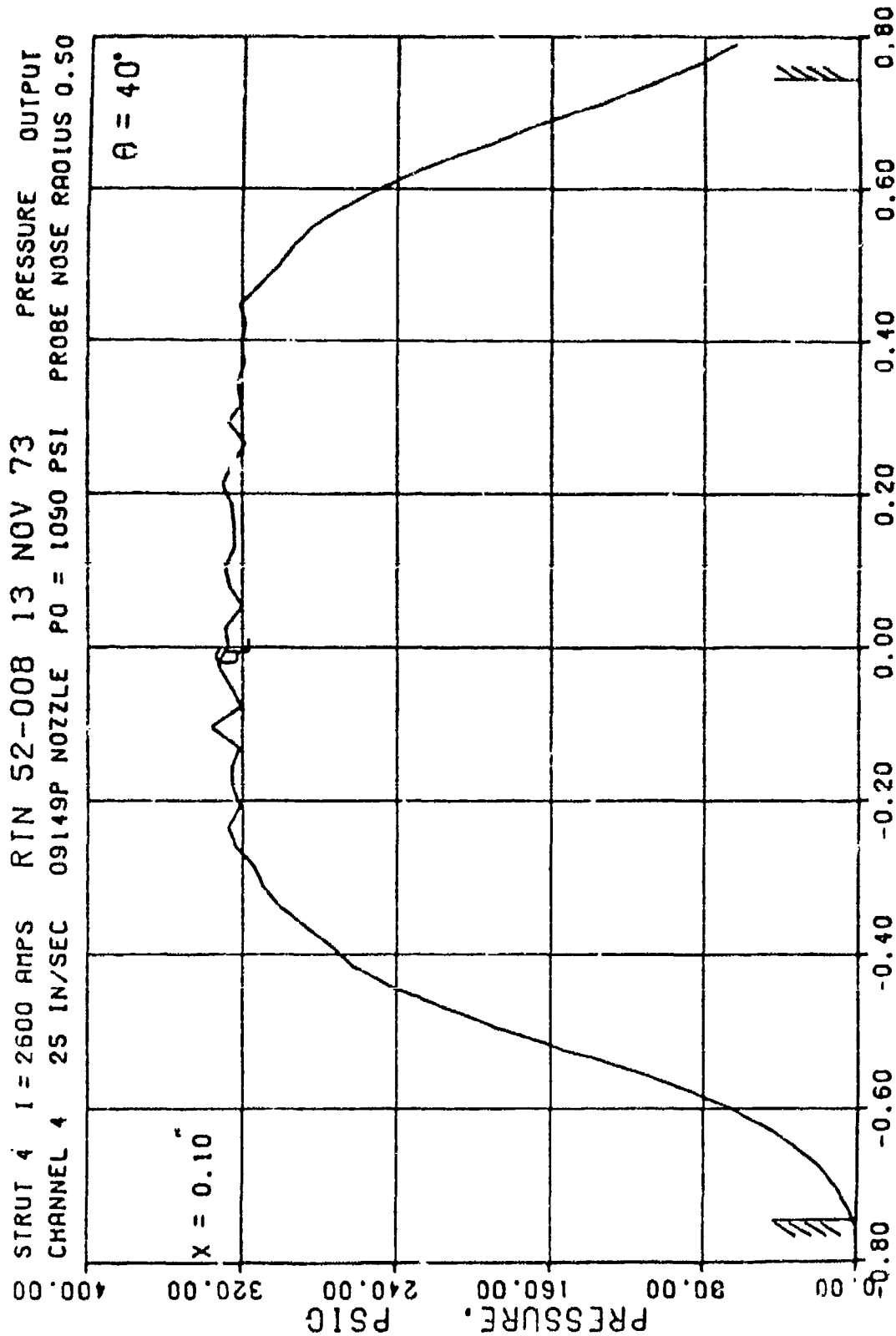Figure 3-27c. Sample Pressure Transducer Output, 1.493 In Nozzle

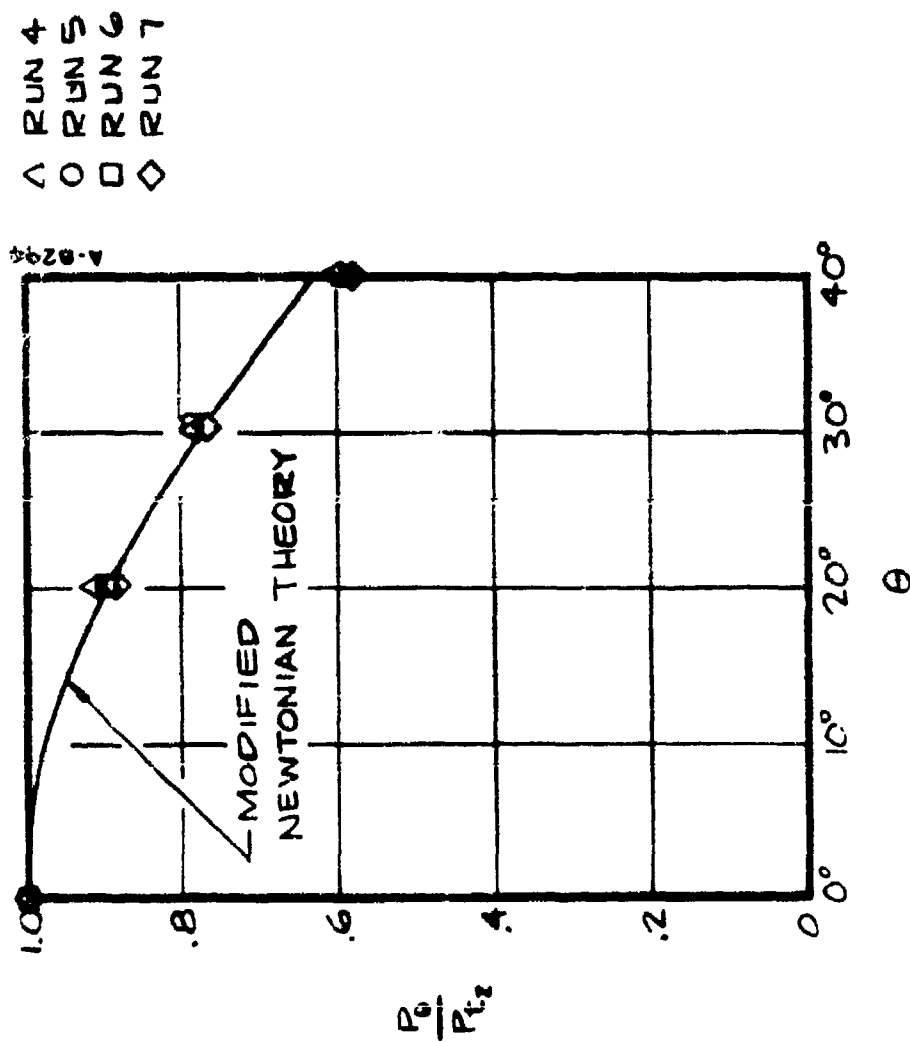Figure 3-27d. Sample Pressure Transducer Output, 1.493 in Nozzle

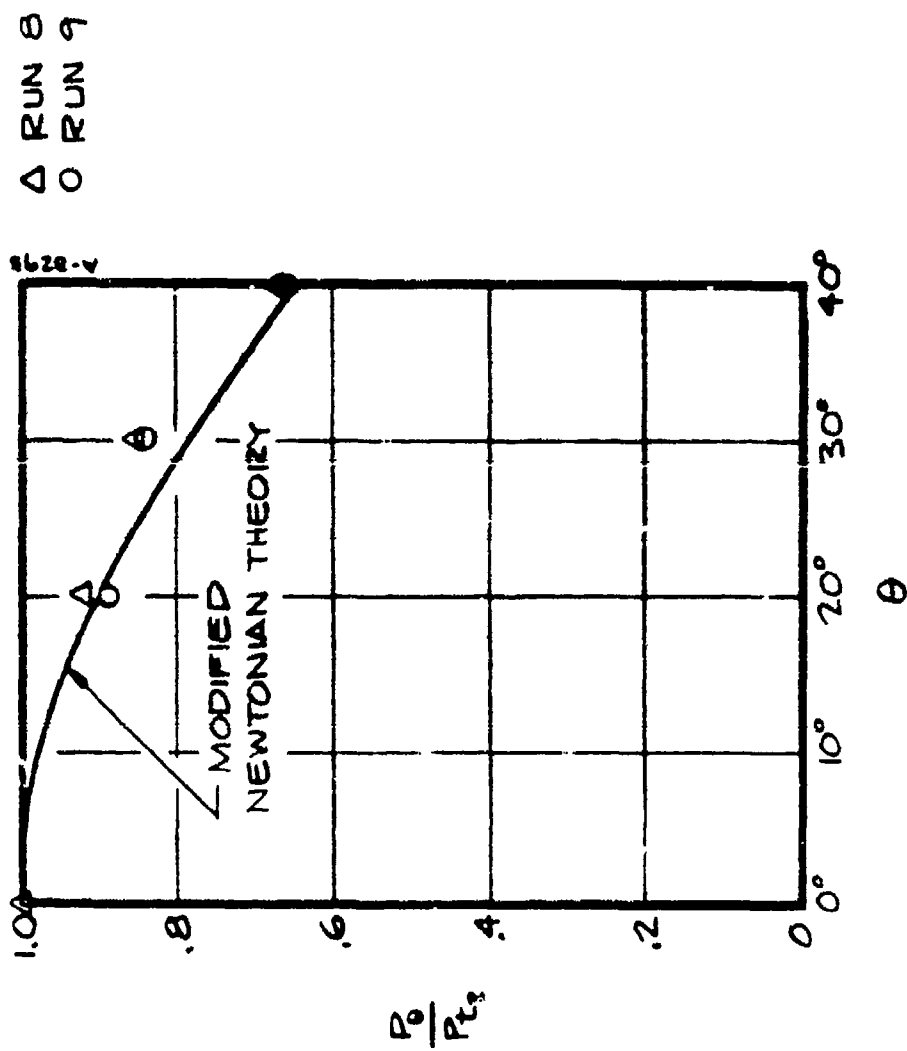Figure 3-28. Correlation of Pressure Distribution, 2.393 in Nozzle

Figure 3-29. Correlation of Pressure Distribution, 1.493 in Nozzle

where P = local surface pressure

P_{t_2} = measured stagnation pressure

P_e = free stream (nozzle exit) pressure

θ = angle between surface normal and free stream velocity vector.

This approximation, as expected, correlates reasonably well with measured data on the spherical nose, although agreement on the 1.493 inch nozzle does show variation from the theoretical results, particularly on Run 008.

The model impact pressure (P_{t_2}) measurements for each run are tabulated in Table 3-1. This table also includes a summary of the arc chamber pressures (P_c) and the ratios P_{t_2}/P_c. These are compared with theoretical impact-to-chamber ratios; both one-dimensional $\gamma = 1.2$ calculations, and variable γ nozzle calculations from Reference 9.

For the higher expansion ratio $D_e = 2.393$ inch nozzle, Table 3-1 shows that the average actual P_{t_2}/P_c ratio is very close to, and midway between, the two theoretical values shown. For the $D_e = 1.493$ inch nozzle, the average actual P_{t_2}/P_c came out somewhat less than the theoretical ratios, implying a γ of 1.13. The reason for this is not apparent since the nozzle dimensions supposedly are quite near the specified values. The average actual P_{t_2}/P_c ratios in Table 3-1 are the factors used to calculate the P_c values shown in the test matrix, Table 2-1.

3.5.2 Heat Flux Data

Heat flux profiles were computed from the null point calorimeter data using the PANDA computer program (Reference 12) by AFFDL. Some typical heat flux profiles are shown in Figures 3-30a through e. These are the heat flux profiles measured by the five operational null point slugs (the sensor at the stagnation point was nonoperational) in the multislug model exposed on RTN-52-005. Similar heat flux profiles are available for all other calorimeters exposed, but they are not included here.

The heat flux data was interpreted in two regards:

1. To check the inferred heat flux distributions over the multislug spherical nose calorimeter model;

2. To check against the procedure used to infer the jet centerline enthalpy levels for each run.

Heat flux profiles such as shown in Figures 3-30a through e were interpreted by estimating a minimum and maximum for the plateau value; this established an uncertainty data band. For the $R_N = 0.75$ inch multislug model, these

TABLE 3-1

SUMMARY OF CALIBRATION DATA

Run	Nozzle (D_E/D^*)	P_{t_2} (psia)	P_c (psia)	P_{t_2}/P_c Experiment	P_{t_2}/P_c Theory[1]	P_{t_2}/P_c Theory[2]
52-004	0.9/2.393	366	1689	.217	.221	.190
52-005		234	1065	.220		
52-006		195	915	.213		
52-007		375	1680	.223		
Average for Nozzle		---	---	.218		
52-008	0.9/1.493	510	1092	.467	0.497	0.532
52-009		461	997	.462		
Average for Nozzle		---	---	.465		

[1]Theoretical calculation based on 1-D, frozen gas, $\gamma = 1.2$.

[2]Results presented in Reference 9 based on real gas 1-D flow.

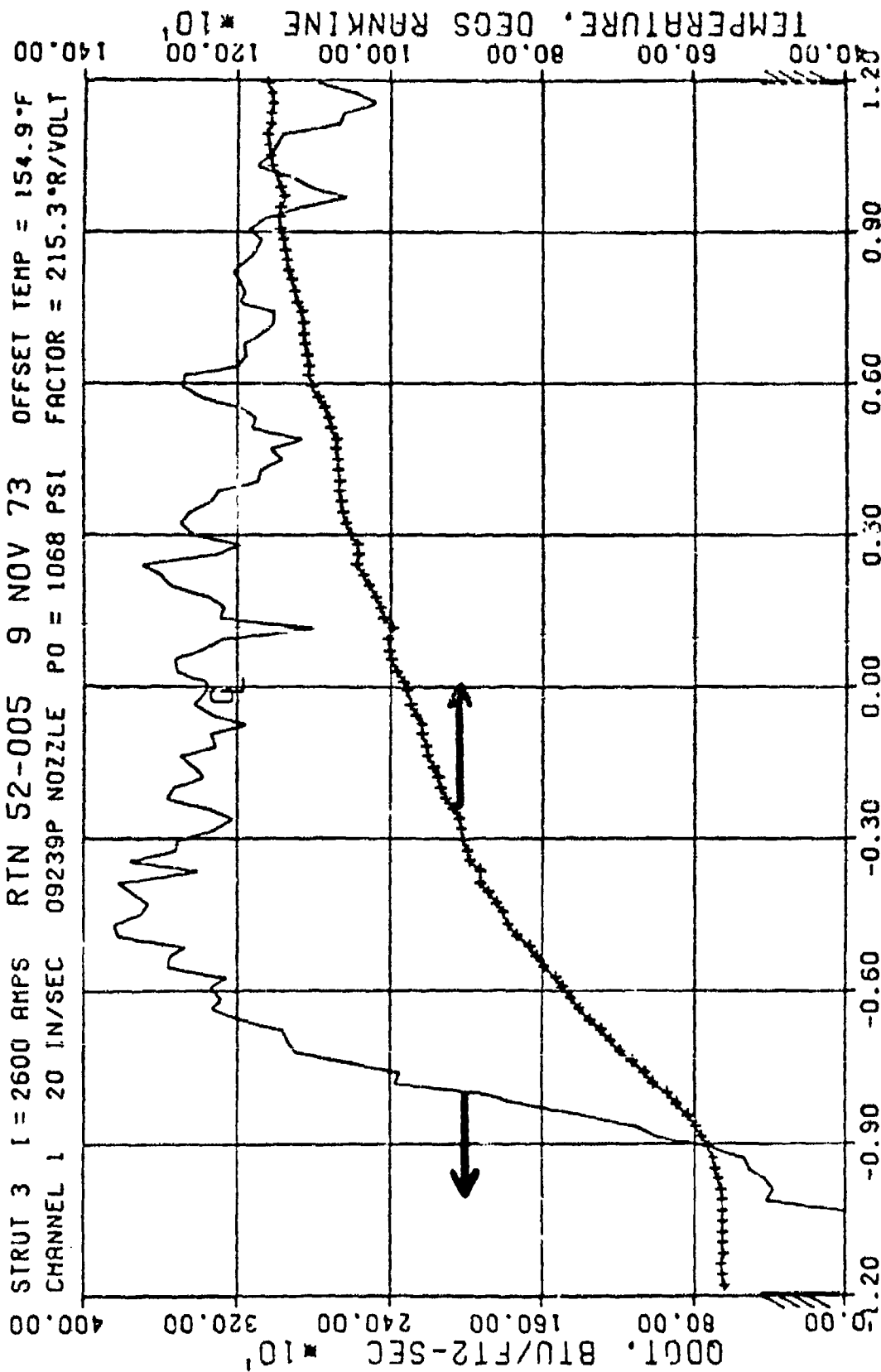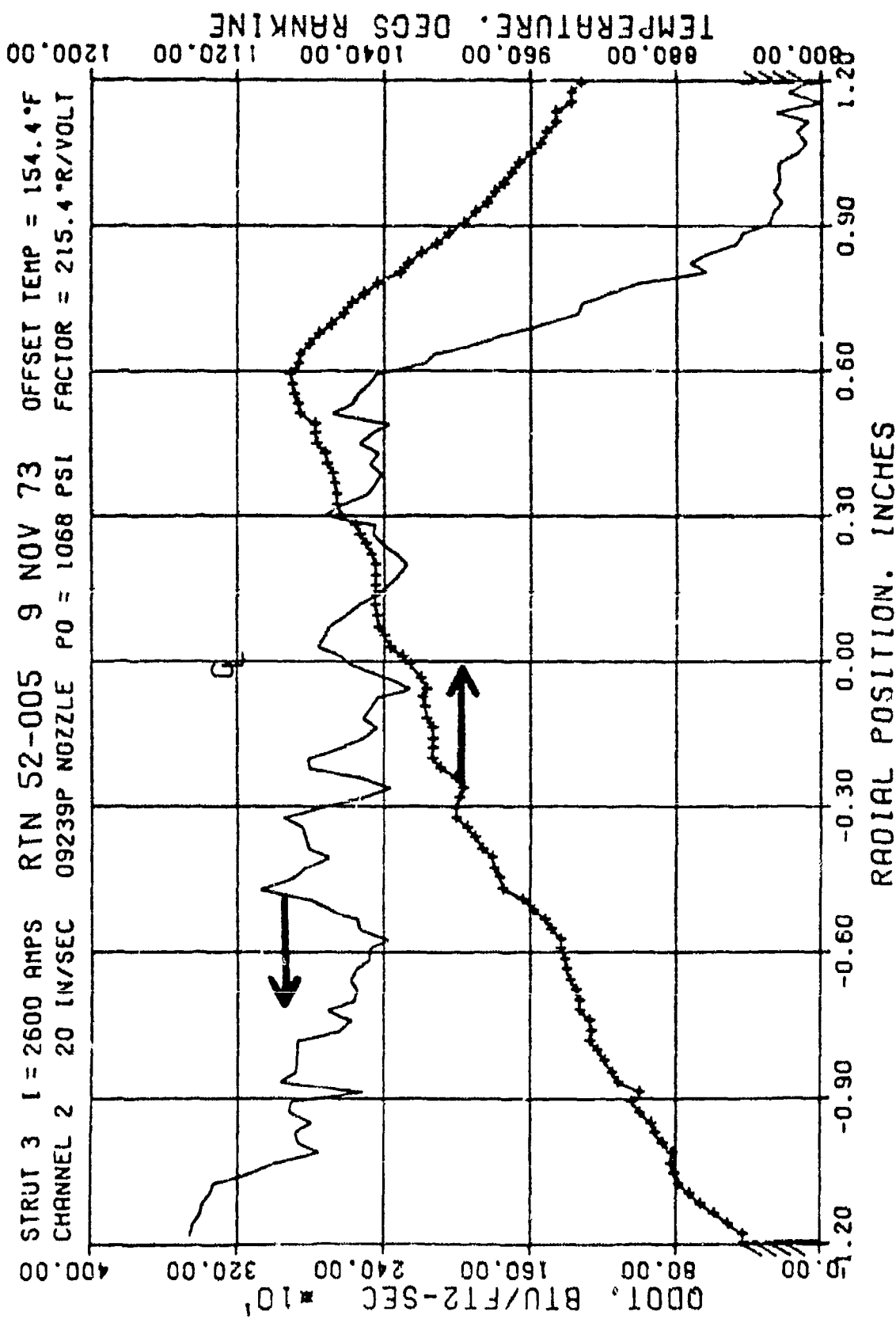Figure 3-30a. Sample Heat Transfer Sensor Output

3-77

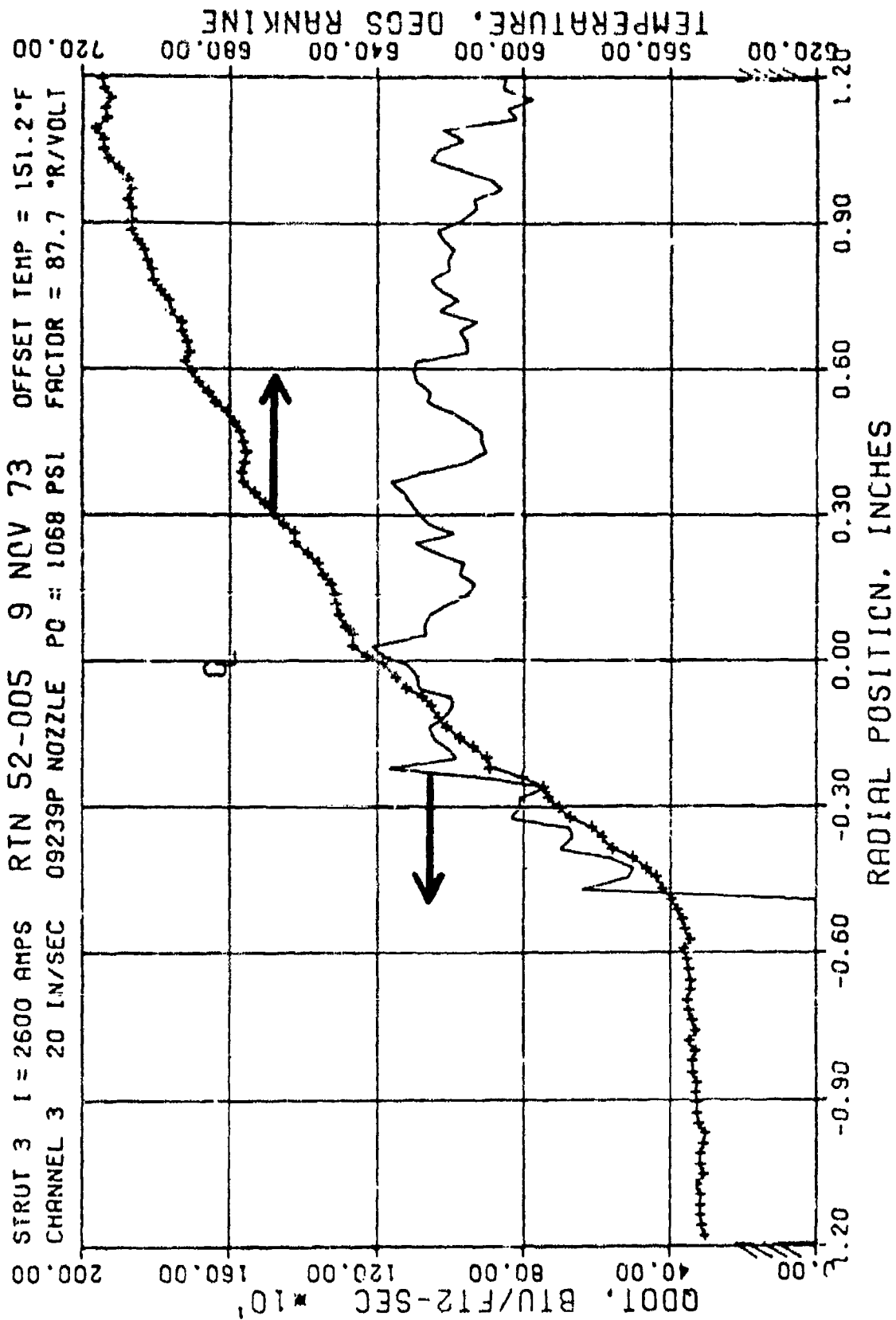Figure 3-30b. Sample Heat Transfer Sensor Output

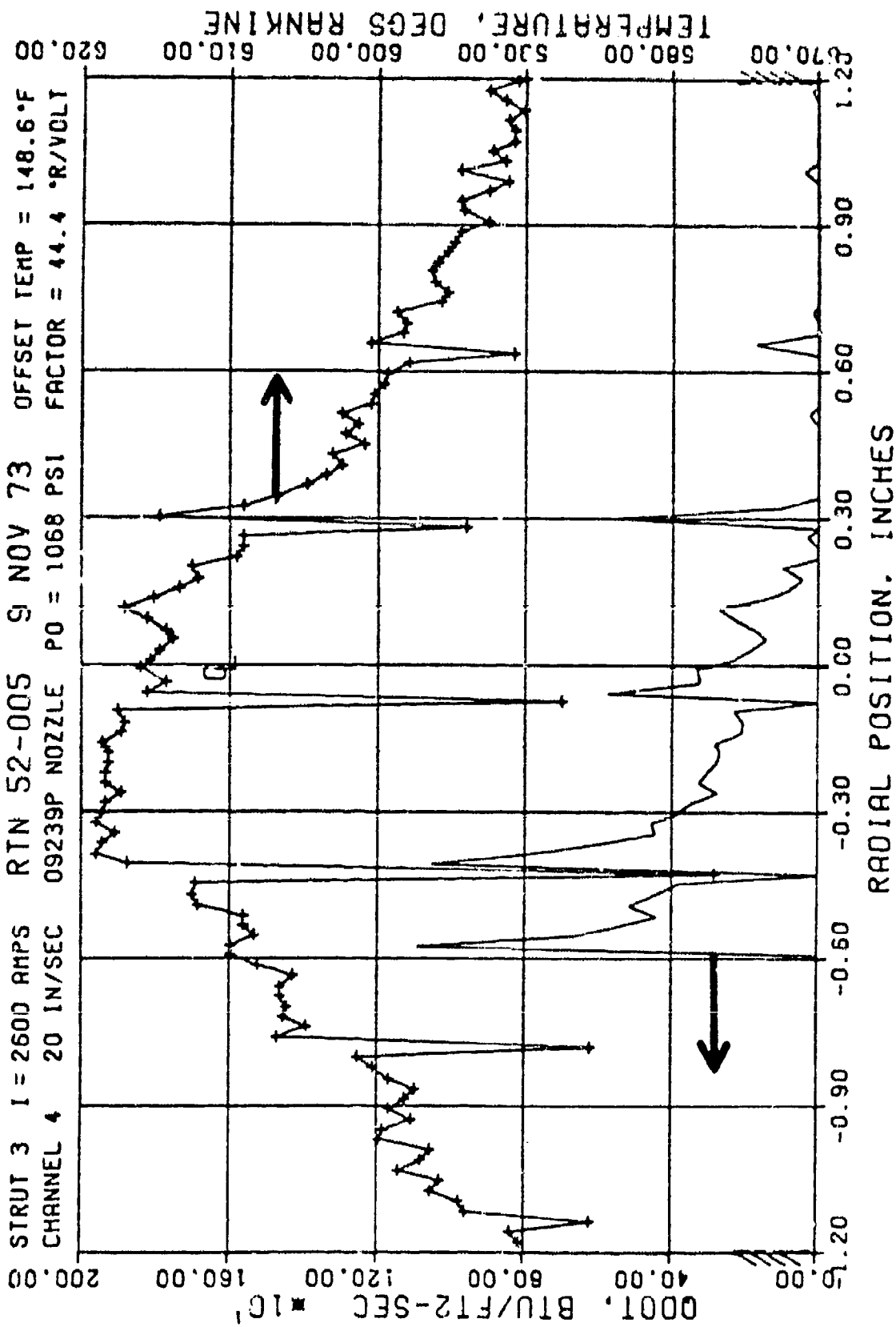Figure 3-30c. Sample Heat Transfer Sensor Output

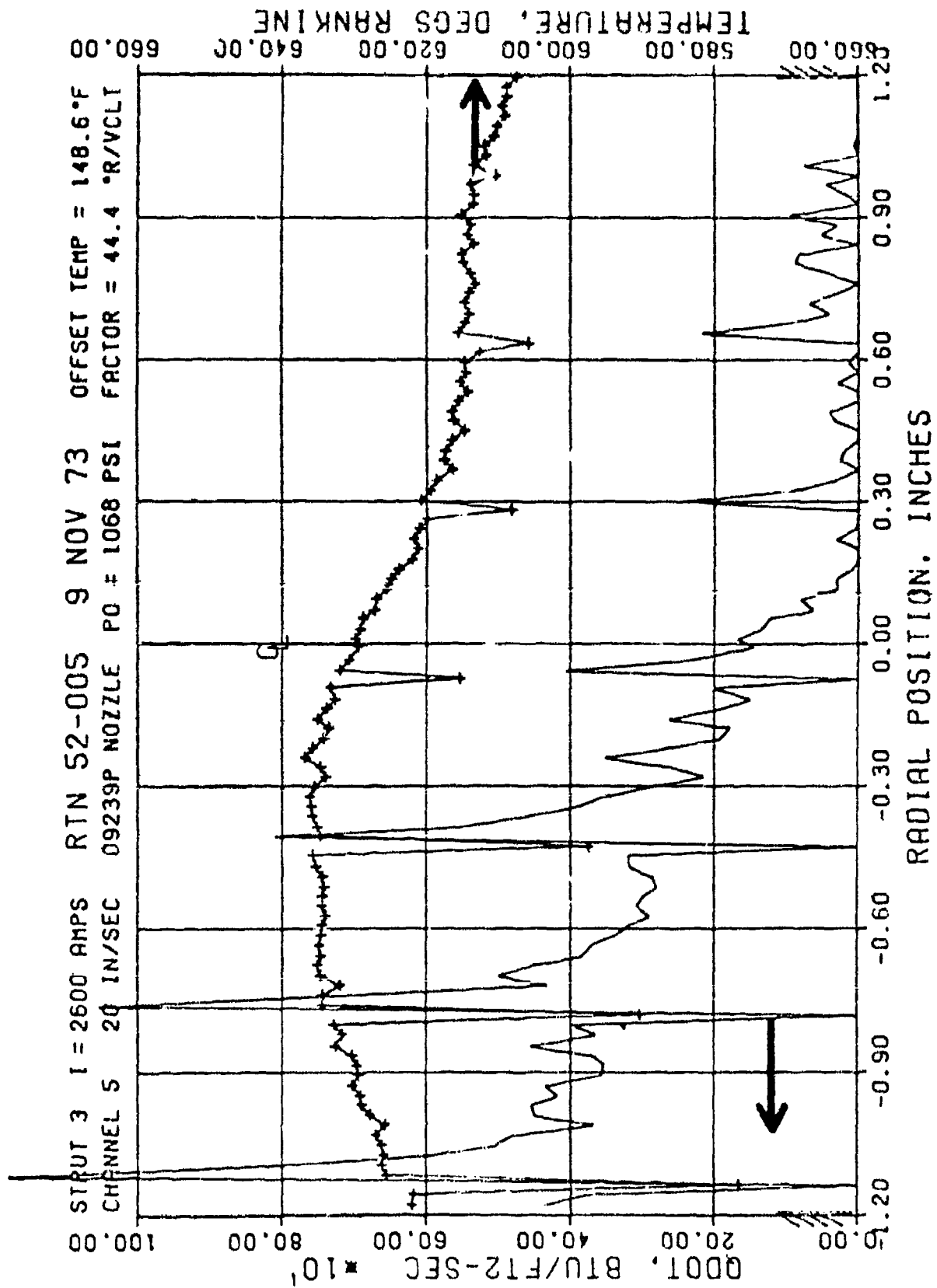Figure 3-30d. Sample Heat Transfer Sensor Output

Figure 3-30e. Sample Heat Transfer Sensor Output

heat flux data bands were plotted versus streamwise coordinate. These heat flux distributions are shown in Figures 3-31a through d. A curve has been drawn through the data bands to aid in interpretation (the curves do not represent theoretical predictions). These heat flux plots show laminar heat flux distributions for these cold-wall, 1.5 mil surface roughness calorimeter models.

The multislug model used for the testing was grit blasted to the 1.5 mil roughness for an earlier test series.

Minimum and maximum interpretations of the stagnation point heat flux levels were also made for the R_B = .25 inch smooth calorimeter models. These data were compared to each other and to theory. To place all of these heat flux values on a more comparable basis, they were all factored to reflect a total enthalpy level of 2000 Btu/lbm using the formula:

$$\dot{q}_{2000} = \dot{q} \, \frac{2000}{H_B}$$

where H_B is the bulk enthalpy measured on the run for which the heat flux $\dot{q}$ was measured.

These adjusted measured heat flux values were then compared to the theoretical heat flux (using simplified Fay-Riddell theory) based on the measured bulk enthalpy. These comparisons are shown in Figure 3-32a (for the D_e = 2.39 inch nozzle) and b (for the D_e = 1.49 inch nozzle). These figures show that, even with the "flat" enthalpy configuration, the heat flux is slightly higher than theoretical based on the bulk enthalpy. This same observation has been made from numerous prior data, although primarily from the D_e = 1.11 inch nozzle.

As part of the AFML contract F33615-71-C-1215, a large quantity of heat flux data obtained at various test conditions has been interpreted to estimate curves of H_C/H_B vs. P_C for the "peaked" and "flat" profile operating conditions. These curves are shown in Figure 3-33. The heat flux data from this series was consistent with the "flat" profile curve shown in Figure 3-32, and so this curve was used to estimate the centerline heat flux values shown in the test matrix, Table 2-1.

Figure 3-31a. Measured Heat Flux Distribution, Run 003

Figure 3-31b. Measured Heat Flux Distribution, Run 004

A-6291

ALL DATA FROM STING 3
$R_N = 0.75'$ EXCEPT WHERE
OTHERWISE NOTED.

STING 2, $R_N = 0.75'$

$\dot{q}$ BTU/FT^2 SEC

6000
5000
4000
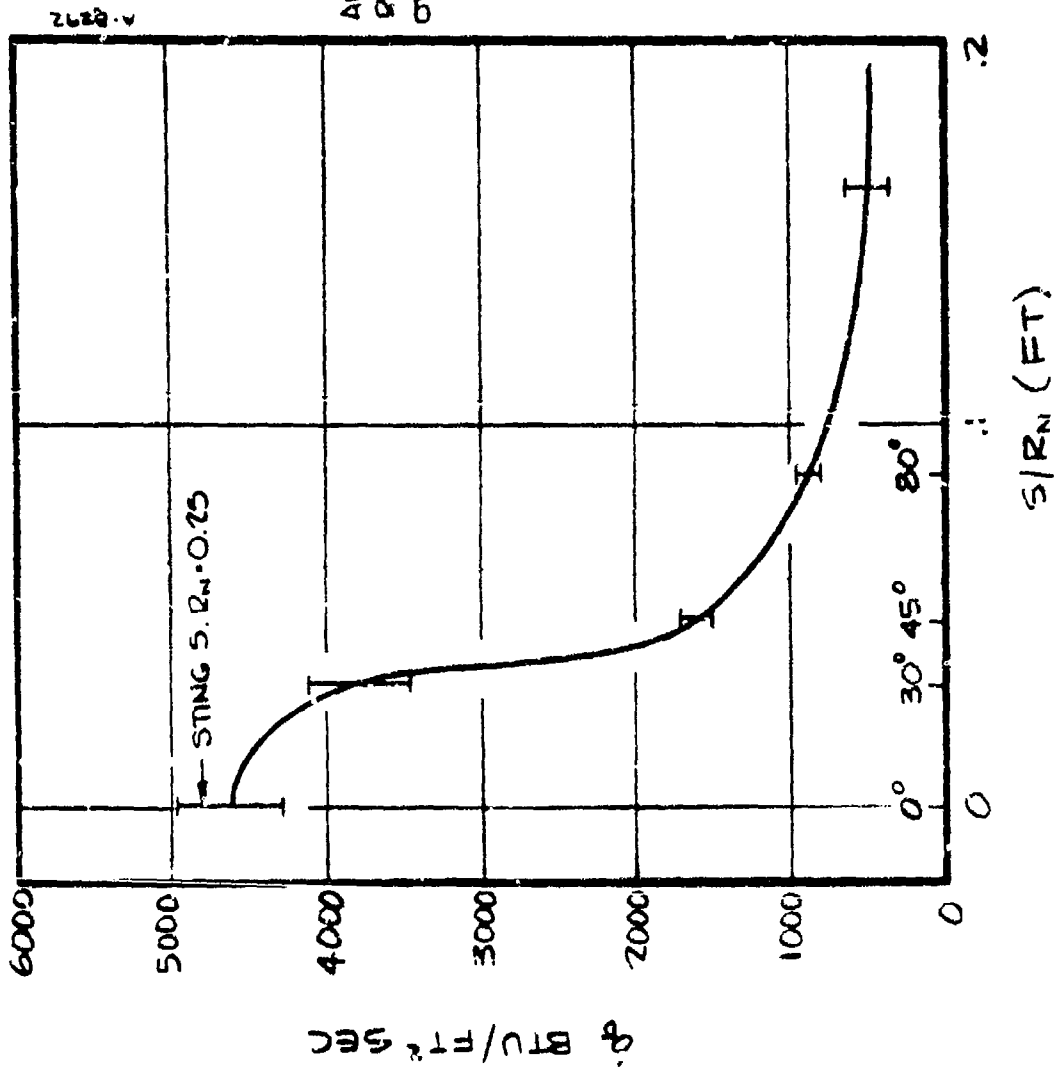3000
2000
1000
0
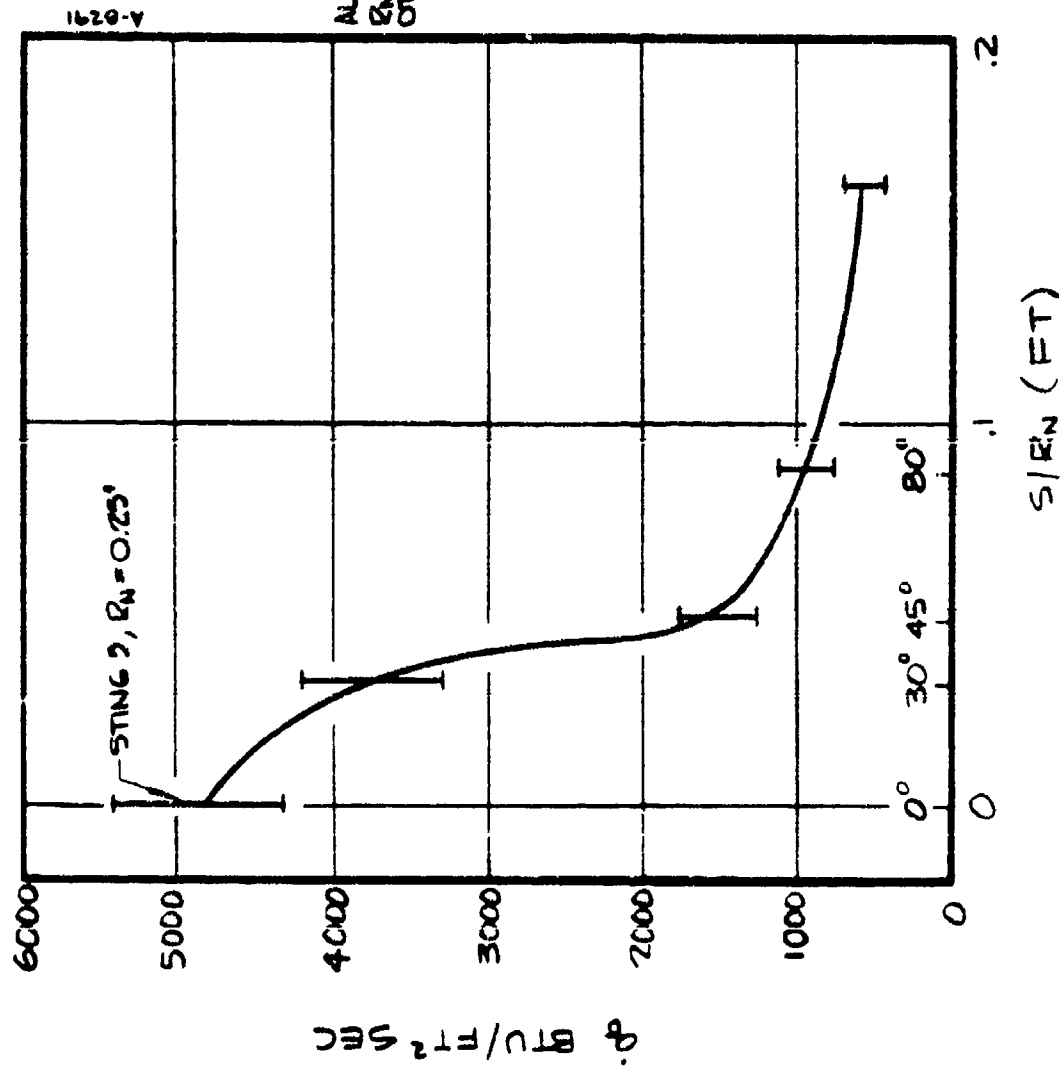
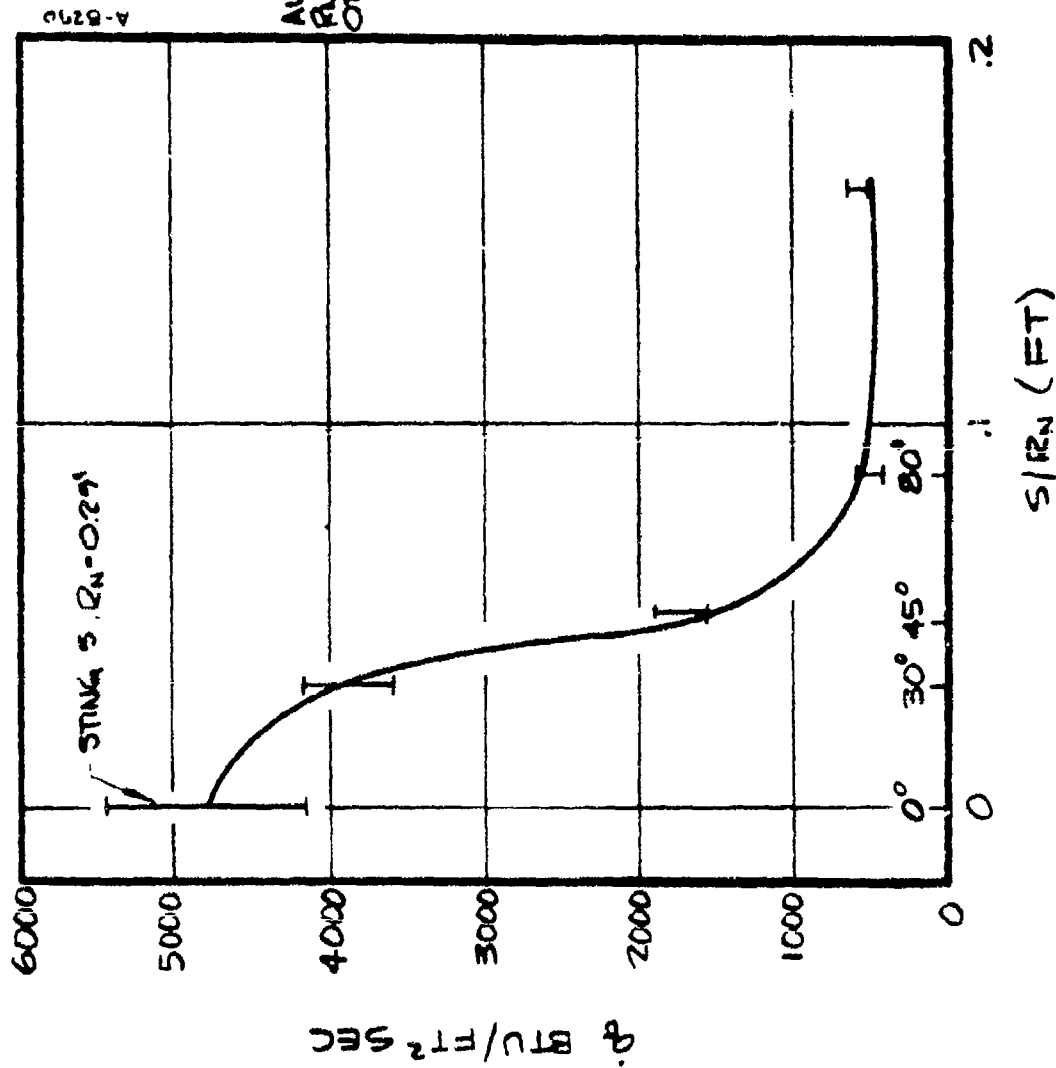$0°$ $30°$ $45°$ $80"$

0 .1 .2

S/R_N (FT)

3-84

Figure 3-31c. Measured Heat Flux Distribution, Run 004
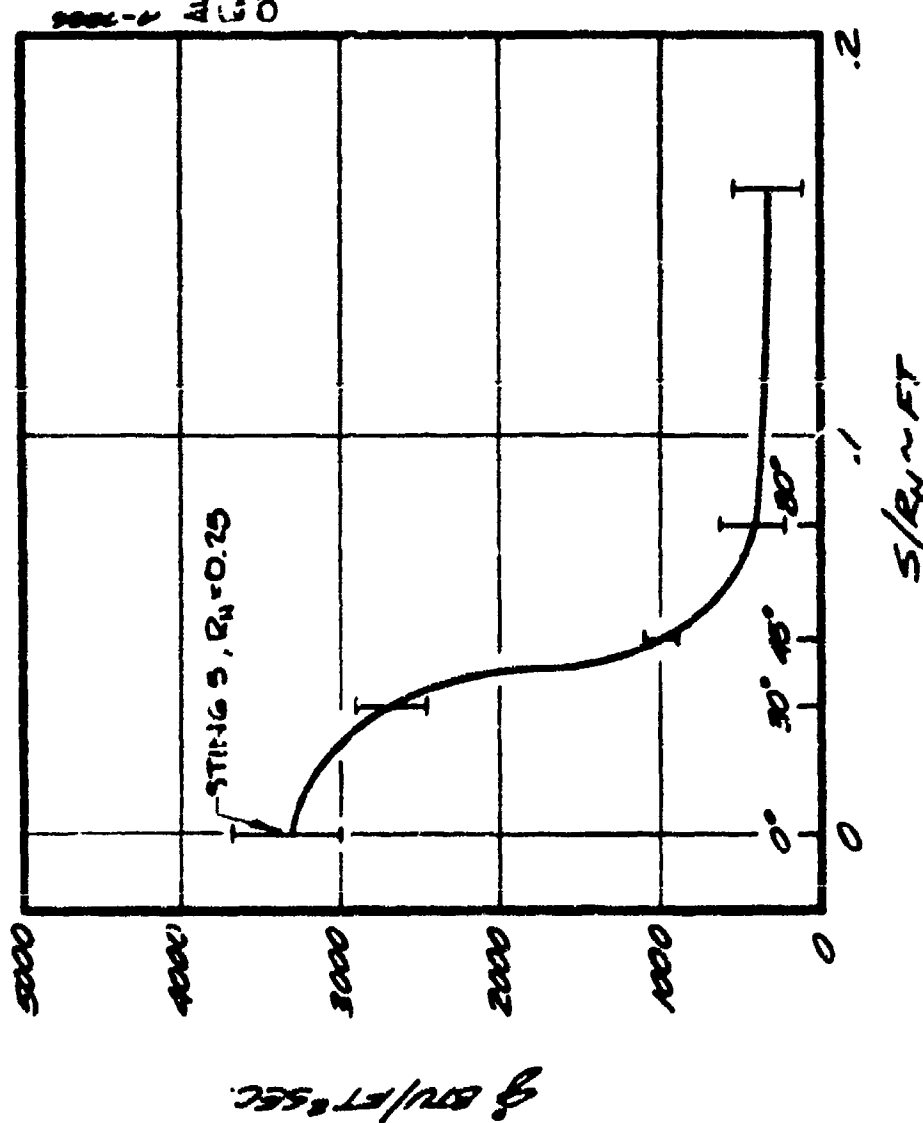
Figure 3-31d. Measured Heat Flux Distribution, Run 005
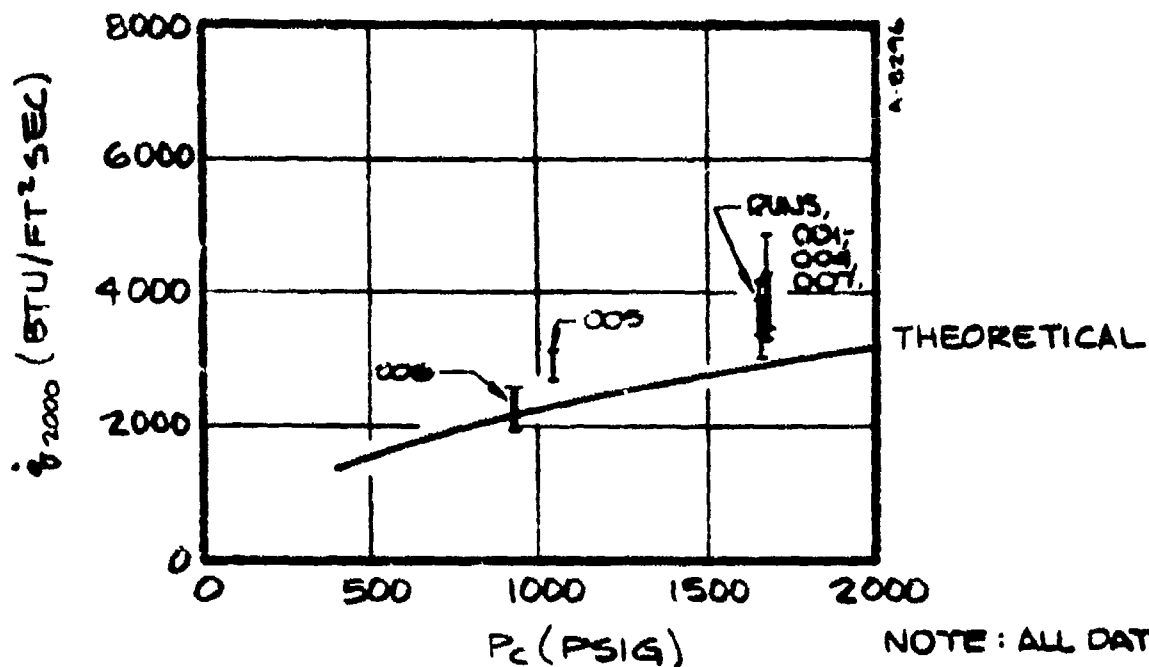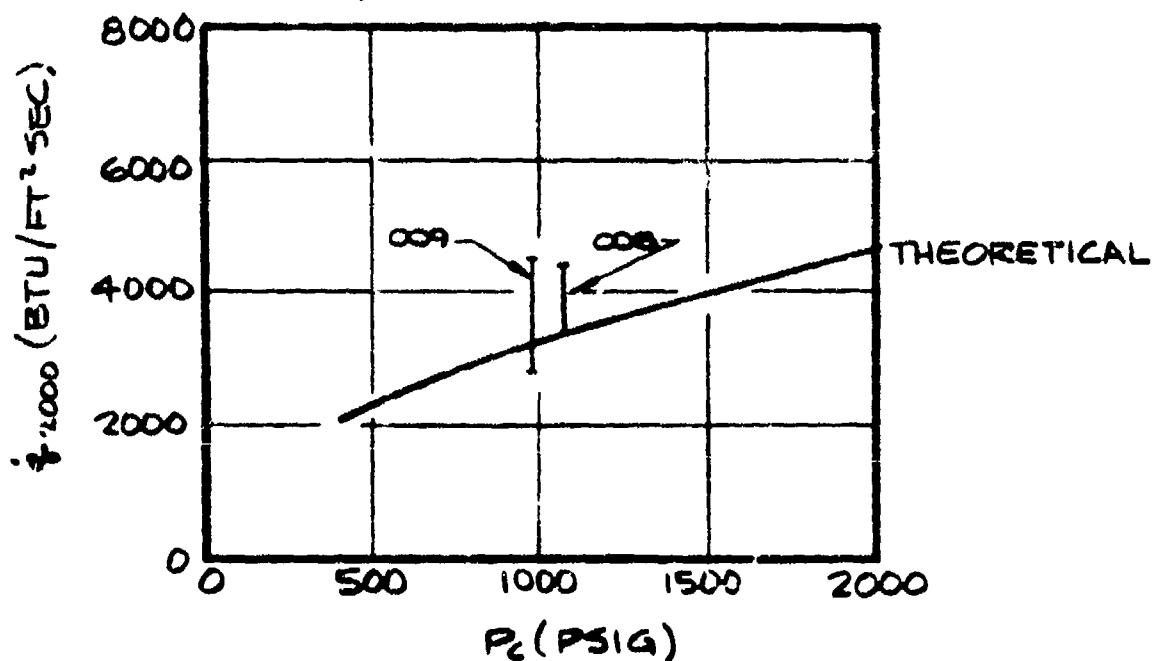
Figure 3-32. Comparison of Stagnation Point Heat Flux Data from This Series (Adjusted to H_g = 2000 Btu/lbm) to theoretical levels corresponding to H_g = 2000 Btu/lbm.

Figure 3-33. Curves Used to Estimate Jet Centerline Enthalpy Levels for the AFFDL 50 MW RENT Arc (From Work Performed as Part of AFML Contract F33615-71-C-1215).

SECTION 4

PRELIMINARY OBSERVATIONS

In general, the test program went smoothly and all data acquisition objectives were met. Relatively minor problems in model design were discovered and corrections to eliminate these problems were successful.

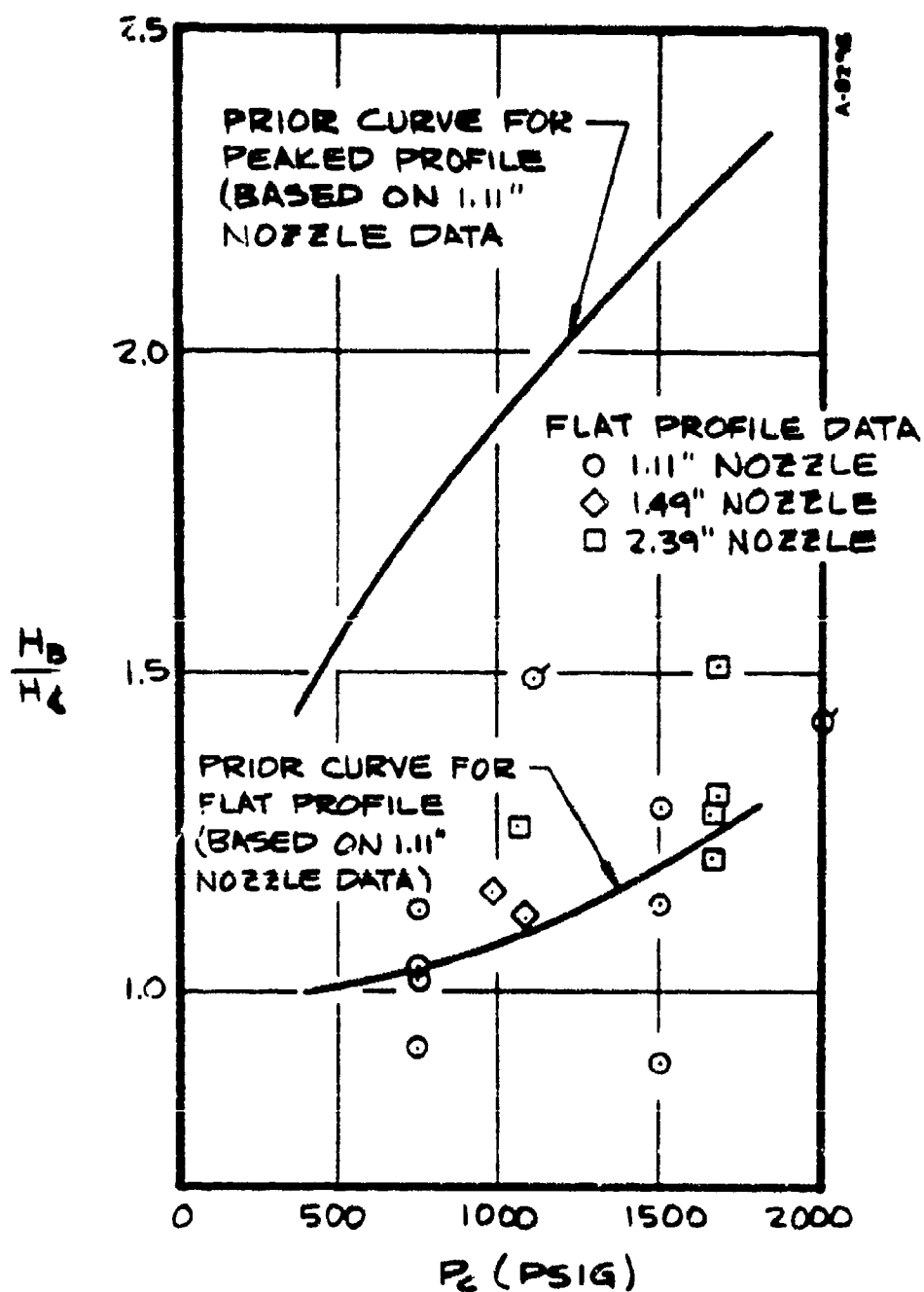The results of the shape change tests (Runs 4, 5, & 7) provide detailed large scale information on shape behavior in "realistic" environments for carbon phenolic and graphite. The model behavior was generally indicative of fully turbulent conditions without major asymmetries or irregular shapes. This was particularly true of the carbon phenolic models which, despite attempts to produce transitional flow, all exhibited well-behaved fully turbulent shapes, although occasional small "knobs" could be seen to form at the stagnation point. With the ATJ-S models, these protrusions or knobs appeared on a more regular basis at the stagnation point and in fact appeared quite similar to previous low temperature ablator tests as illustrated in Figure 4-1 which compares an ATJ-S model with a camphor model tested at $Re_\infty = 5.10^6/ft$ and $M_\infty = 5$ in the NOL hypersonic wind tunnel number 8.
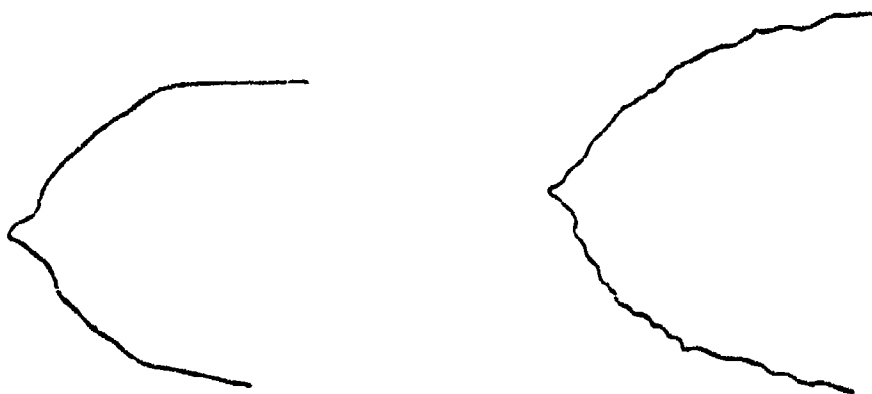
Run 007, Sting 2 (Mid-Test)

a) Graphite

Camphor Run 204 In NOL-8

b) Low Temperature Ablator

Figure 4-1. Comparison of Irregular Shapes

For both the ATJ-S and the carbon phenolic, the sphere/cylinder models seemed to undergo a distinct two phase recession where after transition occurs at about the sonic point, the shape proceeds to sharpen to conic configuration without substantial stagnation point recession and then after achieving the sharpened shape recedes in a relatively uniform manner. The presharpened (30°) configurations for both materials began to recede immediately without having to sharpen thus achieving substantially greater total recession.

The transition tests (Runs 6, 8 and 9) produced satisfactory results except for the two carbon phenolic models. The carbon phenolic at the low impact pressure appeared to char extremely deeply and then delaminate. The carbon phenolic models transitioned early but the shape change and roughness were dominated by the material characteristics rather than the fluid mechanics.

The remaining models all presented useful information on size, shape, and material properties effects on transition. All models tested in the small (1.49 in) nozzle with the exception of the flat faced ATJ-S model exhibited early transition which seemed to remain for a long time in an "intermediate shape" pattern consisting of a laminar region extending up to about the sonic point and then in obviously turbulent region with a fine scale scallop pattern. This pattern slowly sharpens to a configuration similar to that seen with the LTA tests as illustrated in Figure 4-2 which compares a typical 50 MW sample
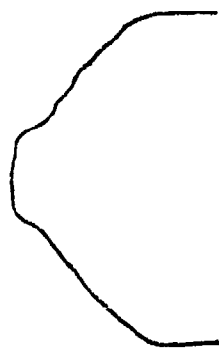
Run 8, Sting 2
a) Graphite
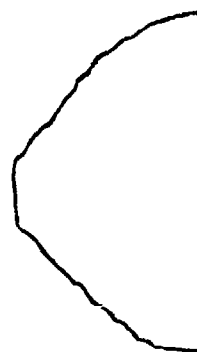
Camphor Run 216 in
NOL-8 (Intermediate Shape)
b) Low Temperature Ablator

Figure 4-2. Comparison of Transitional Shapes

with results from a camphor model tested in the NOL hypersonic tunnel. Detailed information on effects of material and geometry requires further analysis of this data.

The large (0.75 in nose radius) Mod-III model on Sting 3 of Run 006 appeared to be transitional at completion of testing (Figure 3-21c). Large gouges were evident starting at about the 45° location around the nose. Thus, this large nose radius Mod-III appeared to be experiencing incipient transition even at this low pressure (P_{t_2} = 12 atm) test condition.

The flat faced ATJ-S model on Sting 1 of Run 009 appeared to maintain a laminar boundary layer through most of its exposure. This model experienced very little recession (Figure 3-12a). In particular, during the four seconds of exposure, this model did not even ablate to a rounded blunt "laminar" shape as might be expected. It is uncertain whether or not the irregular ablation at the corners of this model near the end of the exposure is indicative of transition.

REFERENCES

1. Powars, C. A., "Test Plan: PANT Program Nosetip Transition and Shape Change Tests in the AFFDL 50 MW RENT Arc," Aerotherm Division, Acurex Corporation, Mountain, View, California, Aerotherm Report TM-73-36, C/N 7010.298, October 1973.

2. Shimizu, A. B., "The Feasibility of Studying the Development of Irregular Ablated Shapes in the 50 MW Arc," TM-73-37, Aerotherm Division, Acurex Corporation, October 1973.

3. Anderson, L. W. and Bartlett, E. P., "Boundary Layer Transition on Reentry Vehicle Nosetips with Consideration of Surface Roughness," TM-71-9, Aerotherm Division, Acurex Corporation, July 1971.

4. Jackson, M. D., Baker, D. L. and Powars, C. A., "PANT Series A - Wind Tunnel Test Data Report," PANT C/N 7040.198, Contract F04701-71-C-0027, Aerotherm Division, Acurex Corporation, December 1972.

5. Anderson, A. D., "Analysis of PANT Series A Rough Wall Calorimeter Data, Part II: Surface Roughness Effects on Boundary Layer Transition," TR-73-31, PANT C/N 7040.272, Contract F04701-71-C-0027, Aerotherm Division, Acurex Corporation, September 1973.

6. Derbidge, T. C., Wool, M. R., and Baker, D. L., "PANT Series D Wind Tunnel Test Data Report," PANT C/N 7040.211, Contract F04701-71-C-0027, Aerotherm Division, Acurex Corporation, January 1973.

7. Baker, D. L., Wool, M. R., Powars, C. A., Derbidge, T. C., "PANT Series C Wind Tunnel Test Data Report," PANT C/N 7040.106, Contract F04701-71-C-0027, Aerotherm Division, Acurex Corporation, January 1972.

8. Maurer, R. E., "Analysis of High Pressure/Hyperthermal ATJ-S Ablation Data and Development of a Recommended Ablation Model (U)," Aerotherm Final Report 73-72, PANT C/N 7040.261, Contract F04701-71-C-0027, Aerotherm Division, Acurex Corporation, June 1973 (CONFIDENTIAL).

9. "The 50 Megawatt Facility, Information for Users," Air Force Flight Dynamics Laboratory, TM-71-17FXE, October 1971.

10. Kennedy, W. S., Rindal, R. A and Powars, C. A., "Heat Flux Measurement Using Swept Null Point Calorimetry," AIAA Paper No. 71-428, April 1971.

11. Wilson, R. G., "Hemispherical Spectral Emittance of Ablation Chars, Carbon and Zirconia (to 3700°K), Article 27, Symposium on Thermal Radiation of Solids, published as NASA SP-55, 1965.

12. Moyer, C. B., "Program for Analysis of Null Point Calorimeter Data (PANDA) Description and Users Manual," UM-71-24, Aerotherm Division of Acurex Corporation, Mountain View, California, 1971.

13. Green, K. A., et al., "AFFDL 50 MW RENT Facility Calibration - Second Quarterly Progress Report for the Period February 12 through June 12, 1970," Contract F33685-70-C-1105, Aerotherm Corporation, Mountain View, California.

REFERENCES (Continued)

14. Bershears, S. R. and Grabowsky, W. R., "Thermal Protection Program - 50 MW RENT Arc Ablation," Aerospace Corporation Report TOR-0059-(S6816-76)-6, November 1970 (C).

15. Kennedy, W. S., et al., "AFFDL 50 MW RENT Facility Calibration - First Quarterly Report for the period October 12, 1969 through February 12, 1970," Contract F33615-70-C-1105, Aerotherm Corporation, Mountain View, California.

16. Green, K. A. and Rindal, R. A., "Phase III Progress Report, AFFDL 50 MW RENT Facility Calibration," Contract F33615-71-C-110" November 1971.